TÉCNICO LISBOA

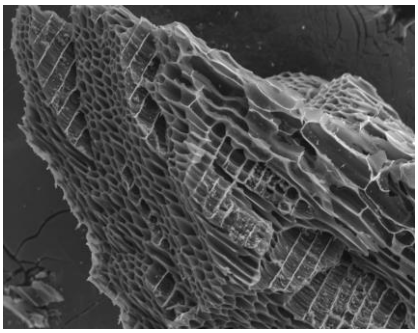

Assessment of biomass and biochar as a porous medium for water retention in soils

Rodrigo Vieira Santos

Thesis to obtain the Master of Science Degree in

Mechanical Engineering

Supervisors: Prof. Ana Filipa da Silva Ferreira

Prof. Miguel Abreu de Almeida Mendes

Examination Committee

Chairperson: Prof. Carlos Frederico Neves Bettencourt da Silva

Supervisor: Prof. Ana Filipa da Silva Ferreira

Member of the Committee: Prof. Ramiro Joaquim de Jesus Neves

December 2021

Abstract

Biomass and its by-products, namely biochar are research objective due to the variety of applications they can have, being mainly due to its porous structure, as the increase of water in soils. It was proposed to evaluate this effect, using two biomasses (pine and eucalyptus), their respective biochars and activated biochars, produced in two different scales, laboratory pine and industrial eucalyptus. Through the characterisation of the materials (BET, Mercury Porosimetry, SEM and TGA) it was observed that both biomasses have a similar thermal decomposition and that the activation has a significant effect on the specific area, 937 m^2g^{-1} and 112 m^2g^{-1} for pine and eucalyptus. While for larger pores, it is found that the pores of the original biological structure have a great influence for the structure of their biochars. SEM images proved elongated pores and that pine has pores in a larger range than eucalyptus. Although the greatest moisture adsorption was in activated pine, due to the CO_2 activated sites, both biomasses also exhibited considerable appetence due to the surface functional groups. A correlation (r=0.95) was found between the total pore volume and the water holding capacity. Regarding water retention curves, in the various mixtures with sand (10%,50% biomass/biochar by volume), an increase in retention was found for plant-available water (maximum observed 50%). For biochars, it is due to their intraporosity, and it is found that smaller pores retain water for higher pressures. For mixtures of 10% the biomasses show a higher increase than the biochars.

Keywords: biomass, biochar, slow pyrolysis, specific area, porosity, water retention

Resumo

Biomassa e os seus sub-produtos, nomeadamente o biochar são objetivo de investigação devido à variedade de aplicações que podem ter, sendo principalmente devido à sua estrutura porosa, como o aumento de água nos solos. Foi proposto avaliar esse efeito, utilizando duas biomassas (pinho e eucalipto), seus respectivos biochars e biochars ativados, produzidos em duas escalas diferentes, pinho laboratorial e eucalipto industrial. Através da caracterização dos materiais (BET, Porosimetria de Mercúrio, SEM e TGA) observou-se que ambas as biomassas têm uma decomposição térmica semelhante e que a ativação tem um efeito significativo na área específica, 937 m^2g^{-1} e 112 m^2g^{-1} para pinho e eucalipto. Enquanto para poros maiores, constata-se que os poros da estrutura biológica original têm uma grande influência para a estrutura dos seus biochars. As imagens SEM, comprovaram poros alongados e que o pinho tem poros numa gama maior que o eucalipto. Embora a maior adsorção de humidade fosse do pinho ativado, devido aos locais ativados por CO_2, ambas a biomassas exibiram também considerável apetência devido aos grupos funcionais superficiais. Constatou-se uma correlação (r=0,95) entre o volume total de poros e a capacidade de armazenamento de água. Em relação às curvas de retenção de água, nas diversas misturas com areia (10%,50% de biomassa/biochar em volume), verificou-se um aumento da retenção para a água disponível para plantas (máximo observado de 50%). Para os biochars, deve-se à sua intraporosidade e constata-se que poros mais pequenos retêm água para pressões maiores. Para misturas de 10% biomassas apresentam um aumento superior aos biochars.

Palavras chave: biomassa, biochar, pirólise lenta, área específica, porosidade, retenção de água

Acknowledgments

I would like to express my words of gratitude towards my supervisors, Prof. Miguel Mendes, Prof. Ana Filipa and Dr. Abel Rodrigues for their great supervision, guidance, support, and encouragement throughout the research, they were fundamental for the realization of this work. I also express my acknowledgments to the professors at the University of Évora, Prof. Manuela Carrott and Prof. Carlos Alexandre, for their support in the experimental work and facilities. And to all the people of the IDMEC laboratory who helped and made possible the development of this work.

The second word of gratefulness goes to my friends and colleagues who accompanied me during all the stages along these difficult years at Técnico, for all the moments that we spent together a lot of thanks. A special recognition to my girlfriend, Rafaela, for the constant support and encouragement.

Finally, the biggest of all thanks goes to my family, especially my parents and brother who always encouraged me throughout the journey and for the tireless effort to always give me the best.

Table of Contents

List of Tables

List of Figures

Nomenclature

A	Section area [m^2]
D	Diameter [m]
D_{ef}	Effective moisture diffusivity [m^2/s]
HHV	High heating value [MJ/kg]
K	Soil hydraulic conductivity [m/s]
k	Hydraulic permeability [m^2]
m	Mass [kg]
Q	Volumetric flow [m^3/s]
r	Radius [m]
R	Universal gas constant [$m^3 \cdot Pa \cdot K^{-1} mol^{-1}$]
RH	Relative Humidity [%]
T	Temperature [ºC]
t	Time [s]
V	Volume [m^3]
V_m	Molar volume [m^3/mol]
X_w	Moisture content [kg/kg]

Greek Symbols

γ	Liquid/vapor surface tension [N/m]
Δp	Gradient Pressure [Pa]
θ	Water content [cm^3/cm^3]
θ	Contact angle [º]
θf_c	Water content at field capacity [cm^3/cm^3]
θ_{paw}	Water content for plant available water [cm^3/cm^3]
θ_r	Residual water content [cm^3/cm^3]
θ_s	Water content at saturation [cm^3/cm^3]
θ_{wp}	Water content at wilting point [cm^3/cm^3]
μ	Dynamic viscosity [kg/(m·s)]
ρ	Density [kg/m^3]
ρ_b	Bulk density [kg/m^3]
ρ_s	Skeletal density [kg/m^3]
φ	Porosity [%]
Ψ	Capillary pressure [KPa]

Abbreviations

aw	Water activity
BET	Brunauer, Emmet, and Teller
db	Dry basis
DTG	Derivative Thermogravimetry
EDS	Energy-dispersive X-ray spectroscopy
EMC	Equilibrium moisture content
EU-AC	Biochar of Eucalyptus activated
EU-C550	Biochar of Eucalyptus at 550ºC
EU-Raw	Eucalyptus raw
FC	Fixed carbon

FTIR	Fourier-transform infrared spectroscopy
GC	Gas chromatography
GtC	Giga tons of carbon
IUPAC	International Union of Pure and Applied Chemistry
M	Moisture
pF	Common log of capillary pressure in hPa
PS-AC	Biochar of pine activated
PS-C600	Biochar of pine produced at 600ºC
PS-Raw	Pine raw
SEM	Scanning electron microscope
SSL	Least Squares Method
SSSA	Soil Science Society of America
TGA	Thermogravimetric analysis
VM	Volatile matter
wb	Wet basis
WHC	Water Holding capacity
WRC	Water Retention Curves
wt%	Weight percentage

Chemical Formulas

$(C_6H_{10}O_5)_n$	Cellulose
C	Carbon
C_2H_2	Acetylene
C_2H_4	Ethylene
C_2H_6	Ethane
C_6H_6	Benzene
Ca	Calcium
CaO	Calcium oxide
CH_4	Methane
CO	Carbon monoxide
CO_2	Carbon dioxide
-COOH	Carboxyl
H	Hydrogen
H_2O	Water
He	Helium
K	Potassium
K_2O	Potassium oxide
Kr	Krypton
Mg	Magnesium
N_2	Nitrogen
Na	Sodium
O	Oxygen
-OH	Hydroxyl
SiO_2	Silicon dioxide

1.Introduction

1.1. Motivation

Biomass is a versatile material that has always been used by mankind, however, due to the challenges that modern society has been implementing both to the planet and to the human being, the increase of research and the use of biomass has gained relevance again. The demand for renewable sustainable energy sources gave to biomass and its by-products an emphasis that had lost with the discovery of coal in the industrial revolution. In fact, energy plays a relevant role which tends to increase in the next decades with population and economic growths. According with the International Energy Outlook 2019 [1], the global gross domestic product (GPD) is expected to grow per year , during the period 2018 to 2050, between 2.4% and 3.7% considering different projected scenarios ,with the greatest influence being given to countries with developing economies (non -OECD countries), mainly due to strong economic growth, increased access to energy markets and rapid population growth. Subsequently this economic growth is linked to an increased demand for energy, nearly 70% in non-OECD countries and 15% in OECD countries. Therefore, world primary energy is expected to grow almost 50% by 2050 with renewable energy becoming the leading source of primary energy consumption (expected growth of 3% per year until 2050). (**Figure *1***)

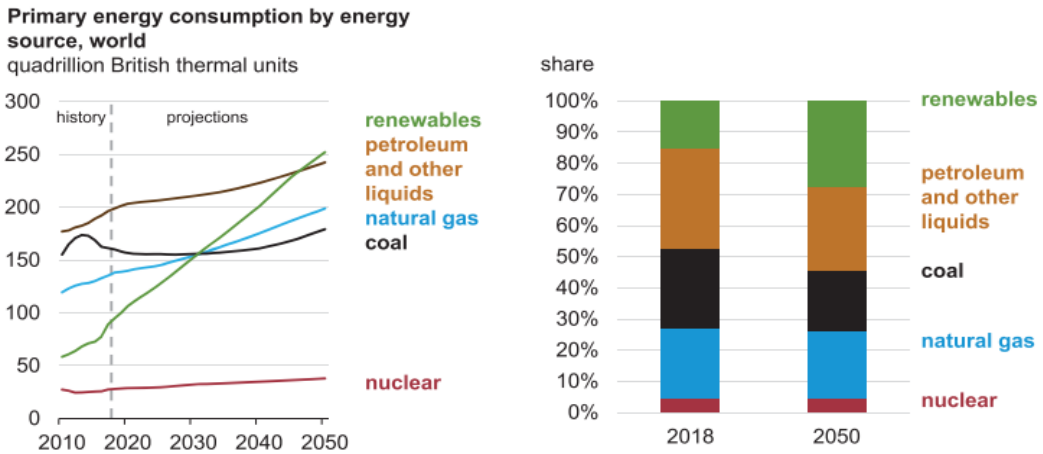

Figure 1-Primary Energy consumption by energy source, World *[1]*

Nowadays the demand for energy is still met mostly through fossil resources (coal, oil and natural gases) which results in high pollution and emission of greenhouse gases, leading to changes in the environment, e.g., climate change and air quality. This is where issues such as sustainable development, emissions reduction, decarbonisation, and renewable forms of energy come in.

The process to combat these changes is already underway insofar that, in 2015 a group of countries signed a climate change treaty (The Paris Agreement), aiming to limital global warming below 2 degrees Celsius (preferably 1.5 ºC), with many countries setting carbon neutrality targets by 2050 [2].To achieve this, the electrification of many sectors is the way forward which gives

renewable energies greater importance and preponderance combined with the fact that energy consumption and the depletion of fossil fuels will continue to rise in the coming years.

Renewable Energies

The concept of renewable energy represents energy which have in common that they correspond to self – renewable energy sources, such as sunlight, wind, water flowing, sea, tides, earth's internal heat or biomass. The later includes feedstock such as waste from agriculture and industry or municipal wate [3]. Currently, between all renewables, hydropower is the largest energy source in the world, nonetheless its share regarding the total renewable generation has been declining in recent years contrasting with wind and solar that have been increasing. In fact, renewables energy consumption continued to grow strongly accounting for over 40% of the global growth in primary energy last year (2019) increasing its share in the energy mix from 4,5% to 5%. Wind generation and solar displayed the largest contribution in accordance with Statistical Review of World Energy [4].

Nonetheless despite energy sources like wind, solar or hydropower have high-cost efficiency, they have the drawback of being intermittent sources of energy, not assuring thereby a continuously power as they are dependent on weather conditions. Biomass and its derivatives conversely can provide power and heat continuously as long as that there is a constant supply of biomass. And in general, is not a problem since it can be obtained through agricultural and forestry practices as well as industrial and urban wastes.

So, analysing the role of renewable energy in the global transformation it can be seen that the biggest growth belongs to wind and solar energy, being complemented with a high increase in efficiencies. However, looking at the roadmap 2050, one can see that energy derived from biomass and all its derivates (biofuels/biogas) will play a major role, since they combined will represent 17% in heat and other direct uses, 10% in transports, and 3% in power (**Figure *2***) [5],[6].

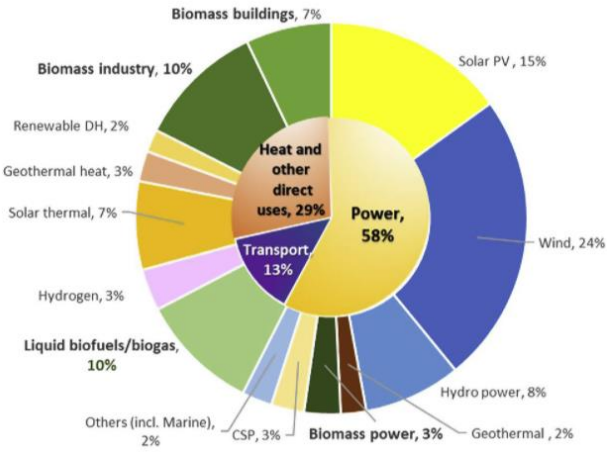

Figure 2- Breakdown of renewables use in total final Energy Consumption Terms, REmaps 2050 *[6]*

Biomass: as a resource

Biomass refers to non-fossilized and biodegradable organic material originating from plants, animals and microorganisms. The biomass includes products, by products, residues and waste from agriculture, forestry, and related industries as well as the non- fossilized and biodegradable organic fractions of industrial and municipal solid wastes. Biomass also includes gases and liquids recovered from the decomposition of non-fossilized and biodegradable organic matter.[7]. By comparison with fossil fuels, it can be renewed and doesn't take millions of years to regenerate. In addition, biomass energy is considered carbon neutral, with no GHG emissions, as it is a constituent part of the carbon cycle (when plants are growing, they absorb CO_2 through photosynthesis, which can then be released in a process such as combustion), therefore being part of the closed carbon cycle the net emissions are zero.[8]

In terms of energy density, biomass represents a step backwards compared to fossil fuels such as oil or gas, but the amount of biomass available worldwide is very representative. Regarding agricultural and forestry practices the wasted derived from harvestable yield is considerable, the global generation of biomass waste is in order of 140 Gt [9] and if this is not used it can also have a negative environmental impacts.

So, biomass can be an instrumental element of energy security and sustainable development, however biomass and their products through conversion processes (discussed below) have a lot of applications beyond energy use, thus making it a resource with enormous scientific and economic potential that has been the subject of much research over the years.[10]

Water usage in agricultural and food industry

As mentioned, biomass and its products, namely biochar can play a role in other issues than energy. Thus, another growing concern besides carbon emissions, is the increasing use of water for agriculture and food industry. According to the OECD and the World Bank[11], currently

around 70% of water is used in agriculture and industry. However due to population growth, urbanization and climate change, competition for water resources is estimated to increase. It is estimated that agricultural production will need to increase by approximately 70% by 2050. The way in which water is managed in the agricultural sector is one of the challenges for the future, involving both the improvement of irrigation systems and the improvement of soils, particularly arid and desert soils, where biomass products (biochar, charcoal when it is used as a soil amendment) can have an effect as a means of increasing water retention.

1.2. Biomass Review

The most important biomass sources are agricultural and forestry residues, animal residues, sewage, algae and aquatic crops. Municipal solid waste and waste streams are also included in the category if they are originated from human activities.

Due to the differences in the variety and quantity of biomass, and in their compositional characteristics, there is no universal way to classify them, but they can be grouped in different groups depending on their purpose. According to their origin and function, they can be classified in two ways[12]:

I. Categorization based on types of biomasses existing in nature (according to ecology or vegetation types).
II. Categorization based on the use and application of biomass as feedstock.

According to the former classification, Vassilev et al.[12] classified various biomass into different groups, which is shown in **Table *1***.

Table 1-Biomass classification: groups, varieties, and species *[11]*

Biomass Group	Varieties and species
Wood and woody biomass	Coniferous or deciduous; Angiospermous or gymnospermous; Stems, branches, foliage, bark, chips, lumps, pellets, briquettes, sawdust, sawmill and others from various wood species.
Herbaceous biomass	Grasses and flowers (alfalfa, arundo, bamboo, bana, brassica, cane, cynara, miscanthus, switchgrass, timothy, others); straws (barley, bean, flax, corn, mint, oat, rape, rice, rye, sesame, sunflower, wheat, others); other residues (fruits, shells, husks, hulls, pits, pips, grains, seeds, coir, stalks, cobs, kernels, bagasse, food, fodder, pulps, cakes, etc.).
Aquatic biomass	Marine or freshwater algae; macroalgae (blue, green, blue-green, brown, red) or microalgae; seaweed, kelp, lake weed, water hyacinth, etc.
Animal and human waste biomass	Bones, meat-bone meal; various manures, etc.

In terms of composition, a distinction can be made between lignocellulosic biomass (wood, plants and leaves), carbohydrates (crops and vegetables) and finally waste biomass which can be

divided into municipal solid waste (MSW), swage, animal, and human wastes, gases derived from landfilling (methane) and agricultural wastes.

The vast majority of biomass is lignocellulosic, so this type of biomass is going to be described in more detail and in this work, this is the type of biomass that will have more emphasis, nevertheless not neglecting the importance of the other types.

1.2.1. Biomass Structure

Structural composition – Cellulose, Hemicellulose and Lignin

The structure of biomass is a complex mixture of organic materials such as carbohydrates, fats, and proteins together with small quantities of minerals such as sodium, phosphorous, calcium and iron. The components of plant biomass can be divided into three groups: extractives, cell wall components and ash. Consequently, the cell wall components are divided into cellulose, hemicellulose and lignin.[13] Lignocellulosic biomass that is considered the most economical and abundant renewable source in the world has as major constituents cellulose (33%-51%), hemicellulose (19%-34%), and lignin (20-30%).(**Figure 3**)

Cellulose is the most common organic compound on Earth and is the primary structural component of cell walls in biomass. Is a long-chain polymer with a high degree of polymerisation (>1000) and large molecular weight, being represented by the generic formula $(C_6H_{10}O_5)_n$. It has a strong tendency to form intra and intermolecular hydrogen bonds, and with the aggregation of linear chain of molecules within microfibrils creates a highly crystalline structure.[14] Thus, gives it high strength, permitting it to provide the skeletal structure of most terrestrial biomass. Hemicellulose is a complex polysaccharide and in contrast to cellulose, are amorphous and have lower degree of polymerisation(50-250)[15]. Lignin is a randomly complex highly branched polymer of phenylpropane and is an integral part of the secondary cell wall of plants, cementing the cellulose fibres in order to hold adjacent cells together.[13]–[15]

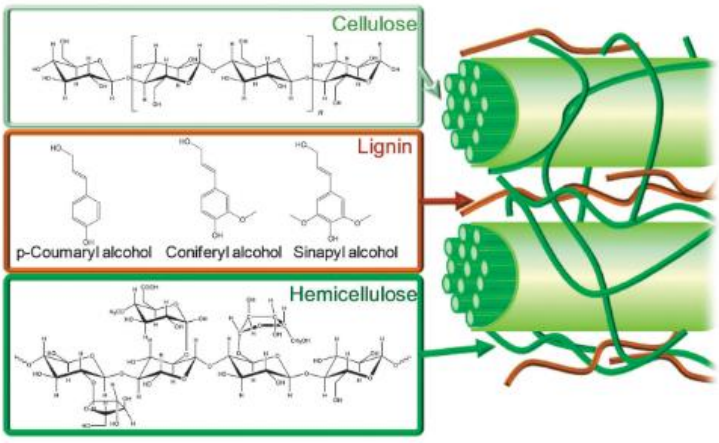

Figure 3-Structure of lignocellulosic biomass with cellulose, hemicellulose, and lignin.[16]

Non-structural composition – extractives and ashes

The components with less prominence in the biomass are called extractives and inorganic matter(ash). Although these components have a small percentage in the biomass constitution, they can have a significant influence on the conversion processes, one example is gasification.

Extractives are substances that can be separated by successive treatments with solvents and can be recovered afterwards by evaporation of the solvents. They have a contribution on properties such as colour, odour and taste. The classification is based on their lipophilic and hydrophilic constituents. Lipophilic extractives, usually called resins, can be non-cyclic compounds (fats, fatty acids and waxes) or cyclic compounds (terpenoids and sterols). Hydrophilic extractives are mostly phenolic compounds (lignans), but can be sugars as well.[15]

Ashes correspond to the inorganic matter (phosphates, carbonates, silicates, chlorides, sulphates, oxyhydroxides, nitrates or hydroxides) presented in biomass, which is usually in lower concentration comparing with organic matter.

Vassilev et al.[12] held an extended overview of the organic and inorganic phase composition of biomass, 93 species carried out between the categories of wood and woody biomass, herbaceous and agricultural biomass, animal biomass and contaminated biomass. This study concluded based on the samples studied that there is a wide variety of composition and properties regarding structural components, extractives and inorganic compounds. The organic matter among the 93 species varies from 54-99% with an average of 93% (dry basis), bulk extractives (various organic and inorganic components) varies between 1-87%, average 10% (dry basis) being higher in herbaceous and agricultural biomass than in wood and woody biomass. Regarding the fluid matter (mineralised aqueous solution associated with inorganic and organic matter), varies between 3-63%, average 14% (dry basis). The inorganic matter (minor and accessory mineral species and poorly crystallized mineraloids) varies between 0.1-46%, average 7% (dry basis).

1.2.2. Conversion Processes

Raw biomass itself has certain disadvantages, such as low energy density and the inconvenience in the form of biomass that can be difficult to handle, store and transport. All this has led to the conversion processes taking a major role, since transforming solid biomass into liquid, gaseous and solid fuels (with better properties) would make it easier to handle this type of fuel. These conversion processes can be achieved in three ways: biochemical, thermochemical, and chemical (referring mainly to acid degradation which leads to lignin-processing, hexoses, pentoses) although the latter is the least used. Through these processes can be obtained different types of fuels, such as liquid fuels (methanol, biodiesel, ethanol, vegetable oil and pyrolysis oil), gaseous fuels (biogas, producer gas, substitute natural gas and syngas) and solid fuels (torrefied biomass, biocoke, charcoal and biochar).

Biochemical conversion

In biochemical conversion, biomass molecules are converted into smaller molecules by bacteria or enzymes. The three types of conversion are:

I. Digestion (anaerobic and aerobic)
II. Fermentation
III. Enzymatic or acid hydrolysis.

In anaerobic digestion the main products are methane and carbon dioxide with a solid residue, while in aerobic digestion (in presence of oxygen) it is produced carbon dioxide, heat, and solid waste. Concerning fermentation, part of biomass is converted into sugars using acids or enzymes, then sugar is converted into ethanol or other chemical with yeast help. These processes are much slower than the thermochemical ones, however, don't require much energy. [17], [18]

Thermochemical conversion

Thermochemical conversion processes, are processes in which temperature has a major influence and they can be divided mainly into:

I. Combustion
II. Torrefaction
III. Slow Pyrolysis/Carbonization
IV. Gasification
V. Liquefaction

Combustion is the oldest mean regarding biomass utilization, chemically speaking is an exothermic reaction between oxygen and hydrocarbon presented in biomass, that is converted in CO_2 and H_2O. It is an important conversion process as it provides heat and electricity, the latter by burning biomass in a boiler and generating power through a steam turbine and can be used as a singular fuel or as a supplement to fossil fuels, thus reducing the amount of carbon dioxide emissions.

Torrefaction is seen as a pre-treatment process, as it prepares the raw biomass for further use. It consists in a slow heating between 200 ºC and 300 ºC (although there is no consensus among authors, none of the maximum temperatures exceed 300 ºC) in an oxygen-free environment or in a presence of a modest amount of oxygen.

Pyrolysis involves rapid or slow heating of biomass in the absence of air or oxygen at a maximum temperature, usually known as pyrolysis temperature, during a certain amount of time to produce non condensable gases, solid char, and liquid products. Considering the heating rate, pyrolysis can be divided as slow or fast, in the former the heating time to pyrolysis temperature is much

longer than the characteristic pyrolysis reaction time and vice versa[17], [19]. In both they generally occur in the absence of a medium (no oxygen or very small amounts) and the characteristics of the products and applications depend very much on the specific operating conditions. Thus, in fast pyrolysis the objective is the production of liquid (bio-oil), the biomass is heated so quickly that the desired temperature is reached before it decomposes, while in slow pyrolysis (or carbonization) the production of biochar is the main objective, the heating is slow allowing time for the condensable vapours to be converted into char and non-condensable gases. In the next chapter, this process together with one of its resulting products which is biochar (a type of char produced from biomass with a wide range of applications) is explored in more detail (from the basis of its theory to the influence of the various parameters).

Gasification is the conversion of solid or liquid feedstock into convenient gaseous or chemical fuel, the difference between gasification and combustion is that the first one packs energy into chemical bonds in the product gas whilst the second one breaks the bonds to release energy. One of the objectives is to increase the hydrogen-to-carbon(H/C) ratio, adding hydrogen and realising carbon from feedstock. Unlike pyrolysis, gasification requires a medium, which can be steam, air or oxygen to rearrange the molecular structure in order to convert solid material into gases or liquids. The gasification process consists of several steps, the first being drying, then pyrolysis in which gases, liquids, oxygenated compounds and solids are releases and react with each other (these reacts can be quite complex) and with the gasifying medium to form the final products.[17], [20]

Liquefaction is the process where the primary goal is the liquid fuel, it can be obtained by pyrolysis, gasification, or hydrothermal process (converting biomass in oil liquid through contact with water at high temperatures and pressures). In **Table *2***, thermochemical processes are summarised regarding operation conditions (temperature, pressure, time) and final products.

Table 2-Thermochemical processes conditions summarised, adapted from [17]

Process	**Temperature**	**Pressure [MPa]**	**Catalyst**	**Drying**
Liquefaction	250-330	5-30	Essential	Not required
Pyrolysis	300-600	0.1-0.5	Not required	Necessary
Combustion	700-1400	>0.1	Not required	Not essential
Gasification	500-1300	>0.1	Not essential	Necessary
Torrefaction	200-300	0.1	Not required	Necessary

1.3. Research Objective

Currently there are certain open issues and critical points that need research and further investigation such as the amendment of desert soils that cannot be used for production, as well as the reduction of water consumption in agriculture and on the other hand the long-term carbon storage. The objectives proposed for this work are as follows:

1. To evaluate and characterize two different biomasses and their respective biochars produced by different thermochemical conversion processes (slow pyrolysis), namely one laboratory process and another industrial process. Also including the activation of both.
2. To portray the porous structure of biomasses and their respective biochars and to study how different processing conditions can affect it.
3. To evaluate the moisture adsorption capacity and its diffusivity, as well as the water retention capacity of the materials.
4. To quantify the effect of biomass and biochars when mixed with soil at different percentages by volume, using silica-based sand as soil, not considering other effects, to understand which parameters have the greatest influence.

1.4. Thesis Outline

The thesis is divided in 7 chapters: Chapter 1 presents an introduction to the motivation regarding the importance of biomass as a resource, with a brief description of its structure and conversion processes. Chapter 2 describes the state of the art in relation to biochar production, namely fast and slow pyrolysis and its applications with special emphasis on soil applications. Chapter 3 shows the materials used during the work, particularly the two biomasses, as well as the characterisation and evaluation methods used. Chapter 4 details the results obtained throughout the work, and a discussion of them is also made. Chapter 5 brings the work to a conclusion with the main outcomes to be highlighted and recommendations for future work. Chapter 6 indicates the references used throughout the work. And finally, chapter 7 contains the appendices.

2. State of the art on biochar production and its potential application

This section presents a literature review of biochar value chain from the biochar production, formation, and its applications. The activation processes during the production of biochar are also taken in account. The key role as a porous medium, water retaining medium for soils are explored, as well the best way to obtain the best effective biochar for this porous medium.

2.1. Biochar production technologies

Pyrolysis as seen in the previous chapter is the thermal decomposition of organic matter with the application of heat in an atmosphere without or with residual air.[19] In order to understand better the pyrolysis reactions, is important to review the chemical reactions behind the transformations of cellulose, hemicellulose and lignin, the main components of biomass.

The thermal decomposition of cellulose is a complex process and has been studied in the literature for several years. Models have been proposed by some researchers such as Shafizadeh, Kilker and Broido, Banyasz. However the current understanding according to Anca-Couce [15], is that cellulose pyrolysis can be divided into two processes which are primary pyrolysis and the secondary reactions. In the first occurs the depolymerization and formation of an intermediate liquid compound (active cellulose) being that later where occurs the fragmentation that produces carbonyl groups and the transglycosilation that produces mostly LGA (levoglucosan). These primary reaction products can lead to secondary reactions in a condensation phase or already outside the cellulose matrix. The char formation is one of the secondary reactions (the explanation of this formation is still not completely clear). Another reaction that occurs is the cracking of volatiles that may occur internally or externally to the cellulose matrix; this phenomenon is more relevant for temperatures above 500 ºC. In relation to hemicellulose, the information in the literature is more limited than for cellulose; however, many similarities have been found between the cellulose and hemicellulose processes.

The lignin has a more complex structure than cellulose and hemicellulose its reaction is also more complex. Thus in a simplified way proposed by Zhou et.al.[21], the first phase occurs the formation of a compound liquid, which will react resulting in pyrolytic lignin, permanent gases and light condensable species (water, carbonyls and alcohols). Subsequently, there are also secondary reactions which may occur in the lignin matrix or outside it and may produce phenolic monomers, char, gases, and light condensable species.

2.1.1. Fast Pyrolysis

According to literature, fast pyrolysis have very short reactions upon to 2 seconds [17], [19].In this process biomass decomposes very quickly to generate mainly vapours and aerosols (volatilization) and some biochar and gas, after that cooling and condensation is form a mobile

liquid (bio-oil). The main product of fast pyrolysis is bio-oil and is obtained in yields up to 75 wt.% in a dry basis[22], depending on different factors such as biomass type, temperature, hot vapour residence time, char separation and biomass ash content. Regarding the temperature, the most used values are between 400 ºC and 600 ºC to maximise the amount of liquid phase.[19] And the vapour residence time should be below 2 seconds to limit the secondary reactions (cracking) of vapour [15].

The configuration of reactors is something that has merited much research due to its importance. The most widely used is fluidized bed reactor (**Figure *4***) both at industrial and laboratory level, since it is able to obtain better heat transfer and mixing conditions. However, other configurations can be named such as, transported bed, circulating fluidised bed, rotating cone, ablative, screw and microwave reactors. Despite the type of reactor, the fundamental characteristics are moderate temperature (around 500 ºC), residence time below 2 s, high heating rates (>100 ºC), short solid residence time and rapid quenching of product vapours to transform in bio-oil.

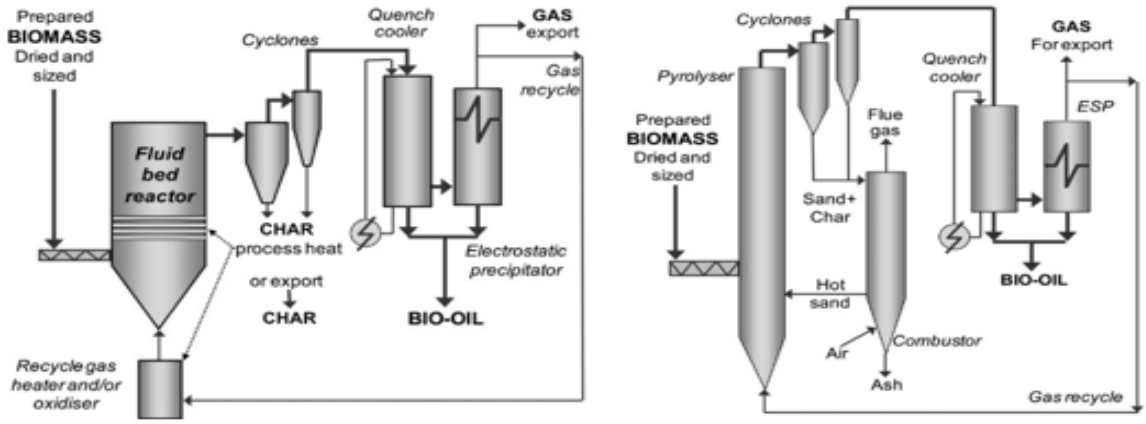

Figure 4-Fast-pyrolysis showing bubbling fluid bed reactor(left) and circulating fluid bed reactor(right) adapted from [22].

Another important parameter is the particle size of biomass, Van de Velden et al.[23] showed that the biomass particle size should be theoretically under 200 µm, however the typically range used is between 100 µm and 3000 µm.

2.1.2. Slow Pyrolysis/Carbonization

Overview

Slow pyrolysis has been used more for charcoal production in recent years and hence has been referred to more as carbonization, they are often used interchangeably, however slow pyrolysis can be considered a broader term, which covers both carbonization as well as torrefaction (i.e., a low temperature pyrolysis process that serves as a pre-treatment process)[19],[24]. The primary goal of this process is to obtain high yields of solid product (char), generally characterized with

low heating rates when compared with other conversion processes. Thus, slow pyrolysis is a derivation of a pyrolysis process in the sense that consists in heating the feedstock in an inert environment (with N_2 for example) or in a limited oxygen environment and depends on the following parameters:

I. Temperature
II. Residence Time
III. Heating Rate
IV. Pressure
V. Type of feedstock (biomass), its composition (% of hemicellulose, cellulose and lignin) and particle size
VI. Reactor Types

Temperature

Temperature is a very important parameter as it affects many characteristics of the products including their yields. According to literature a broad range of temperatures has been tested for slow pyrolysis, ranging from 300 ºC to 1000 ºC.[25]–[27] Studies also show that reaction temperatures used in slow pyrolysis have a great influence on product yield of biochar. The yield of char decreases with the increasing in reaction temperature (300 ºC to 800 ºC) [19] due to the degradation of cellulose that gives place to a more stable an hydrocellulose, which gives higher biochar yield at temperature less than 300 ºC and at a temperature higher than 300 ºC, cellulose depolymerizes hence producing volatiles. [26] In terms of liquid (bio-oil) yield has the same behaviour, first increases then decreases with temperatures above 450 ºC. [28]

Despite of that in many studies the temperature increase led to a decrease in biochar yield, Kathrin Weber and Peter Quicker [29] reviewed a large number of experiments on biochar production to give a general overview of the properties that can be achieved, concluding that with the increase in temperature the quality of biochar have increases, namely in terms of low heating value (LHV), fixed carbon content, porosity and surface area (very important properties as is seen in the next sections).

Heating Rate and Residence time

Heating rate is also very important, as it dictates the speed at which the pyrolysis temperature is reached, as opposed to fast pyrolysis that can heating rate can be as high as 100-1000 ºC/s, the slow pyrolysis is between 0.01 to 2.0 ºC/s [19], in fact the higher the heating rate the higher the condensable gases and consequently more liquid phase (bio-oil), as showed by Kumar et al.[30].However, heating rate does not define the final product, residence time plays an important role as well. To maximize the biochar production, along with slow heating rate is used also a long residence time that can vary between hours until days. In general, with a slow heating, a gradual

removal of volatiles occurs which allows secondary reactions to occur between solid particles and volatiles, leading to secondary biochar formation.

Pressure

The pressure can be varied but in the carbonization process, the pressure is normally not controlled and is therefore close to the ambient pressure. In recent times, much research has been done on a carbonization process, called hydrothermal carbonization, which is carried out in a temperature range between 180-350 ºC in which biomass is submerged in a water reservoir under high pressure (2-6MPa). Heidari et.al [31] held a review on the current knowledge and challenges of hydrothermal carbonization. However, since is not the focus of this thesis the review of this process is not extensive.

Reactor Types

In terms of reactors**,** they can be divided in terms of production, batch or continuous. The batch reactors are steel and brick kilns and retorts, the fundamental difference between them is that the latter the heat to process pyrolysis is generated externally and is transferred to biomass by means of a direct or indirect heating, in both cases heating may be generated by the combustion of pyrolysis gases and vapours.

Continuous reactors can be of various types, depending on their configuration. A well know example is the Lambiotte process, where the biomass is provided by gravity means, gases including pyrolysis vapours move counter. Currently toward the top of the reactor where they are extracted and cooled. Consequently, through condensation some valuable chemicals are recovered and the non-condensable are burnt in the reactor below the region where pyrolysis takes place. However, the most commonly used and modern in the industry, that have arisen with the interest in biochar, are the rotary kilns and screw pyrolizers. The first one consists of a feed hopper that provides biomass to a concentric rotating drum, to ensure mixing of biomass, which is then heated by direct or indirect means. Pyrolysis by-gases, after combustion in an afterburner are used to provide indirect heating to the rotating drum. The screw pyrolizers have a similar principle, except the transport of biomass that is made by means of a rotating, helical screw (allowing for a proper control of biomass residence time) (**Figure *5***)[24].

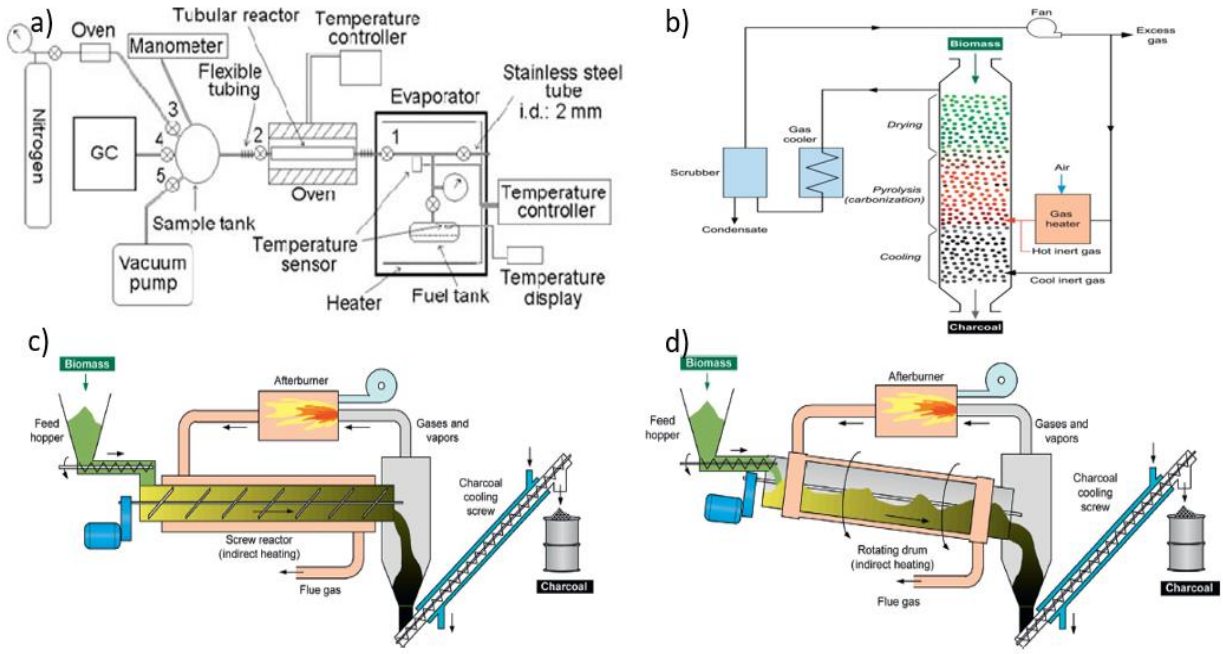

Figure 5- Scheme of biomass carbonization process showing a) batch reactor, b) Lambiott process, c) rotary kiln and d) screw pyrolizer, respectively. Adapted from [24].

2.1.3. Pyrolysis Products

As mentioned in the previous sections, pyrolysis is a transformation (breakdown) of larger complex molecules into many smaller molecules. The products can be classified in three types:

I. Liquid (e.g., heavier hydrocarbons, tars, and water)
II. Solid (char and carbon)
III. Gaseous (e.g., CO_2, H_2O, CO, C_2H_2, C_2H_4, C_2H_6, C_6H_6)

The amount of these products depends on the process and on several factors such as the heating rate and the residence time. In fact, if the purpose is to maximize char production should be used slow heating rate and long residence time, if is to maximize liquid should be used moderate final temperature (450-600 ºC) and short residence time and finally if is to maximize gas, moderate heating rate, high final temperature (700-900 ºC) and long residence time should be used[19].

Bio-oil (mixture of complex hydrocarbons containing oxygen and water) is obtained, as already described, by rapid and simultaneous depolymerization and fragmentation of the hemicellulose, cellulose, and lignin components of biomass. Biochar is the solid yield, containing a large amount of carbon. The gases can be divided into condensable and non-condensable gases, being the condensable gases the heavier molecules which condense upon cooling adding then to liquid yield, and the non-condensable gases the mixture of low molecular weight gases (CO_2, CO, CH_4).

In proximate analysis, the yield of the liquid and gaseous part is generally lumped together as volatile matter (VM), and the solid yield as fixed carbon (FC).

According to the studies[19], [22], [32] , the **Table *3*** presents the solid, liquid and gas yield average values for both processes (fast and slow pyrolysis).

Table 3-Product yields for slow and fast pyrolysis

Process	Char yield	Liquid yield	Gas yield
Slow Pyrolysis	35%	30%	35%
Fast Pyrolysis	12%	75%	13%

In the following sections, the focus of study in this work is on the solid product resulting from slow pyrolysis, biochar.

2.2. Biochar characterization and applications

The term biochar also known as charcoal is a carbonaceous product which results from the thermal treatment of natural organic feedstock in an oxygen limited environment [33], as already seen. Biochar has an aromatic carbon-rich structure which makes it more stable chemically and biologically in comparison to the carbon source from which it produced, this turns biochar difficult to breakdown and was already shown that the mean residence time of stable fraction can range from several hundreds to few thousand years.[34] As expected biochar is not a single material in the way that its characteristics depend on the biomass and the production method.

In fact, the concept of biochar can be connected to the environmental neutral carbon cycle, where the plants decomposes quickly after its death and then CO_2 is released back to atmosphere to neutral the carbon cycle. With the biochar, the natural carbon cycle is uncoupled because instead of plant decomposition, biochar technology sequesters the carbon in a resilient and stable form resistant to decomposition. So, generally, biochar slows the return of CO_2 from soil to atmosphere hence making negative the carbon cycle. Therefore biochar has a huge potential and looking at the global picture the world harvest more than 6.5 GtC (giga tons of carbon) per year of biomass, of which 3.25 tonnes can be converted into biochar and biofuels corresponding to 6500 million barrels of crude oil.[35]

2.2.1. Biochar's Properties

Before analysing the chemical and physical properties of biochar, it is very important to quantify the yields of the production process which, as already seen in the pyrolysis section, depends on several parameters, fundamentally the temperature and the type of feedstock. Thus, the important yields to define are mass yield, energy yield and fixed carbon yield. Pereira et.al [36] concluded that biomass with larger lignin is preferable to achieve high values of mass yield. Whereas

hemicellulose and cellulose contribute more to condensable gases the lignin being more stable contributes also to biochar yield.

Chemical Properties

The composition of biochar is a crucial in determining its use. Here in this subsection is reviewed the chemical properties of biochar such as the proximate and elemental composition, energy content, values of pH, reactivity, degradation, and self-ignition processes that depend on process conditions, temperature, and residence time.

Atomic Ratios

As carbonization is a process that involves changes in chemical structure, it's natural that occurs release of functional groups that contain hydrogen and oxygen. Resulting in the decrease of the respective ratios with carbon, called atomic ratios H/C and O/C. These ratios are represented in the so called van-Krevelen diagram [37]. Weber and Quicker [28] with the collection of results from several studies showed that the trend is the reduction of H/C and O/C ratios in both woody, herbaceous and straw biomasses. **Figure *6*** shows the evolution of the fuels components during carbonization and can be concluded that the oxygen released is approximately the double of hydrogen release.

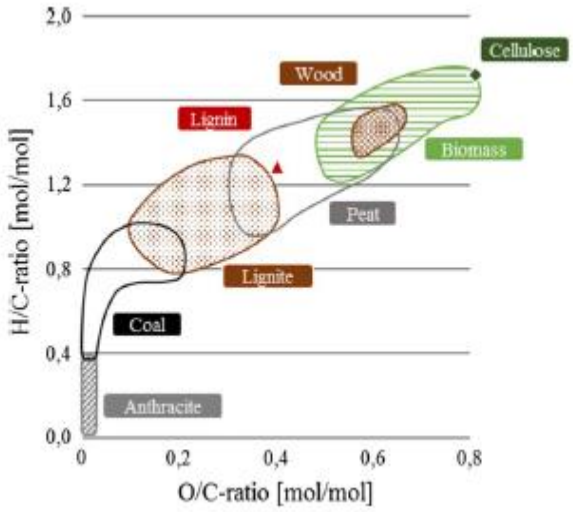

Figure 6- Van Krevelen diagram for natural carbonization processes adapted from [37]

Regarding elemental composition, which is done by elemental or ultimate analysis, biochar may reach carbon contents of more than 95% and oxygen contents of less than 5% with the increasing in temperature. And consequently, once the carbon content in biochar increases with temperature the energy content increases as well.

Fixed Carbon (FC) and Volatile matter (VM)

Fixed carbon content is the material that remains in the solid structure after the volatile components are expelled. Some applications, like metallurgical, require very high fixed carbon contents which only can be obtained with high temperatures (FC higher than 90% demands temperatures of 700 ºC). Thus, once more the increase in temperature leads to a higher fixed carbon content resulted from the devolatilization process.

Functionality

The functional groups on the surfaces of biochar are very important, as they will determine many of its applications. The thermal decomposition of biomass leads to the detachment of functional groups and hence the release of hydrogen and oxygen. With the research done in [38], [39], biochars with low H/C ratios (corresponding to high temperatures of carbonization) have overall less functional groups and more aromatic groups than biochars produced by low temperatures. Aromatic structures have a high influence in thermodynamic stability and are important for application such as metallurgical purposes or soil amendment. These structures depend either of operative temperature as of feedstock. According to [29] the presence of at least two different aromatic structures in biochars is defended, randomly organized aromatic rings that form an amorphous phase and condensed polyaromatic sheets comprising a crystalline phase. The type and quantity of functional groups have influence on the alkalinity (ability to neutralize acid in soils) and they can be for example carboxyl -COOH or hydroxyl -OH.

pH and cation exchange capacity

Raw biomass is typically acid or mildly basic with pH ranging between 5 and 7.5, because most functional groups released during pyrolysis (carboxy, hydroxyl, formyl groups) are acidic in nature.[40] Consequently, it occurs an increase in pH value with the increase of the degree of carbonization, i.e., the remaining solid becomes more basic as more the functional groups are released. According to Weber and Quicker [29], the maximum pH values are in the range of 10 to 12 for temperature above 500 ºC, emphasising that again pyrolysis operative temperature has a predominant influence (increase of pH with increase of temperature). Additionally the pH value can be raised by increasing the residence time, although it is proved in [39], [41] that the greatest effect is registered in the first 5 to 10 minutes of carbonization, due to that most acidic functional groups of biomass are released early in the carbonization process.

Ash content and composition

During pyrolysis the water is completely removed, however most of ash remains with the solid by-product. It is important to know the ash content and its composition since it can influence possible applications. The major dependency of ash content is the type of biomass and as obvious it increases with the increasing temperature. Vassilev et al.[42] reviewed a wide range of biomass

ash compositions and concluded that the main components of biomass ash are SiO_2, K_2O and CaO.

Physical Properties

In addition to the chemical transformations during carbonization, there is also a breakdown of fibrous structure of biomass, leading to changes in physical properties. The most important factors influencing the objectives and discussion of the results of this work are presented below.

Density and porosity

The design and operation of handling and processing facilities of any bulk material takes its density in account. Different concepts of density may be distinguished: bulk density, envelope density, particle density, true density (**Figure *7***). The density variations are inverse with increasing temperature, due to the fact that the devolatilization of gases creates a porous structure in the biochar, so the greater the porosity, the lighter the biochar per unit volume. The porosity of wood varies depending on its type, but according to [43] it roughly lies between 50 and 55%. Furthermore, regarding bulk density it can be considered that occurs a decrease from raw materials to biochars at different temperatures, with the greatest responsibility falling on the drying of the raw material. However, if the true density of biochar (considering only the solid), an increase occurs with increasing temperature due to shrinkage of the solid matrix of the material.[44]

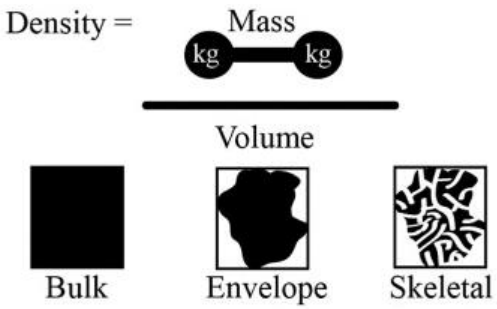

Figure 7- Different types of densities

Surface Area, Pore Volume Pore Size distribution

As porosity changes along with the escaping of volatile gases during the carbonization process also occurs to the surface area of biomass. This property is usually measured by BET (Brunauer, Emmet, and Teller) analysis (which is descried in more detail in section 3), and is connected to other biochar properties (e.g., water holding capacity and cation exchange capacity). In **Figure *8*** [45], is visible the increase of surface area with temperature and the big offset that occurs around 500 ºC, and the decrease for higher temperature (>800 ºC) might be due to the shrinking solid

matrix. However, looking at biochar as a porous structure, knowing the specific surface may not be enough for certain applications. Still, according to [29], there is a clear correlation between the micropore volume and the surface area.

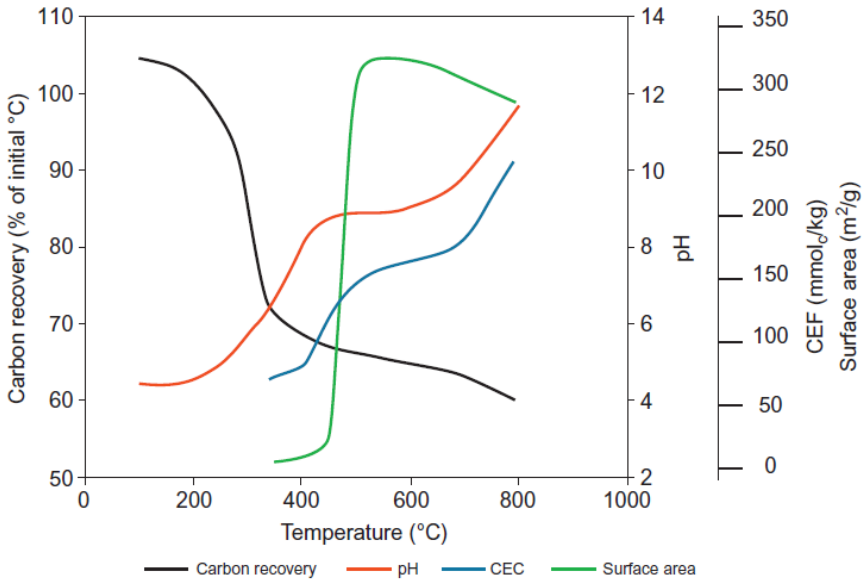

Figure 8- Qualitative diagram showing properties changes of biochar with temperature of its production.[45]

Pores in biochar extend over several orders of magnitude, so they can be classified as macro-pores (1000-0,05 µm), mesopores (0,05-0,002 µm), micropores(<0,002 µm) [46], which is the same classification by IPUAC (International Union of Pure and Applied Chemistry). It is therefore fundamental to know the volume of the pores and their size distribution, because the abundance of very small pores may not be useful for certain applications such as the adsorption of pollutants since, as they are very small, they might not be accessible. Similarly, an abundant number of micropores may have no relevance for plant-available water, because plants cannot overcome the capillary forces associated with these pores. Pycnometry or mercury porosimetry are examples of methods to characterize these properties.

Activation is the most widely used and effective method to increase biochar surface area and porosity. It can be done by physical and/or chemical activation.[47]

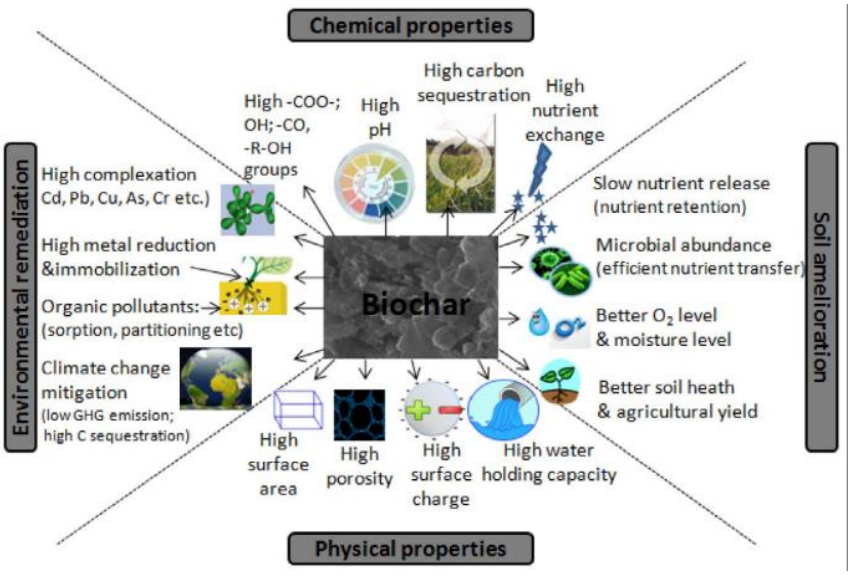

Figure 9-Biochar characteristics and suitability for specific applications [48].

2.2.2. Biochar's Applications

Depending on the characteristics of biochar there are a lot of biochar applications (**Figure *9***), can be used for composting, animal farming, building sector, textile, cosmetics, and energy production without any requirement in enhancement in chemical and physical properties. However there are few that need specific improvements in chemical and physical properties of biochar for applications such as soil conditioner, biogas production, decontamination, and treatment of water.

The major applications for biochar are solid fuels, soil amendment and activated carbon. Some studies have shown that the high heating rates favour the formation of pores in pyrolysis, and thereby following the correct operating conditions biochar may be produced with favourable BET surface area , high adsorption properties and high combustion reactivity [27],[49],[50].

In the next section, is given more emphasis to the application of biochar as soil amendment (improve soil quality and fertility), mainly in relation to increasing the amount of retained water which is the main focus of this work.

2.3. Soil Amendment – Biochar's effects on water soil

Sand-based soils (normally have a high hydraulic conductivity and a low ability to retain water and nutrients, and therefore many plants have difficulties in surviving under such conditions. In China there are large areas where plants and crops cannot thrive due to low water storage. Severe droughts due to climate change result in the degradation of these soils, i.e., desertification and sandification, consequently increasing water loss through evaporation and decreasing the water retention capacity of the soils on these lands [51]. According to the 4th round of national desertification and sandification monitoring carried out by the State Forestry Administration of China from 2005 until 2009, the desertified and sandified land areas of China were 2 623 700 km^2

and 1 731 100 km^2, respectively [52]. It is therefore necessary to act to reverse these effects and one of the measures will be to improve the physical hydraulic properties (include the soil water retention and hydraulic conductivity) of these soils, namely, to improve water retention. Soil hydraulic properties are important indicators in order to evaluate the soil physical quality and are highly related with the edaphic storage and movement of substances (e.g., water, air, and nutrients) being important indicators for evaluate the soil physical quality. Many studies have reported that the application of biochar in soils could improve these physical properties of soils. The following section discusses the effects biochar can have.

Chemical and biological properties

In general, studies show that incorporation of biochar into soils increases soil pH, cation exchange capacity and the amount of extractable nutrients such as Ca, Mg, K and Na, which are beneficial for soil fertility and nutrient retention.[53], [54]

Physical Properties

Since biochar is a porous material and is characterised by a low bulk density, it might have a positive influence at absorbing water and increasing water retention. There are two ways in which the soil water content can be affected. Under the direct way, in which the biochar as a porous structure retains water in its pores and then increases the soil water content. Or the indirect way in which the biochar added with soil will bind with other edaphic components improving the soil structure and aggregation, increasing thereby the amount of soil water [55]. So, to understand water retention in soils and for example how this can have a positive influence on the amount of water available to plants, it is necessary to understand the mechanisms of soil water retention. Firstly, the water retention curves are used, being curves that represent the water content (θ, g/g or m^3/m^3) as a function of the soil water matric or capillary potential Ψ, expressed in kPa, which is ultimately the work necessary to be done per unity of pure water in order to transport the soil water to a considered point. These curves are characteristic for different types of soils and allow to understand how much water is available in the soil depending on the potential that is being exerted. (**Figure 10-a)**)

It is, therefore, necessary to introduce the concepts of field capacity (θ_{fc}), permanent wilting point (θ_{wp}) and plant available water (θ_{paw}), which represents the water content retained in soil after excess of water has been drained away, the minimum water content required by a plant to not wilt and the water content available to the plant being given by the difference between the field capacity and the wilting point. By convention, the saturation is the water content at Ψ = 0 kPa, the field capacity at Ψ = -33 kPa and wilting point at Ψ = -1500 kPa. It should be noted, as represented in **Figure *10***, that the Ψ can be expressed as the common log of the pressure in hPa (pF scale).

By introducing biochar into the soil (especially into sandy soils which, as can be seen in **Figure *10*-a)**, have more difficulty in retaining water), the amount of porosity of the soil itself

increases(e.g. Liu et.al.[56]), in terms of interporosity (the porosity between the particles of the soil and the biochar) and intraporosity derived from the particles of the biochar.

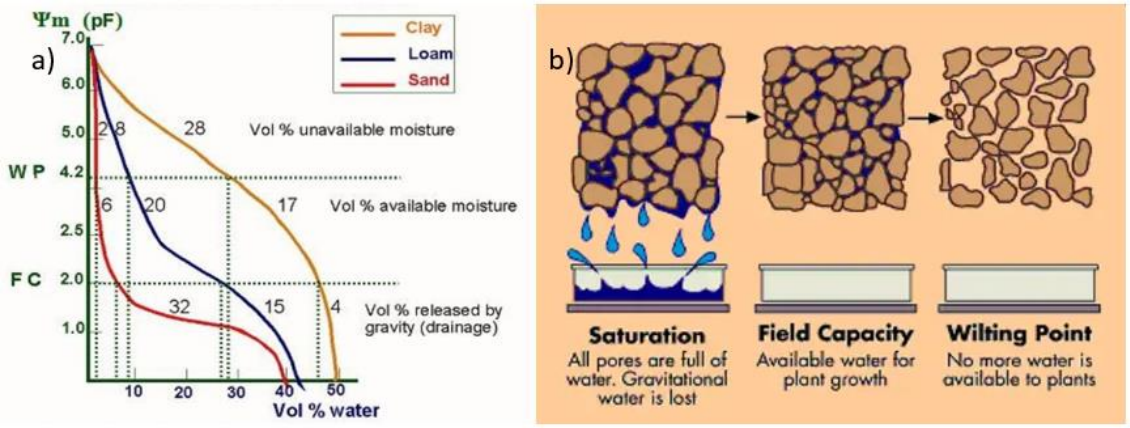

Figure 10- a) Example of water retention curves adapted from [57] and b) saturation, field capacity and wilting point.

Furthermore, biochar can have an influence on soil hydraulic conductivity (K, m/s), which is a physical property that measures the ability of the material to transmit fluid through the pore space in the presence of a hydraulic gradient, which is presented in the Darcy's Law. This law is an equation that describes the flow of a fluid through a porous medium, valid for steady state, laminar flow and incompressible fluid. Stating, for one-dimension through a section area (A, m^2), that the volumetric flow (Q, m^3/s) is proportional to hydraulic conductivity (K) and to hydraulic gradient ($\frac{\partial h}{\partial x}$, m/m), as follow:

$$Q = KA\frac{\partial h}{\partial x} \quad (1)$$

Where, considering the relation static fluid pressure $\frac{\partial p}{\partial x} = -\rho g \frac{\partial h}{\partial x}$ and the relation between hydraulic conductivity(K) and hydraulic permeability(k):

$$K = \frac{k\rho g}{\mu} \quad (2)$$

It can be written the Darcy's law in a general form:

$$Q = -\frac{kA}{\mu}\frac{\partial p}{\partial x} \quad (3)$$

where $\rho[\frac{kg}{m^3}], g\left[\frac{m}{s^2}\right], k[m^2], \mu\left[\frac{kg}{m\cdot s}\right], p[Pa]$ represents the fluid density, gravitational acceleration, hydraulic permeability, dynamic viscosity and gradient pressure, respectively.

Applied Studies

Liu et.al.[56] used a simple biochar and sand system in order to understand the mechanisms that allow how the internal pores of the biochar and the pores between the biochar and the sand particles affect water retention in soils. In their experiments, the addition of biochar (2 wt% biochar

into the sand) increased the initial water content and field capacity. Three particle sizes were used for both biochar and sand: fine <0.251 mm, medium 0.251-0.853 mm; coarse 0.853-2.00 mm. Controlling particle size and porosity, thus allows the development of conceptual models that connect biochar properties to soil water benefits. It was then proposed that the increased water content in sandy soils for low (Ψ) potential values is due to the intraporosity of the biochar while for high (Ψ) values (where capillary pressure is the main component of soil water potential) is due to increased interporosity which was found to be the case for more elongated biochar particles. Suggesting that biochars with higher intraporosity and a more irregular shape are more effective in increasing water storage.

Zhang et.al.[51] used 4 different types of biochar (Pine and Poplar 450 ºC and 550 ºC) to evaluate the hydraulic properties and water evaporation in sandy soils of a province in China. It was concluded that biochar has a strong absorption ability (being the pores structure the most important factor) compared to sandy soil. The hydraulic conductivity decreased gradually with increasing biochar addition. They also concluded that particle size has an important influence on the physical properties and that when grinded into powder its structure is destroyed (mainly the macropores) for this reason adding biochar powder to sandy soil does not decrease the water loss by evaporation from the soil itself.

Abel et.al.[58] evaluated the impact of biochar (feedstock maize) with a specific area of 217 m^2/g on different soil types, sandy and loamy sand (clay, silt and sand composition). It's concluded that the addition of biochar is more beneficial for sandy soil, as the available water capacity increased from 9% (water volume per sample volume basis) of the sandy soil to 24% with the introduction of 5 wt.% biochar. Whereas for loamy sand it was less.

Myles Gray et.al.[59] studied the effects of porosity and hydrophobicity on water uptake by biochars. He analysed biochars produced from two types of feedstocks (hazelnut shells and fir chips) at three production temperatures (370 ºC, 500 ºC and 620 ºC) and to distinguish the effects of porosity from hydrophobicity he performed tests in water and in ethanol (contact angle is zero). In both materials the higher temperature biochars absorbed more water than the lower temperature ones. However, in ethanol comparing the same feedstock the absorbed capacity was very similar. Comparing the different feedstocks, fir chip biochars absorbed more water than hazelnut shell ones due to higher porosity. They therefore concluded that for water holding applications, designing biochar requires two considerations: creating sufficient porosity through the choice of feedstock and determining the production temperature in order to reduce the level of hydrophobicity (they showed the higher the temperature, the lower the aliphatic functional groups, the lower the hydrophobicity).

Lijian Leng et.al [47] conducted an engineering review of the surface area and porosity of biochar, concluding that they play a key role in its applications as wastewater treatment and soil remediation. Furthermore, the type of biomass and pyrolysis temperature were considered as the

most influential factors, being the lignocellulosic biomasses, mainly wood and woody, the most recommended. In terms of temperature, a moderate temperature (400 to 700 ºC) is suitable for the development of the pore structure.

Razzagi et.al. [60] through a review reported that although there are many studies suggesting the use of biochar as soil amendment by improving physical properties, the heterogeneity of the experiments conducted in terms of biochar characteristics, experimental conditions and soil properties makes it difficult to make a comparison and extrapolation of results.

2.4. Conceptual Model-Equilibrium Moisture content

In general, moisture has a fundamental effect on the properties and biological behaviour of various materials. It is also important to understand the theory on which these materials absorb moisture, particularly in hygroscopic materials such as woody biomass. How these materials absorb more or less moisture can have an effect, whether in a practical application of controlling a controlled space or when it is mixed with soil in the field. Kosmas et.al. [61] , evaluated the effect of water vapour adsorption on soil moisture content in semi-arid climatic conditions, indicating that at night-time periods water adsorption is very important for areas of high moisture oscillation. Therefore, as biomass and biochars obtained from it are suitable materials to adsorb moisture, it is relevant to study how they do it, since when mixed with soil they can increase its soil moisture content.

To understand how a certain biomass or biochar adsorbs moisture, the so-called moisture sportion isotherms (**Figure *11***) are determined. These represent the relationship between the water content and the water activity (a_w), which is the partial vapour pressure of water in a solution divided by the standard state partial vapour pressure of water. This means that in an open atmosphere it is equivalent to the relative humidity, RH. Due to the complexity of the sorption processes, the isotherms cannot be determined explicitly by calculation, and have to be determined experimentally. An increase in a_w is usually accompanied by an increase in water content, but in a non-linear way. Therefore, for each point on the curve, the equilibrium moisture content (EMC) is determined.

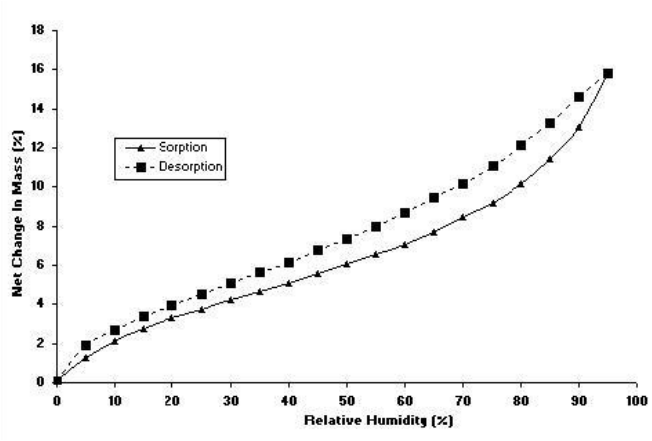

Figure 11- Moisture Sportion Curve

The sorption process is complex because it depends on physical and chemical adsorptions. However, at low relative pressures, adsorption by sites occurs which depends on the functional groups (it is generally known that at high amounts of oxygen functional groups the adsorption properties increase), followed by micropore filling and progressive monolayer formation ($0<p/p_0<0{,}1$) (being p/p_0 the pressure divide by saturated pressure., the relative pressure). For the interval of $0.1<p/p_0<0.5$, multilayer formation occurs and for the remaining interval ($0.5<p/p_0<1$) the process that is called capillary condensation in the mesopores (2-50nm) occurs. The capillary condensation process is described by the Kelvin equation which is given by:

$$\ln\left(\frac{p}{p_{sat}}\right) = \frac{2\gamma V_m}{rRT}\cos(\alpha) \tag{4}$$

Where p is the actual vapour pressure, $p_{sat}[Pa]$ is the saturated vapour pressure when the surface is flat, $\gamma[\frac{N}{m}]$ is the liquid/vapor surface tension, $V_m[\frac{m^3}{mol}]$ is the molar volume of the liquid, $R[m^3 \cdot Pa \cdot K^{-1} \cdot mol^{-1}]$ is the universal gas constant, $r[m]$ is the radius of the droplet, and T[K] is temperature. By the equation 4, holding the other variables constant, as soon as r increases p decreases towards p_{sat} and the vapour grow into liquid. This relation will depend on the angle of contact with the surface if the contact angle is negative the relation of p is the opposite.

3. Materials and Methods

This chapter includes the experimental procedures used in this work concerning biochar production (two types of process), physical activation of the biochar, characterization of the biomass and biochar and three tests related to moisture adsorption and water retention.

3.1. Biomass

The biomasses used in this work are woody biomass: Pine Sawdust ("Pinus"), Eucalyptus ("Eucalyptus Globulus") (**Table *4***). The Pine Sawdust was supplied by the IDMEC Laboratory (Mechanical Engineering Institute – IST) and the Eucalyptus was obtained on an industrial scale supplied by the company Bio Green Woods®, located in the Leiria district. [**Figure *12***]. In terms of pre-treatment all biomasses were dried for 24 hours in an oven to remove moisture, and then sieved to obtain a particle size in the range 400-1000 µm. The sieving method used is USP General Test 768 Method I [62] and the sieves used follow the standard ISO 3310.

Table 4-Information related to biomass

Biomass	Type	Process Type	Provided by	Abbreviation
Pine Sawdust	Woody	Batch	IDMEC Laboratory	PS
Eucalyptus	Woody	Continuous	BioGreen Woods®	EU

In relation to the tests involving mixtures, the type of sand used is a silica-based sand. It was also sieved and washed according to the previously mentioned standards and then the pore size distribution was determined using the Malvern Series 2600 (figure in appendix A).

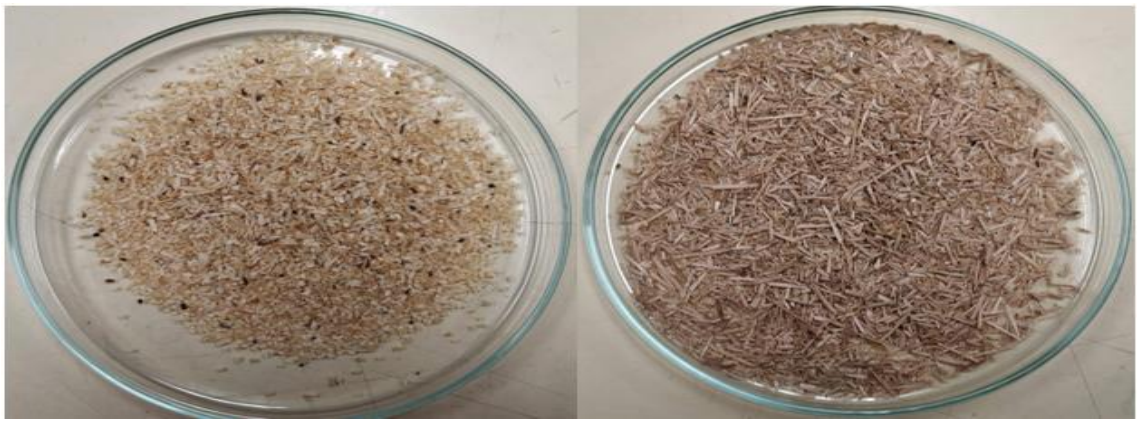

Figure 12-Pine Sawdust (left) and Eucalyptus (right)

Table *5* represents the breakdown by volume percentage used in the tests between biomass/biochar and sand (silica-based). In terms of nomenclature, PS- Raw is the designation for pine sawdust biomass, PS-C600 for pine biochar produced at 600 ºC, PS-AC for activated

pine biochar, EU-Raw for eucalyptus biomass, EU-C550 for eucalyptus biochar at 550 and EU-AC for activated eucalyptus.

Table 5- Breakdown of the percentages by volume used between biomass/biochar and sand.

Test	**Biomass/Biochar [Volume%]** PS-Raw PS-C600 PS-AC EU-Raw EU-C550 EU-AC	**Sand [Volume %]**
• **Equilibrium Moisture Content**	100%	-
• **Water Holding Capacity** • **Water Retention Curves**	-	100%
	100%	-
	50%	50%
	10%	90%

3.2. Methods

Figure *13* shows the scheme representing the work's methodology, which is divided into several parts, such as the materials used (two types of woody biomass), the processes used (batch and continuous/industrial processes), the characterisation methods (proximate analysis, Thermogravimetric analysis, Scanning Electron Microscopy analysis, Brunauer-Emmet-Teller(BET) and Mercury Porosimetry), the evaluation tests (equilibrium moisture content test, water holding capacity and water retention test) and finally the parametric models. In the equilibrium moisture content, 4 biochars and 2 biomasses (PS-Raw, PS-C600, PS-AC, EU-Raw, EU-C550, EU-AC) were considered isolated without any mixture. While for the water holding capacity and water retention curves, these 6 samples were considered alone and subsequently mixed with sand at percentages of 10%biochar-90%sand and 50%biochar-50%sand. Tests were also carried out for 100% sand to use as a control. These percentages were selected in order to have the extremes of biochar representation and assess the influence of the percentage on the results (**Table *5***).

In the following sub-sections, the different parts of the project are described in more detail.

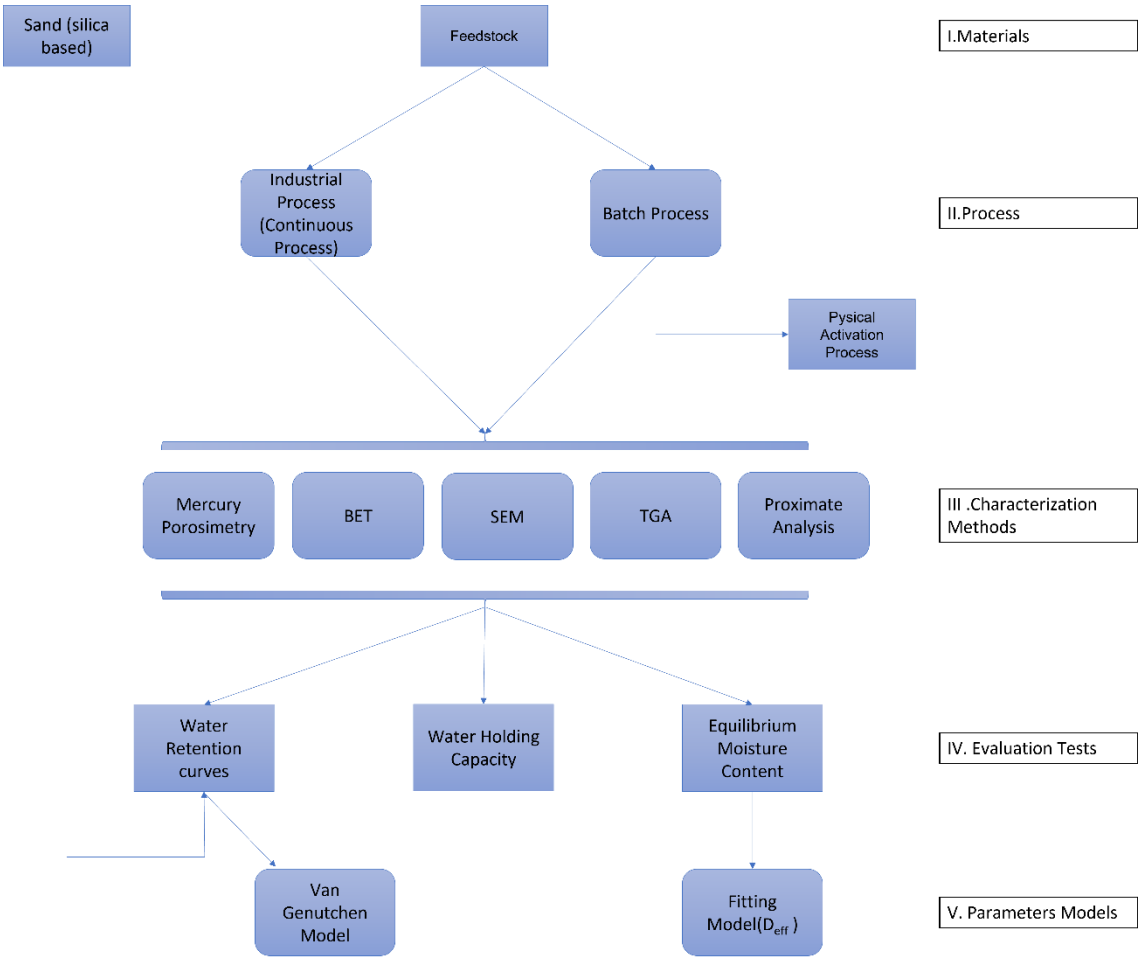

Figure 13-Methodology of the present work for biochar production, characterization, and performance evaluation.

3.2.1. Biochar Production-Experimental Setups and Process Conditions

The biochar production processes used were different, one as batch controlled in laboratory while on the other hand the second one is done continuously and controlled industrially by Bio Green Woods®.

Batch Process

Experimental setup is shown in **Figure *14***. It consists of a horizontal reactor of controlled atmosphere with constant volume and the internal tube is made of alumina with an internal diameter of 4 cm and a length of 55 cm. The inner tube is also insulated with fibreglass. Heating is done by an electrical resistance, being controlled by the Eurotherm 3216 controller (a PID temperature controller) and the wall temperature is constantly monitored by means of an s-type thermocouple. The reactor also has a water-cooling system which has the function of cooling the flanges, made of steel, located at the ends. So, at the first end we have the inlet which is responsible for the entry of the desired gas to the atmosphere inside the reactor and at the opposite end we have the exhaust gas outlet. The system also has two rotameters, since it is

possible to put a mixture of gases in the atmosphere of the reactor, thus allowing the control of its flow rate. A tube connects the gas source to the rotameter near the reactor entrance, this tube has a T-shaped splitter coming from the other rotameter if the purpose is to introduce another gas in the system. The biomass is introduced in a rectangular crucible, carrying an amount between 1 to 2 grams (depending on the density of the biomass), in each test two crucibles are placed in the centre of the reactor in a symmetrical way, since according to the reactor temperature profile the desired temperature remains constant in these positions.

In terms of procedure, the biomass is placed in the crucibles positioning them in the central position of the tube, then purged with the carrier gas N_2 for 10 min at a flow rate of 1L/min (left rotameter), to ensure an oxygen-free atmosphere and thereafter maintain the flow rate. The heating rate used is 33 ºC/min and the residence time one hour. The type of biomass used in this type of process was Pine Sawdust and the temperature range considered is between 300 ºC and 600 ºC, since the offset in surface area occurs around 500 ºC[19]. Each test was analysed at least 3 time, i.e., six samples were considered for error analysis.

To produce an activated biochar, a CO_2 flow rate was introduced with the right rotameter in order to make a physical activation. The procedure is the same as to produce biochar at 600 ºC and, based on other investigation [50], [63], [64], after one hour of residence time the temperature was increased to 800 ºC introducing a flow rate of 104 ml/min by one hour.

Subsequently the mass yield, Ym , was then determined with the following equation:

$$Ym = \frac{m_{final}}{m_{initial}} \tag{5}$$

Where m_{final} is the mass of the biochar obtained and $m_{initial}$ is the mass of raw biomass. These calculations allow obtaining the mass yield curve for pine sawdust for temperatures ranging 300 to 600 ºC. **Table *5*** summarises the test conditions and the products obtained.

Table 6-Tubular reactor test conditions and biochars nomenclatures

Feedstock	Particle Size [µm]	Temperature[ºC]	Heating Rate[ºC/min]	Residence time[min]	Activation Temperature[ºC]	Biochar nomenclature
Pine Sawdust	400-1000	300	33	60	-	PS-C300
		400				PS-C400
		500				PS-C500
		600				PS-C600
		600			800	PS-AC

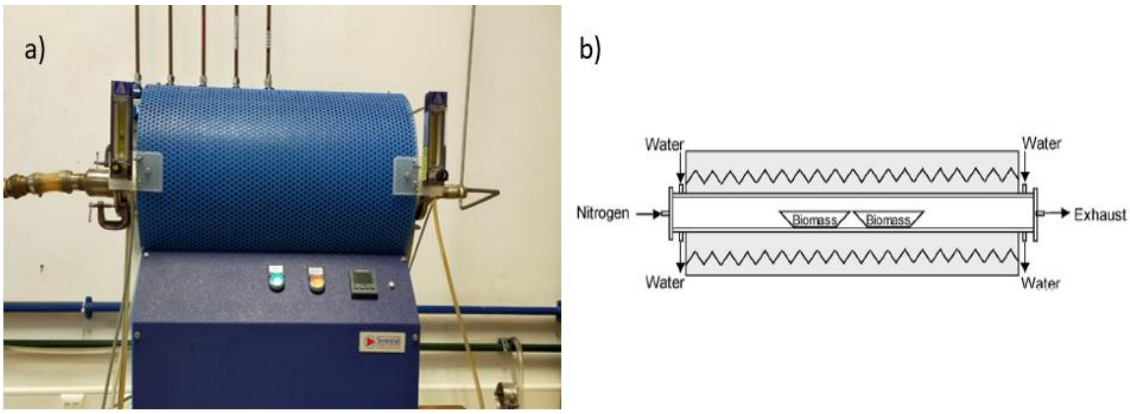

Figure 14-a) Tubular reactor furnace; b) reactor scheme from [65]

Industrial Process

The conversion process associated with Eucalyptus biomass was carried out by the company *BioGreenwoods*® using a continuous production reactor (**Figure *15***). This reactor is a screw pyrolizer, consisting of an elevator conveyor, responsible for taking the biomass to the feeding system, this one is a screw that takes the biomass to the carbonization zone with the controlled atmosphere. There, operative parameters such as temperature and residence time are settled depending on the speed imposed on the screw. At the final end of the reactor there is a combustion chamber that recirculates the exhaust gases, which pass through a heat exchanger, supplying energy to the system itself, and then exit through the exhaust gas duct. A discharge screw is responsible for removing the biochar from the system. For this work two types of materials were supplied, the first one a biochar produced at a temperature of 550 ºC and the second one an activated biochar (**Table *7***). The information in relation to the other parameters was not provided by the company.

Table 7- Industrial reactor test conditions and biochar nomenclatures

Feedstock	Temperature[ºC]	Heating Rate[ºC/min]	Residence Time[min]	Activation Temperature[ºC]	Biochar Nomenclature
Eucalyptus	550	NA	NA	-	EU-C550
	550	NA	NA	NA	EU-AC

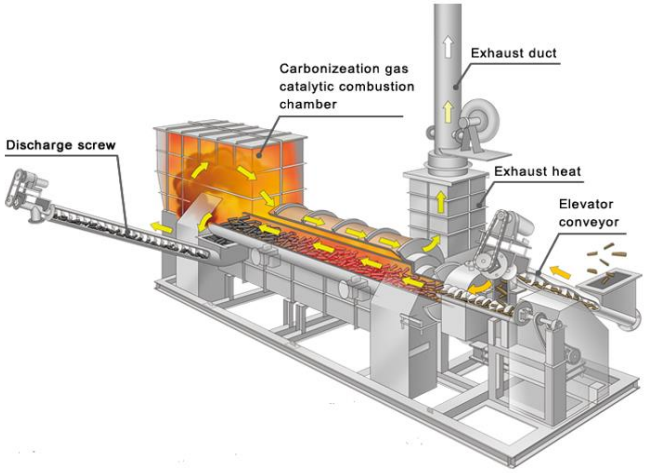

Figure 15- Continuous carbonization scheme. The feedstock is discharge through a spindle that transports it to a chamber where slow pyrolysis takes place. The process also features exhaust gas recirculation [66]

3.3. Characterization of material

Biomass and biochar are characterized by its composition, thermal decomposition, surface topography, surface area and porosity. This series of analysis methods is presented in detail below.

3.3.1. Proximate Analysis

Proximate Analysis gives the composition in terms of gross components such as Moisture (M), volatile matter (VM), ash (ASH) and fixed carbon (FC) [13]. These elements are presented in percentage.

Volatile matter of a fuel is the condensable and non-condensable vapours when the fuel is heated, the amount depends on the rate of heating and the temperature to which it is heated. Its determination was made using the Nabertherm P330 muffle furnace following the standard EN 15148:2009 (“Solid Biofuels – Determination of the content of volatile matter”). Besides other details, it consists in keeping the material for 7 min at 900 ºC. (Equation 6)

Ash is the inorganic solid residue left after the fuel is completely burned. The standard EN ISO 18122 (“Solid Biofuels- Determination of ash content”) was followed and after performing all the preparation steps in the desiccator the test consists of heating to 250 ºC for one and a half hours, followed by heating to 500ºC for two hours. (Equation 7)

Moisture (which can remain in two forms, external and inherent moisture) is a major characteristic of biomass and is determined according standard EN ISO 18134-3 (“Solid Biofuels – Determination of moisture content “). The process consists of drying at 105 degrees for two to three hours for 1g of sample and repeated weighing until the mass variation is less than 1 mg. (Equation 8)

Fixed carbon represents the solid carbon that remains in the char of biomass after devolatilization and is computed by difference as presented in equation 9.

The composition of biomass can be expressed on different bases, depending on the situation. The most common are as received basis, air-dry, total dry, dry and ash-free. (**Figure *16***)

$$VM\% = \frac{(m_{cruc} + m_{ds}) - (m_{cruc} + m_{dev\,s})}{(m_{cruc} + m_s) - m_{cruc}} \times 100 \quad (6)$$

$$ASH\% = \frac{(m_{cruc} + m_{ash}) - m_{cruc}}{(m_{cruc} + m_s) - m_{cruc}} \times 100 \quad (7)$$

$$M\% = \frac{(m_{cruc} + m_s) - (m_{cruc} + m_{ds})}{(m_{cruc} + m_s) - m_{cruc}} \times 100 \quad (8)$$

$$FC\% = 100 - M\% - VM\% - ASH\% \quad (9)$$

$$HVV\left[\frac{MJ}{kg}\right] = 0.3536FC\% + 0.1559VM\% - 0.0078ASH\%\ [dry - basis] \quad (10)$$

Where m_{cruc} , $m_s, m_{ds}, m_{dev\,s}, m_{ash}$ represents the crucible, sample, dry sample, devolatilized sample and ash mass, respectively. The results are presented in as received basis and then with M% converted to dry basis results.

Furthermore, in order to assess the possibility of using the material as a fuel, a correlation, proposed by Parikh et.al [67] was also used to determine the gross calorific value on the basis of the approximate analysis.(Equation (10))

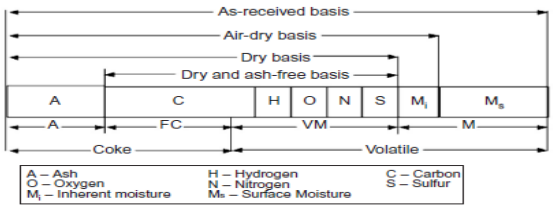

Figure 16-Basis of expressing biomass composition [13].

3.3.2. Thermogravimetric Analysis (TGA)

The thermogravimetric analysis was performed in Perkin Elmer STA 6000 Simultaneous Thermal Analyzer (**Figure 17 a**)). The precision of the weighing was ±0.01% and the sensitivity of the mass measurements was 0.1 mg. TGA tests were performed in a range of 8-10 mg of biomass using temperatures from 25 to 800 ºC (uncertainty of ±1 ºC), the program used has a 5 min step of constant temperature and helium (H_e) constant flux in order to stabilize and replace air with H_e. After the first 5 min, the heating starts with a heating rate of 10 ºC/min in H_e flux. Each sample was analysed at least three times, and the average values were considered. The thermogravimetric (TG) curves show the sample weight loss as a function of temperature and the

derivative (DTG) curves show the rate of weight loss with temperature.[65] To analyse the data was used a moving average with a 60 period.

3.3.3. Scanning Electron Microscopy (SEM)/ EDS analysis

Morphology and chemical composition of biomass and biochars were analysed using a scanning electron microscope (SEM), the instrument used was JEOL model JSM-7001F (**Figure *17* b)**). It is also equipped with an energy dispersive X-ray spectroscopy (EDS) detector allowing to measure the ultimate composition of a sample with a resolution of around 10 µm (results can be found in appendix B). The samples, to improve conductivity, need to be covered by a thin metallic film. This analysis are used to evaluate the morphologic of the biochar particles after different treatments as well as the raw biomasses. Furthermore, SEM images are suitable to obtain details about the biochar pore structure.[19] These techniques are excellent to detect biochar macropores, and they are used frequently in biochar characterization researches. However, microscopy computerized tomography have some issues regarding the selection of representative samples and viewing orientations, definition of edges between solid and pore, and development of images analysis protocols to quantify porosity.[46] For error analysis each sample was analysed three times.

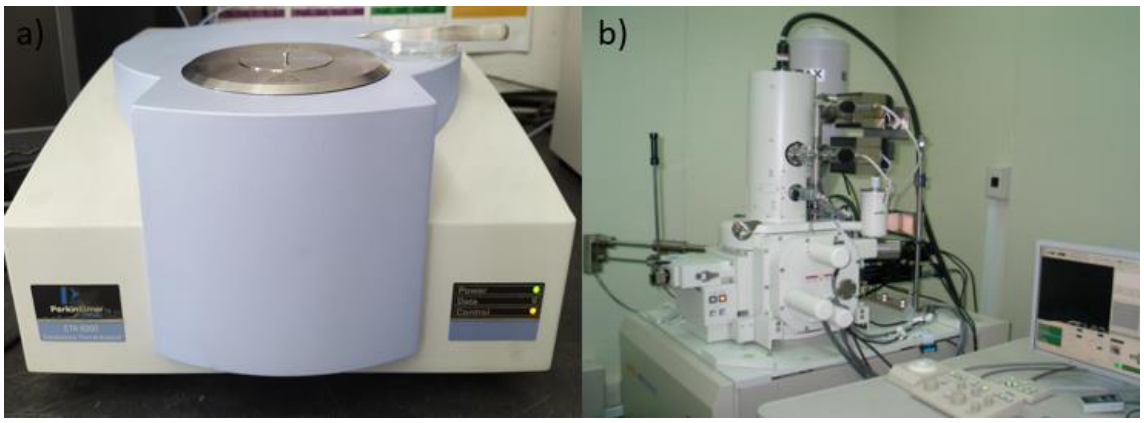

Figure 17- a) Perkin Elmer STA 6000 (Évora University – Chemistry Laboratory); b) JEOL model JSM-7001F

3.3.4. Brunauer-Emmett-Teller (BET)

BET test is a theory developed to describe the physical adsorption of gas molecules on a solid surface, serving as the basis for an analysis technique to measure the specific area of a material. It was developed by Bunauer, Emmett and Teller hence its name. In this work to determine the surface area of the samples and their isotherms the following equipments were used: Quantachrome model Autosorb iQ (K_r at 77K) and Quadrasorb (N_2 at 77K) equipped with vacuum systems with termolecular pumps (**Figure *19* a)**). In terms of experimental conditions, degasification was previously carried out in vacuum, with a thermo molecular pump, for 3 days at ambient temperature followed by 4h at 60 ºC (biomass) and 8h at 200 ºC (biochar), with a heating ramp of 2ºC/min until the final temperature. The specific areas were determined from the

adsorption of N_2 at 77k, except for the raw biomass that was determined through Kr at 77K (it presents a low area not being possible to obtain a result with N_2), following the recommendations of IUPAC.[68] These analyses were obtained with the collaboration of the university of Évora in the chemistry laboratory.

Total pore volume (V_T) is determined from nitrogen held as liquid as P/Po=0.95, and the average pore radius from $r_p=2\ V_T/S_{BET}$, is evaluated. However, since BET analysis is an gas adsorption test it has some limitations, one of which is the range of pores it can measure which is relatively small and relative to small pore sizes, generally below 4 nm[69], therefore to classify and investigate the material as a porous structure it is necessary to use other methods such as mercury porosimetry and water retention curves (pF curves) which are described in section 3.3.5 and 3.6, respectively.(**Figure *18***)

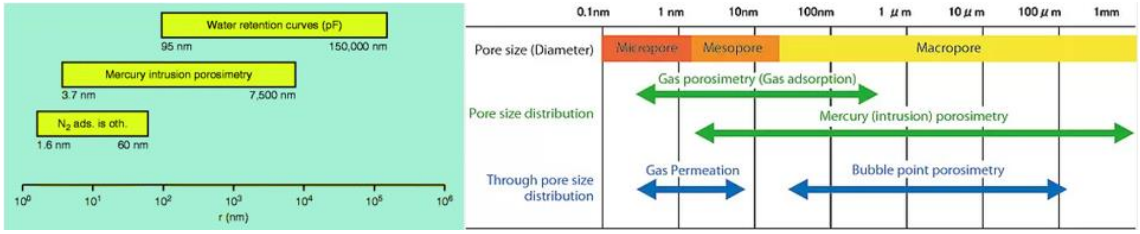

Figure 18-Limits of Pores size range and analysis methods [69].

3.3.5. Mercury Porosimetry

Mercury porosimeter is a device which is able to generate suitably high pressure and measuring simultaneous both pressure and volume of mercury taken up by a porous material. This method was used to obtain various aspects of this porous structure such as pore diameter, pore size distribution, total pore volume, surface area and absolute and bulk density. AutoPore® IV 9500 Series was the instrument used [**Figure *19* b)**]. Mercury does not wet most materials and will only penetrate pores when forced to do under high pressures. Thus, an apparatus is used to evacuate the atmosphere around the sample (with vacuum) and surround it with mercury. The sample is contained inside a penetrometer, which is a long capillary tube, the end of which is bulb shaped. With the vacuum controller, the gases and vapours are removed from the sample, then the valve of the vacuum is closed, and the penetrometer is tilted so that the end is immersed in mercury. The control valve is slowly opened allowing air to enter the mercury chamber, the mercury is forced up the capillary stem and into the bulb. Finally, the filled penetrometer is removed and inserted into a porosimeter for pore analysis.[70] The entry of mercury into pores requires applying pressure in inverse proportion of pore size. So, bigger pores (fill first) smaller pressures and smaller pores bigger pressures. This equipment has a range of low pressure between 0 to 345 kPa, which translates to pore size range of 360 to 3.6 µm and a range of high pressure between atmospheric pressure to 228 Mpa, corresponding to 6 to 0.003 µm. Equation 7, also known as Washburn equation, is the basis of mercury porosimeter method to determine pore size distribution:

$$D = \frac{-4\gamma cos\theta}{P} \quad (11)$$

Where D,γ,θ,P correspond to pore diameter [mm], surface tension [dyne/mm], contact angle [º] and applied pressure [dyne/mm^2] respectively.

In these tests, the samples were analysed after drying at 105 ºC for 16h, and the results are presented for the whole reading range (maximum pressure 228 Mpa), considering as contact angle 140º (125º for extrusion) and a surface tension of 480 dyne/cm.

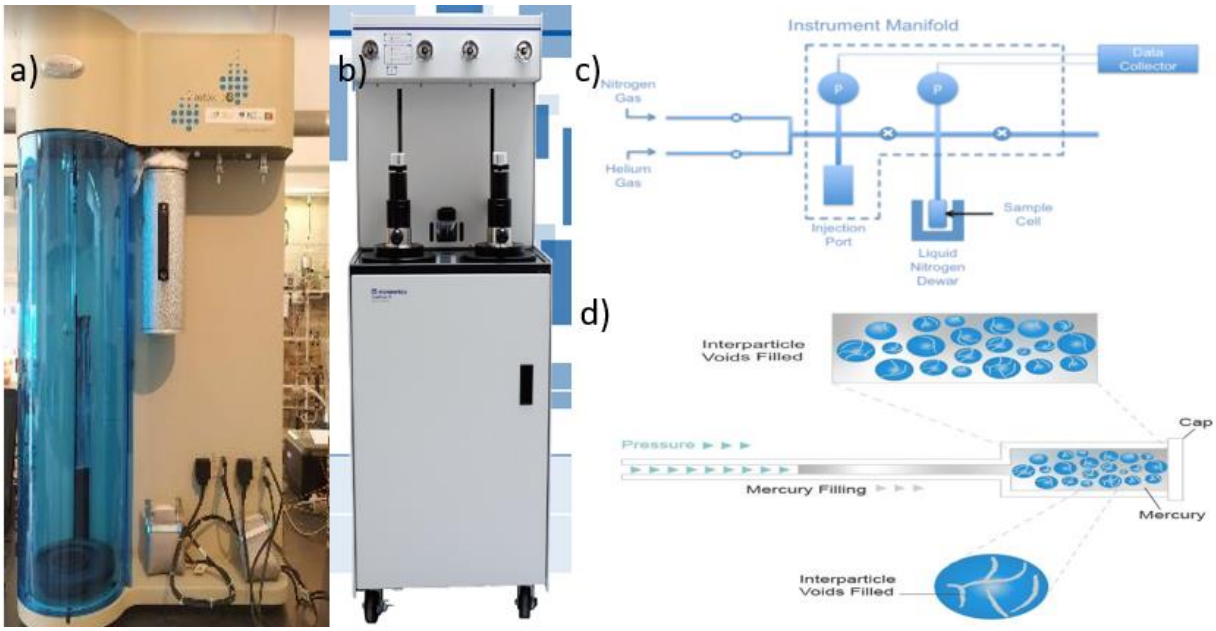

Figure 19-a) Quantachrome model Autosorb iQ (Évora University – Chemistry Laboratory); b) AutoPore® IV 9500 Series; c) Scheme of BET test; d) Scheme of Mercury Porosimetry test.

3.3.6. FTIR

Fourier transform infrared spectroscopy [71] was perfomed using *perkinelmer spectrum two FT-IR spectrometer* which thus allows obtaining a curve of transmittance/absorbance as a function of wavenumber and consequently through the peaks of this curve it is possible to identify the functional groups present on the surface of the material (in this case, biomass and biochar). Therefore, enabling the complement of the study in relation to the structure of the material (characterization from the chemical point of view).

3.4. Equilibrium Moisture Content Curves

As biomass and biochar are hygroscopic materials, to assess their adsorption capacity, a moisture adsorption test was carried out. The aim was also to understand the effect of the different conditions of biochar production on moisture adsorption. Ideally, the intention would be to use a Dynamic moisture sorption technique, which is a gravimetric technique, that measures how fast

and how much of the solvent (moisture) is adsorbed by the sample. It is done by varying the moisture concentration around the sample and measuring the change in mass. Thus, obtaining the moisture sorption isotherms, which are curves representing equilibrium moisture content [g/g] vs relative humidity (often represented as water activity) as represented in [72]. However, to do this it would be necessary to have a chamber with a controlled atmosphere and to change the conditions inside the chamber in order to obtain the isotherm.

Therefore, in order to obtain a point on that curve (corresponding to a value of relative humidity) and to evaluate the transient behaviour in moisture adsorption of the different samples, the following method was elaborated [**Figure *20***]: After drying the samples for 24 hours at 105 ºC in an oven, a constant volume, 4 cm^3, of sample was measured in a 10 cm^3 volumetric cylinder with a precision of 0.1 cm^3. Then the sample is spread evenly on a petri dish surface (also dried and placed in a desiccator) with a diameter of 70 mm and a height of 15 mm and is placed back in the oven for 1h. After this time, it is weighed and placed again for 1h in the oven until the difference between weighing is less than 0.1 mg. Ensuring that the sample is completely dry, it is placed in a closed room with a hygrometer and the variation in mass is determined using a KERN ABT 120-5DM precision balance (accuracy of 0.01 mg), first at 15 min intervals, then at 30 min intervals and finally at 1h intervals until a difference of less than 0.1 mg is recorded, thus reaching the equilibrium. The temperature and relative humidity values are monitored throughout the test using the hygrometer and the test is only valid if they remain constant at all times. Detailed figures of the process are in appendix A.

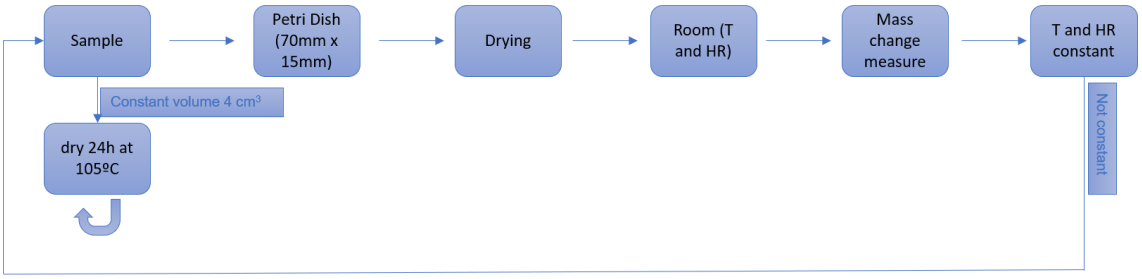

Figure 20-Scheme for equilibrium moisture content test

3.4.1 Water mass transfer applied to a film (1D model)

In order to estimate the water diffusion coefficient through the studied biomasses and biochar, a mass balance was applied to the control volume specified in **Figure *21*** [73]. Then the mass conservation on film is given by the equation 12:

$$\frac{\partial(\rho_s X_w)}{\partial t} + \vec{\nabla} \cdot \left(\overrightarrow{V_w}\rho_s\right) = 0 \qquad (12)$$

Where $\rho_s[\frac{kg}{m^3}]$, $X_w[\frac{kg}{kg}]$, $\overrightarrow{V_w}$ $[\frac{m}{s}]$, $\vec{\nabla}$, $t[s]$ are the density of the material, moisture content of the material, is the velocity vector of moisture, nabla operator (stands for divergence) and time, respectively. The first part term of the equation represents the temporal variation, while the second represents the spatial variation.

Considering the mass flux unidirectional, the equation 13 can be written as:

$$\frac{\partial(\rho_s X_w)}{\partial t} = D_{ef}\frac{\partial^2(\rho_s X_w)}{\partial z^2} \tag{13}$$

Where $D_{ef}\left[\frac{m^2}{s}\right], z[m]$ represent the effective moisture diffusivity and the film depth, respectively.

The assumptions for applying the transient method are shown in **Figure *21*** and are listed as follows: (i) the external (convective) resistances to mass transfer were neglected because its assumed that the air is constantly mixed; (ii) the water diffusion coefficient in the film (D_{ef}) is constant at for the RH investigated; (iii) diffusion was considered unidirectional because of the thickness (δ) was much smaller than the other dimensions; (iv) at the beginning of the experiments, the moisture content was homogeneous throughout the film and (v) the film did not swell.

Thus, considering these assumptions the dimensionless average concentration ($\bar{\theta}$), is obtained through equation 15 using the separation of variables and applying the Fourier Series [74]:

$$\bar{\bar{\theta}} = \frac{W_a - W_{eq(RH2)}}{W_{eq(RH1)} - W_{eq(RH2)}} \tag{14}$$

Where W_a, $W_{eq(RH2)}$, $W_{eq(RH1)}$ are the average film moisture content after an elapsed time t, initial film moisture content (t=0) and the moisture content when the sample reaches the equilibrium with RH_2.

$$\bar{\bar{\theta}} = \frac{8}{\pi^2}\sum_{n=0}^{\infty}\frac{1}{(2n+1)^2}\exp\left[-\left(\frac{(2n+1)}{2z}\pi\right)^2 \cdot D_{ef} \cdot t\right] \tag{15}$$

Where n is the number of the series used. For the estimation of the effective diffusivity several series indexes were considered, namely n=1, n=3 and n=10 and it was concluded that the value obtained for n=3 and n=10 was equal. Therefore, the values for n =3 were considered. It was

also considered that the initial moisture content of the film is zero as they go through the drying process.

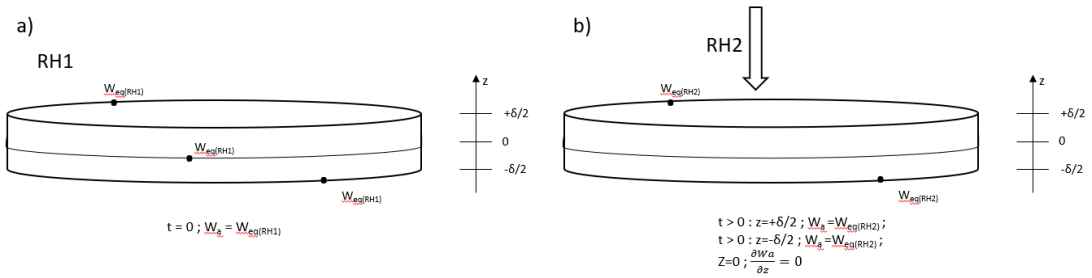

Figure 21- Control volume representation of the initial and boundary conditions for the transient method used to determine the effective diffusivity. a) represents the initial conditions; b) represents the conditions during the transient phase.[73]

3.5. Water Holding Capacity

For measurement of water holding capacity (WHC) of the studied samples with different physical structure, a constant volume of sample ,12 cm^3, was placed in an acrylic tube with a diameter of 32 mm, a height of 50 mm and with one end covered with a wire mesh reduced in size so as not to allow particle of less than 400 microns to pass through, allowing total water permeability [figure in appendix A]. Then the tube with the sample is imbibed in a glass beaker with deionized water for 24 hours. The direction of the water is upwards (imbibition) and slow enough not to cause changes in the structure of the materials. The sample with the tube is then fixed in a bigger container in order to let excessive water drain for about 15 min (i.e., until there is no more dripping from the sample). Wet sample is then weighted and consequently dried in an oven at 105 ºC until no more weight loss is registered. Similar methods has been reported in the literature [55], [75]. Water holding capacity is computed by using equation 16:

$$WHC(g/g) = \frac{M_2 - M_3}{M_3 - M_1} \tag{16}$$

Where $M_1[g], M_2[g], M_3[g]$ are tube weight, total weight of wet sample and acrylic tube, total weight of dry sample and acrylic tube, respectively. The volume ratio is obtained by multiplying the density of the water and the dry sample. All the measurements were repeated at least three types to ensure reproducibility of results and were done at the same time to ensure the same conditions.

3.6. Water Retention Curves (pF curves)

3.6.1. The experimental approach

As presented in sub-section 2.3.1 the water retention curves were obtained for different points of matric or capillary potential: saturation point (ψ = 0 kPa), field capacity points (ψ = 10 kPa and ψ

= 33 kPa) and wilting point (ψ = 1500 kPa). It is common to present these values in logarithmic form through the following equation:

$$pF = \log\ (\psi) \tag{17}$$

With ψ , the pressure applied in hPa. Then on pF scale the points that are calculated are the saturation, pF 2.0, 2.5 and 4.2.

Different apparatus were used to measure the different pressure points. For the saturation point and for 10 kPa (pF 2) a sand suction table (**Figure 22-a**)) was used. For the points of 33 kPa and 1500 kPa a ceramic pressure vessel with a ceramic plate and regulated air system used to control the pressure inside the vessel (**Figure 22-b, c**)). The procedure then consisted of:

1) prepare the sample and place it in a ring with a fixed volume and covered at one end with gauze (allowing the water to pass through but not the sample).
2) Place the sample on the suction table and then allow water to enter the suction table to saturate the samples through imbibition (for 24 hours to make sure they are saturated). At the end of the process a weighing is done.
3) After saturation, the water inlet valve of the table is closed, and the outlet valve is opened and through the suction level regulator it is placed at a height of 100cm below the water level corresponding to pF 2. It is waited for the necessary time until no more water leaks from the sand box meaning that the samples have already reached equilibrium. A weighing is carried out again.
4) Then the sample is placed in the pressure vessel on top of a saturated ceramic plate and is closed tightly and through the air regulating system, a pressure of 33 kPa (pF 2.5) is set and again it is waited until no more water leaks out of the vessel (water coming out from under the ceramic plate). When equilibrium is reached, a reweighing is carried out.
5) Subsequently the same is done as in point 4 but increasing the pressure to 1500 kPa (pF4.2).
6) Finally, the sample is dried in an oven at 105 ºC, and consecutive weightings are made to ensure that the variation in mass is less than 0.01g.

The water content (θ) is then calculated as follows:

$$\theta_i \left[\frac{cm^3}{cm^3}\right] = \frac{(m_{wi} - m_{dry})/\rho_w}{V_{ring}} \tag{18}$$

Where,$m_{wi}[g], m_{dry,}[g], \rho_w[g/cm^3], V_{ring}[cm^3]$ represents the mass of wet sample at each applied pressure, the mass of oven dry sample, the density of deionized water (1 g/cm^3) and the volume of the sample ring[56]. It is used deionized water to exclude osmotic potential effects. Regarding the rings used, it was first made a trial with several samples with the industrial eucalyptus biochar (since the availability is high) with the conventional steel rings (**Figure *22*-d**)) used (5 cm diameter and 3 cm height, corresponding to 58.9 cm^3 of volume). Subsequently, in order to obtain these curves also with the biochar produced in the laboratory (smaller quantity), a

test was made with the same samples in pvc rings (**Figure 22-e**)) of dimensions 2.54 cm diameter and 2 cm height and the sample was placed so as to have a constant volume of 8 cm^3. Comparing the results, reproducibility was obtained and then the tests were performed on the pvc rings.

Figure 22-a) Sand suction table; b) Pressure Vessel and air regulator system; c) Ceramic Plates; d) Steel Ring; e) PVC ring

3.6.2. Van Genutchen Model

To estimate the water retention curves, is used an empirical model called Van Genutchen Model [76] commonly used in studies related to soil water retention curves as carried out by Liu et.al. [56] and by Abel et.al.[58]. It is a one-dimensional model that relates soil water content with soil water potentials and is given by:

$$\theta(\psi) = \theta_r + (\theta_s - \theta_r) \cdot \left[\frac{1}{(1 + (\alpha|\psi|)^n}\right]^{1-\frac{1}{n}} \quad (19)$$

Where $\theta(\psi)[\frac{cm^3}{cm^3}]$ is the volumetric water content at given matric potential ψ , $\theta_s \left[\frac{cm^3}{cm^3}\right]$ is the saturated water content when $\psi = 0$, θ_r is the residual water content $[\frac{cm^3}{cm^3}]$ and α and n are shape parameters, representing the inverse of the entry pressure and the pore size distribution, respectively.

3.7. Statistical Analysis

All the measurements were repeated at least three types to ensure reproducibility of results and were done at the same time to ensure the same conditions. Standard deviation was also

calculated and represented in the graphs with error bars. Pearson correlation was used to correlate variables and is described by the following equation:

$$\rho = \frac{\sum_{i=1}^{n}(x_i - \bar{x})(y_i - \bar{y})}{\sqrt{\sum_{i=1}^{n}(x_i - \bar{x})} \cdot \sqrt{\sum_{i=1}^{n}(y_i - \bar{y})}} \quad (20)$$

Where $x_i, y_i, \bar{x}, \bar{y}$ are the variables measured and their respective means.

And to do the equation fitting with the experimental data it was used the non-linear least squares method, which is a form of analysis to fit a set of *m of* observations with a non-linear model on *n* unknown parameters. The error is given by:

$$SSL = \sum_{i=1}^{m} r_i^2 \quad (21)$$

Where r represent the fitting bias:

$$r_i = y_i - f(x_i, \beta) \quad (22)$$

Where y_i are the experimental points and $f(x_i, \beta)$ are the model function dependent on the variables x and β.

4.Results and discussion

In this section the results are presented and the comparison and discussion around them is also carried out. Firstly, the analyses regarding the raw material used are presented, secondly the results from the laboratory carbonization method are presented, thirdly the characteristics of the materials obtained are presented and discussed, regarding their composition, porous structure, surface area, hydrophobicity, their thermogravimetric decomposition, and the surface topography. Subsequently, the capacity to adsorb moisture in the transient phase, the water holding capacity and finally the water retention curves with the biomass/biochar elements and also mixed with sand are evaluated.

4.1. Biochar Production

The curve representing the mass yield of the laboratory process for biomass carbonization at an electrically heated horizontal tube furnace for the conditions presented in section 3.2.1 is shown in **Figure *23***. As expected, a reduction in the mass yield is observed with the temperature increase, due to the release of condensable, tars and non-condensable gases due to the breakdown of the various constituents of the pine biomass. There was a mass yield reduction from 38.47% to 20.11%, for 200 ºC and 600 ºC, respectively. However, there is a more significant reduction between 300 ºC and 400 ºC of 12.78% than between 400 ºC and 500 ºC of only 4,94%. This is explained by the fact that pine is a lignocellulosic biomass with its composition being mostly based on cellulose, hemicellulose and lignin (with about 48,1%, 23.5% and 28.4%, respectively according to [12]) and by analysing the thermodecomposition of these constituents it is found that cellulose decomposes mostly around 380 ºC, hemicellulose around 300 ºC and lignin gradually decomposes throughout the temperature range. Hence the greater drop in mass yield between 300 and 400 ºC. In addition, it is verified that the difference between 500 ºC and 600 ºC is relatively small (0.64%), since there the greatest effects are due to the lignin and given the higher residence times, formation of char from secondary reactions may occur in the meantime, preventing the decrease in mass yield from being so significant.

To check that the devolatilization was complete for temperature of 600 ºC (which was the main temperature point of the study) and to ensure that the residence time used was sufficient to remove the volatiles from the biomass, the gases were recorded using *Gas Chromatography*. Gases such as H_2, N_2, CH_4, CO and CO_2 were identified. Several samples of gases were taken along the process, and it was verified that at the end of the residence time (1h), only N_2 was verified which was the used carrier gas, therefore the devolatilization was complete. (Figure in appendix B)

In the production of activated carbon through biochar at 600 ºC (**Table *8***), the mass yield obtained was 11.79% with a standard deviation of 1.16%. This low yield is due to the activation by CO_2 which causes the burn-out to increase since the oxygen particles in the CO_2 will activate the biochar surface [50]. Namely the main reaction that occurs can be described as follows:

$$C + CO_2 \rightarrow 2CO\ (CO_2\ activation) \quad (23)$$

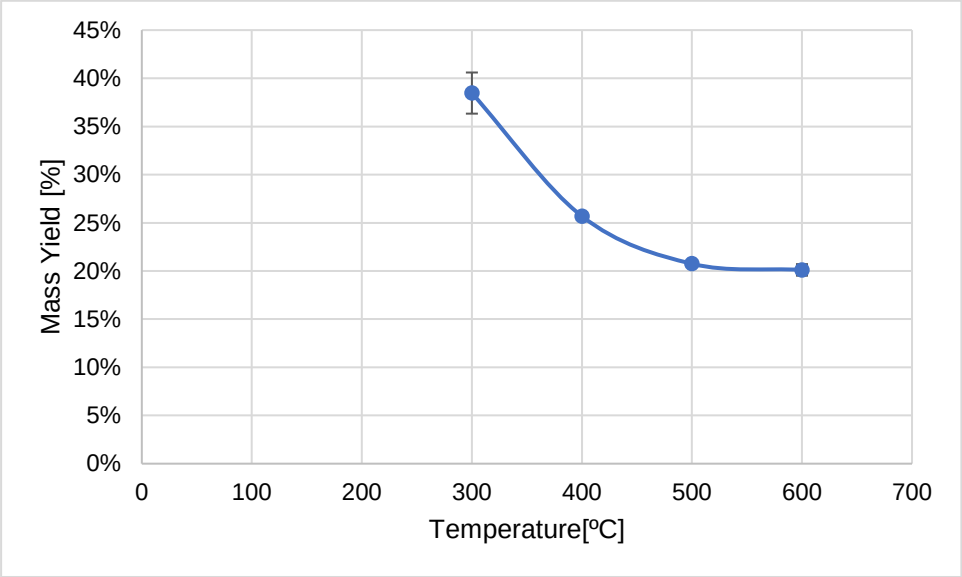

Figure 23- Mass yield curve for a temperature range from 300 ºC to 600 ºC for Pine Biomass.

Table 8- Mass yield of the physical activation process described in section 3.2.1. n=3

	Mean Mass Yield	**Standard Deviation**
PS-AC	11.79%	1.16%

4.2. Characterization of laboratory and industrial biomass and biochar

In this section, the materials evaluated are the Pine and Eucalyptus biomass (PS-Raw and EU-Raw, respectively), the pine biochar produced at 600 ºC (PS-C600), the activated Pine biochar (PS-AC), the Eucalyptus biochar supplied by BioGreenwoods® (EU-C550) and the activated Eucalyptus biochar also supplied by the company (EU-AC).

4.2.1. Proximate, thermogravimetric and hydrophobicity analysis

Proximate Analysis and Thermogravimetric Analysis (TGA)

In section 3.3.1 is provided a comprehensive description of the proximate analysis test, which gives an overview of the constituents in a general way and not in an elementary way (which would be a much more expensive test) and can draw conclusions whether the type of biomass is suitable for the intended application or not. Since the most biomasses are hygroscopic (the property that certain materials have of absorbing water) it is important to represent the approximate analysis on a dry basis [**Figure *16***] since the moisture contained in the base as received may lead to some doubt in the interpretation of the results.

Table *9* and **Table *10***, show the result for the studied biomasses in these same conditions respectively. Both PS-Raw and EU-Raw present high values of volatile matter (86.85% and 88.34%), meaning that they may have the ability to release a lot of gases during the thermochemical processes in which they are involved. Among the obtained biochars, both have a considerably high value of fixed carbon, which is the carbon content that remains in the solid structure after the volatile components are driven off, since the carbonization process has as one of the main objectives that fixation of carbon. Although the differences are not very distinct, the PS-C600 was the one which presented a lower volatile matter (15.16%) and higher ash content (1.39%), while EU-C550 carries the highest percentage of volatiles (18,89%). This proves that the processes used are different and that the conditions used in the production of EU-C550 do not maximise the volatiles release. However, comparing with EU-AC, it is possible to see an improvement in the process in order to obtain a biochar with less volatile matter and a higher carbon fixation (18.32 % and 81.23%). The PS-AC values were not present, due to the very low mass yield of the activation process, it was no possible to obtain enough mass to comply with the standards described in section 3.3.1. These results are in accordance with what is discussed in [29], since the temperatures between 250 and 350 ºC the FC values are about 50-60% and to obtain higher than 90% requires temperatures around 700 ºC, so the values obtained fall within this range.

To clarify the devolatilization process and to support the data obtained in the proximate analysis, a thermogravimetry (**Figure *24***) and the corresponding derivative curves (**Figure *25***) were performed. Considering PS-Raw, it can be seen that there is an initial mass loss of values around 5%, which is related to the moisture present in the material, as already mentioned, due to the fact that it is a very hygroscopic material. Afterwards, between 100 ºC and 250 ºC, there is practically no mass variation, since this is the temperature range for which torrefaction occurs, where the mass yield is very high, and a slight carbon fixation occurs. Between 300 and 400 ºC occurs the largest drop in mass variation, due to the release of volatiles, and compared with the decomposition of hemicellulose and cellulose we can see that the major release of these constituents occurs at 250 ºC and 350 ºC, respectively. As already mentioned, the pine composition is mostly cellulose and hemicellulose (48.1%,23.5%), so in this temperature range this mass drop is of great influence of these two constituents. Looking at **Figure *24* (right)**, the lignin gradually decomposes along the temperature (more resistant element), the same happens with the pine after 400 ºC, being therefore the most relevant factor after that temperature. Due to limitation in the number of tests available it was not possible to obtain the TGA curves for the Eucalyptus biomass. However, as the results of the approximate analysis are very similar (1.5% for volatile matter and 1% for fixed carbon), its lignocellulosic composition does not vary significantly according to [12], and through the TGA performed in another study [77], the behaviour of the curve is quite similar to that of pine, occurring the largest drop in mass loss in the range of 250-400 ºC.

Regarding biochars, analysing the TGA and DTA curves, there was no mass variation until 400 ºC, starting to have some residual mass loss from 400 to 500 ºC and afterwards for the PS-C600 and EU-C550 a more accentuated mass fall occurs until 600 ºC and consequently then the mass loss rate remains constant until 800 ºC. For the activated carbon of both biomasses the peak loss rate occurs around 700 ºC, and this loss is lower compared to biochars, since they lose more mass during their production process due to activation.

In the eucalyptus biochars, it would be expected that a release of volatiles would still occur at a lower temperature than the one at which it is carried out (550 ºC), since it is an industrial process, the heating rate and residence time used are not sufficient to guarantee that the reaction associated with the slow pyrolysis take place. Regarding the biochar produced in the laboratory (pine), it would be expected that there would be only mass variation from 600 ºC and for activated from 800 ºC, since the gas analysis with GC allowed to conclude that in the tests performed no release of volatiles was occurring. However, as already mentioned, the reactions involving the pyrolysis process are quite complex and not yet fully understood (they are the subject of much research) so considering the heating rate, in TGA the heating rate was 10 ºC/min, much lower than that used in the tubular reactor of 33 ºC/min, thus allowing the release of gases from 400 ºC due to this slower rate.

Table 9- Proximate analysis for eucalyptus and pine biomasses and the respective biochars on an as-received basis.

	As Received Basis			
Sample Type	Moisture (%)	Volatile Matter (%)	Ash (%)	Fixed Carbon (%)
PS-Raw	10.46	77.76	0.44	11.34
EU-Raw	9.68	79.79	0.12	10.41
PS-C600	7.53	14.01	1.28	77.17
EU-C550	5.65	18.89	0.79	74.67
EU-AC	6.61	17.11	0.42	75.86

Table 10- Proximate analysis for eucalyptus and pine biomasses and the respective biochars on a dry basis

	Dry Basis				
Sample Type	Moisture (%)	Volatile Matter (%)	Ash (%)	Fixed Carbon (%)	Calorific Value [MJ/kg]
PS-Raw	-	86.85	0.49	12.66	18.01
EU-Raw	-	88.34	0.13	11.52	17.84
PS-C600	-	15.16	1.39	83.46	31.86
EU-C550	-	20.03	0.83	79.14	31.10
EU-AC	-	18.32	0.45	81.23	31.58

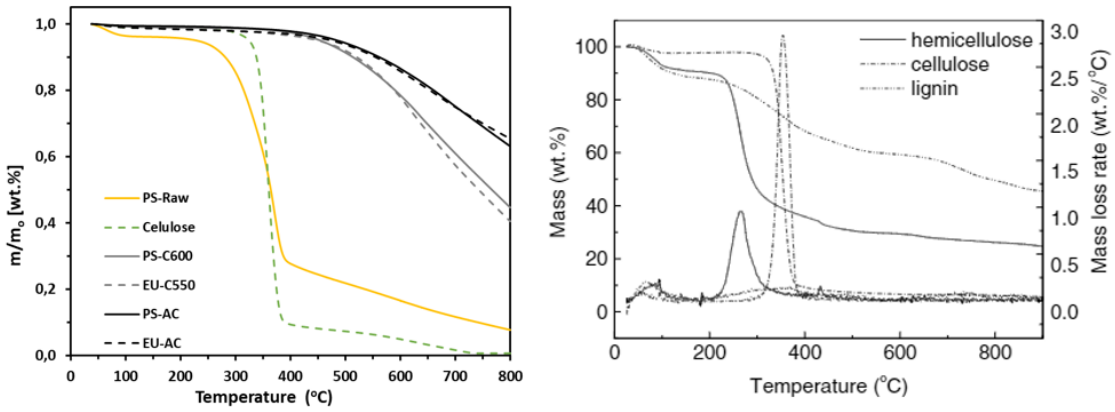

Figure 24- TGA of PS-Raw, PS-C600, PS-AC,EU-C550, EU-AC and Cellulose (Left) and TGA curves of hemicellulose, cellulose and lignin adapted from [78] (Right).

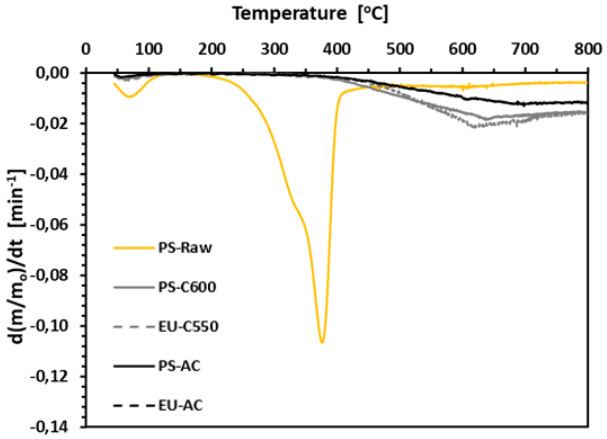

Figure 25- Differential thermal analysis for PS-Raw, PS-C600, EU-C550, PS-AC and EU-AC.

Surface Functionality

As mentioned in the introduction and state-of-the-art chapters (chapters 1 and 2), biomasses are known to have surface functional groups, which can lead the materials to be more or less hydrophobic. However, during the production of biochars (through thermochemical processes, namely slow pyrolysis in this study), a change in the chemical composition on the surface can occur. **Figure *26*** depicts the transmittance curves for the various wavelengths for pine biomass and its biochars. For PS Raw there is a broad transmittance band between 3650 and 3250 cm^{-1}, indicating hydrogen bond. This band confirms the existence of hydrate (H_2O), hydroxyl (-OH), ammonium, or amino. A narrow band at below 3000 cm^{-1} (2935 and 2860 cm^{-1}) is also visible, showing aliphatic compounds. Whereas the transmittance band observed between 1200 and 900 cm^{-1}, corresponds to alcohol and hydroxy compounds (primary alcohols C-O stretch). It can also be seen that looking at the spectrum of PS-C600 there was a large decrease in the peaks , which proves that the thermochemical process allows the deformation of these surface functional groups. In PS-AC it is possible to see a sloping down baseline for small wavelengths, this is due to the technique itself, as the effect of carbon black becomes greater with deeper light penetration

at the low wavenumber end. This results in a spectrum where the baseline descends at the right end. Therefore, it is not possible to have a clear conclusion about the functionality of the PS-AC surface, however some functional groups are expected due to the reaction with CO_2. (Table with the FTIR bands can be found in appendix B)

These results are in agreement with that presented in several studies, namely by Myles Gray et.al.[59], where it is indicated that there is a decrease in abundance and diversity of functional groups with increasing temperature in biochar production.

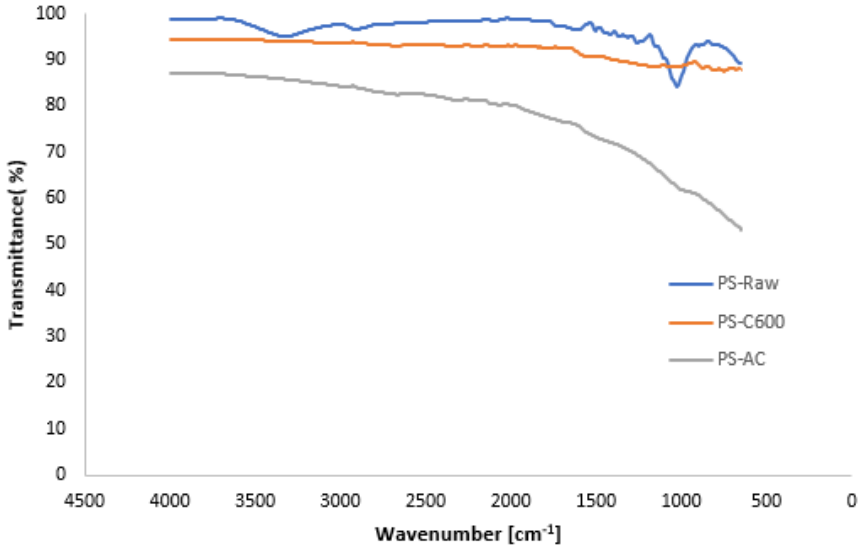

Figure 26- FTIR Analysis for materials produced in the laboratory process.

4.2.2. Porous Structure

BET and Isotherms

In physical adsorption research, the domain of the experimental information is the adsorption isotherm which is a plot of equilibrium quantities adsorbed (n_{ads} in mmol g^{-1}) against the relative pressure (p/p_0) of the adsorbate. The computerized equipment is programmed to re-assemble the adsorption data in the coordinates of Brunauer-Emmett-Teller (BET) to provide the optimal straight line through data, in order to obtain the value of surface area. These adsorption isotherms result from controlled physical adsorption of a gas in to the porous material[79]. The BET equation doesn't predict surface areas but predicts monolayer coverage (mmol g^{-1} of adsorbate). In some materials as activated carbons, adsorption might occur such that several layers of adsorbate molecules are adsorbed together. It is called volume filling and occurs in the largest of micropores. When it occurs in mesoporosity is designated as capillary condensation and must not be included in values of n_{ads} (mmol g^{-1}). So any value beyond 1000 m^2g^{-1} should be associated with capillary condensation and volume filling and should be treated with special attention.[79]

The adsorption isotherms of PS-C600, PS-AC and EU-AC are shown in **Figure *27***. According to IUPAC there are six types of isotherms (**Figure *28***). Type I adsorption isotherm is for very small pores or microporous adsorbents, adsorption occurs by filling of micropores. Type II and type IV were detected for non-porous or microporous adsorbents with unlimited monolayer-multilayer adsorption. When monolayer formation of the adsorbed molecules is complete, the multilayer formation begins to take place corresponding to the “sharp knee” of the isotherm. As the relative pressure approaches unity, a sudden increase shows bulk condensation from adsorbate gas to liquid. Type III and V correspond to weak substrates in which the interactions between adsorbates is greater than between adsorbates and adsorbents, occurring capillary condensation in the latter. In type VI occurs the layering. Then after analysis of the isotherms presented in **Figure *27*** it can be concluded that all of them correspond to type I isotherms.

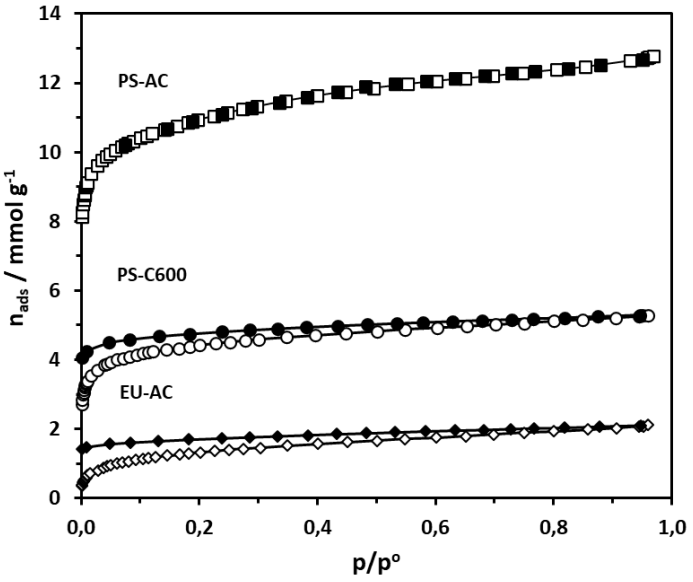

Figure 27- Isotherms obtained by BET (N_2 at 77K] for PS-AC (square), PS-C600 (circles) and EU-AC (diamond). Black means adsorption and white means desorption.

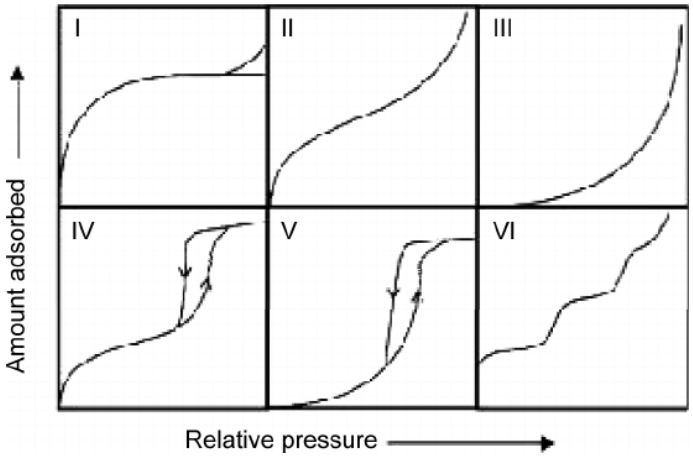

Figure 28- IUPAC classification of adsorption isotherms.[80]

Table *11* contains the values referring to the specific area of pine, eucalyptus, their respective biochars and consequently the total micropore volume (within the BET test range). The average pore radius is also presented, calculated based on the total volume and surface area. To compare the evolution of the specific area through the pyrolysis process and consequently activation, the raw biomass was also tested. However, as can be seen in **Table *11***, the value obtained was residual (0.34 m^2g^{-1}). Besides, it was obtained with krypton, gas that is only used for low specific areas and is not recommended by IUPAC. On the other hand, for the biochar at a temperature of 600 ºC, it shows a substantial increase in the specific area to 345 m^2/g, thus providing that until a temperature of 600 ºC there is an increase in the specific area of biochars, as presented by Leng et.al.[47] where several pyrolysis studies are presented in which the specific area for different biomasses increases with temperature up to 600 ºC. Showing thus that the pyrolysis temperature is considered the predominant parameter influencing the surface area of biochar. It was also found that physical activation of the pine biochar also had a considerable effect, since its specific area increased to 937 m^2g^{-1}, representing an increase of 150% approximately.

Table 11- Specific areas, micropore volume and pore radius of biomass and its biochars.

Sample	A_{BET} [m^2g^{-1}]	V_T [cm^3g^{-1}]	R_p[nm]	A_{BET} [m^2g^{-1}] from literature	Reference
PS-Raw	0.34*	-	-	-	-
EU-Raw	<5	-	-	-	-
PS-C600	375	1.84e-01	9.81e-01	392	[81]
PS-AC	937	4.43e-01	9.46e-01	809	[82]
EU-C550	20	-	-	335	[83]
EU-AC	112	7.30e-02	1.30	673	[84]

*****Determined by Kr adsorption at 77 K following IUPAC recommendation for extremely low surface areas; n=1 due to cost-bases constrains (number of repetitions).
a) due to low specific area < 5m^2/g it was not possible to obtain a value with Autosorb iQ

For Eucalyptus products the same procedure was followed, however for raw Eucalyptus it was not possible to obtain a specific result since its specific surface area is very low (it is guaranteed to be lower than 5 m^2g^{-1}). For its biochar produced at 550 ºC a value of 20 m^2g^{-1} was recorded, while for the activated correspondent a value of 120 m^2g^{-1} was recorded, corresponding to an increase of 460%, representing well the activation effect. As already mentioned, the slow pyrolysis process is complex since it depends on many variables, namely raw material, temperature, heating rate and residence time, however the value obtained for the EU-C550 is relatively low since in [47] , a trend was recorded for several types of biomasses and the specific area value increased significantly from 500 ºC, mostly to values in the hundreds. This indicates that the process may not be optimised in relation to the dependent parameters mentioned. In addition, there was a bottleneck in the pores, i.e., a constriction in the passage from larger pores to smaller pores, since it was difficult to obtain equilibrium in the nitrogen adsorption, resulting in the consequence that it was not possible to obtain its isotherm. In the activation despite there is a very significant increase, when compared with the value obtained for pine it is found to be approximately eight times lower, and although the detail of the activation process is not given, being pine and eucalyptus two wood biomasses with similar structural compositions the differences should not be so significant. Those evidences suggest that the biochar production and activation for eucalyptus feedstock could be significantly enhanced.

Thus, it is concluded that for both PS-C600 and PS-AC, the pyrogenic nanopores (voids that form within the carbon structure as a result of chemical changes during pyrolysis) comprise the majority of biochar surface area, and therefore provide the most sites for nutrient adsorption, cation exchange and soil microbial as well as filter contaminants from aqueous streams. This is in agreement with that presented by Chun et.al [85], in which chars produced at high temperatures from crop residues were tested for their ability to adsorb benzene and nitrobenzene from water exhibiting their ability for adsorption.

Table *11* also shows a column where the comparison of specific area values with values presented in the literature is made. First for the PS-C600, Keiluweit et.al.[81] obtained for pine sawdust with a particle size less than 1.5 mm, having been subjected to slow pyrolysis for one hour in an inert atmosphere at 600 ºC, obtained a value of 392 m^2g^{-1}, a value very close to the one obtained in the laboratory (the heating rate was not specified). For PS-AC, Chu et.al [82] obtained for pine sawdust an activated carbon of 809 m^2g^{-1} at 600ºC, however the activation process used was different, it was used chemical activation with a precursor H_3PO_4. For EU-C550, was found in literature a eucalyptus biochar with a specific area of 335 m^2g^{-1}, much higher than the eucalyptus biochar studied, however the pyrolysis conditions used by Fernandes et.al.[83] were different (pyrolysis with 8h of heating time and 14h of residence time at 500º C). In any case it is an indication that higher values can be obtained, for which indicates that the industrial process can be optimised. This, bearing in mind that the raw materials, exert influence on the processes, and may be different. Similarly, for EU-AC, a study by Mopoung and Dejang [84] obtained a value of 673 m^2g^{-1} for a temperature of 600 ºC through an physical activation with

steam, comparing these results it can be seen that it is six times higher, corroborating the hypothesis that it can be enhanced.

Mercury Porosimetry

As described in section 3.3.4, BET analysis only detects pores on the nanometre order (less than 4nm according to Jeng et.al.[47]), so to have a better model of the porous structure of both biomasses and their respective biochars, a mercury porosimetry analysis was performed, covering a range of pore size from 392 µm to 6 nm. The pore size distribution [mL/g] (left) and the cumulative intrusion value [mL/g] (right) are shown in **Figure *29*** and **Figure *30*** for pine and eucalyptus, respectively.

Analysing the pore distribution for pine and its respective biochars present in **Figure *29***, it can be seen that for raw pine there is a continuous pore distribution from 392µm to approximately 1 µm, with higher amount in the range between 391µm and 119µm,following with a decrease in the range 119µm to 53µm, with the highest contribution in the range 52 µm to around 10 µm. For the PS-C600 biochar, it is observed that there is similar to raw pine as there is a continuous distribution of pores from 392 µm to 1 µm, with the highest peaks in the range between 392 µm to 150 µm and 32 µm and 6 µm. Comparing this biochar with the raw biomass, it can be seen that the pore distribution is similar although there is a slight offset of narrowing of the biochar pores as can be seen in **Figure *29***, due to the fact that there is an alignment and “unclogging” of the pores during pyrolysis with the release of volatiles, which can be proved with the decrease in the density of the materials. The pore size distribution of both (PS-Raw and PS-C600) have a positive Pearson correlation of 0.734 (r=0.734), being the difference justified by what is mentioned above.

Comparing PS-C600 with PS-AC, the pore distribution is practically similar, which is to be expected since the formation process of both biochars is the same, the latter differing in that it is physically activated with CO_2, which as shown in **Table *11*** will differ at the level of nanopores by significantly increasing their specific area. The difference is that for the activated biochar there is a small amount of pores in the interval from 9 nm to 6 nm (mesoporosity) in the order of 0.07 mLg^{-1}, consequence of activation. The pore size distribution of both (PS-C600 and PS-AC) have a positive Pearson correlation of 0.987 (r=0.987), proving the similarity.

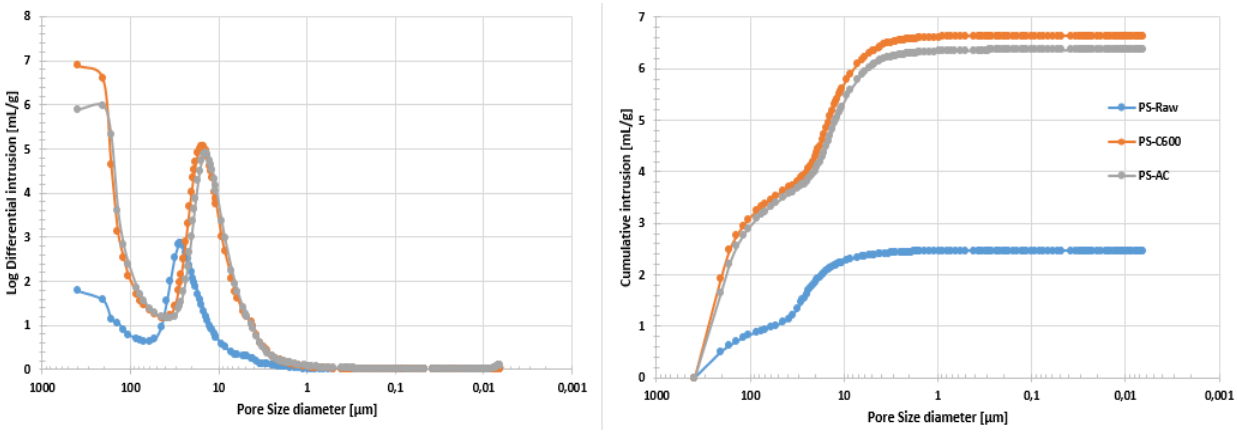

Figure 29- Log differential intrusion [mL/g] (left) and Cumulative Intrusion [mL/g] (right) vs Pore size diameter [µm] for PS-Raw, PS-C600 and PS-AC.

For EU-Raw, represented in **Figure *30***, a continuous distribution is verified for the whole range (400 µm to 6 nm), with a higher stage in the larger pores (400 µm to 166 µm) corresponding to 0.37 mLg^{-1}, followed by a decrease with the minimum at 14 µm corresponding to 0.10 mLg^{-1} , increasing again with a practically constant stage between 5 µm and 1 µm representing 0.17mLg^{-1} and reaching a maximum at 0.6 µm (0.2mLg^{-1}) , reducing again registering a last increase from 8 nm to 6 nm (0.05mLg^{-1}).

While for EU-C550 there is also a continuous distribution across the range, with a higher amount in larger pores between 400 µm to 200 µm (1.25 mLg^{-1}) with a valley between 200 µm and 6.5 µm with the minimum at 25 µm (0.17 mLg^{-1}). Subsequently a peak occurs at 6.5 µm (0.58 mLg^{-1}) followed by a new valley between 6.5 µm and 59 nm with a minimum at 0.28 µm (0.12 mLg^{-1}) culminating in a local maximum at 59 nm (0.22 mLg^{-1}). Finally, there is a decrease between 59 nm and 9 nm, reversing at 9 nm for an increase to 6 nm (0.1 mLg^{-1}). Analysing EU- AC, it can be seen that the pore size distribution is practically the same as that presented for EU-C550, which agrees with the results for pine biomass. The pore size distribution of both eucalyptus biochars have a Pearson correlation of 0.990 (r=0.990), providing this same agreement. However, the correlation between EU-C550 and EU-Raw is 0.696 (r=0.696), which is not as significant as in the case of pine.

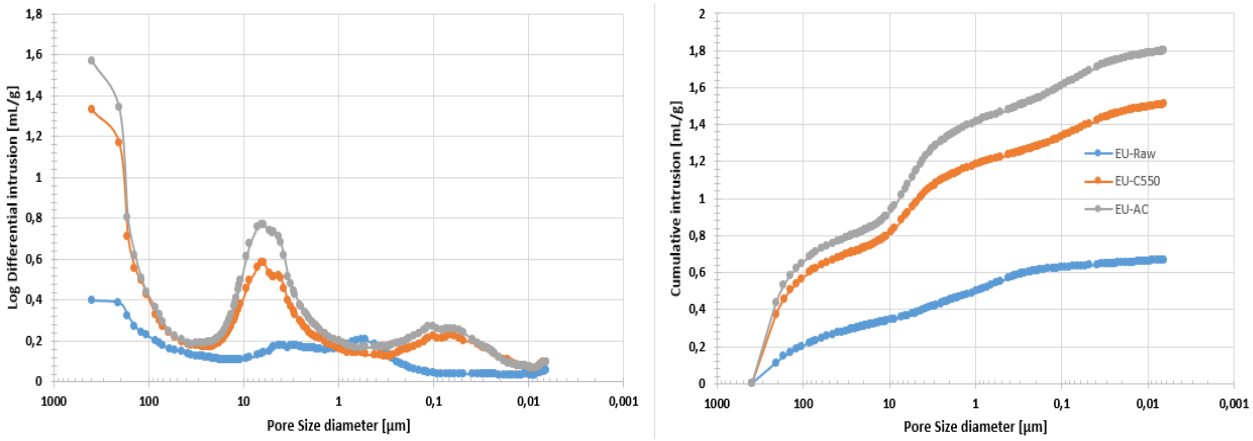

Figure 30- Log differential intrusion [mL/g] (left) and Cumulative Intrusion [mL/g] (right) vs Pore size diameter [µm] for EU-Raw, EU-C550, EU-AC.

Table *12* presents the various parameters from the mercury porosimetry test, total intrusion volume [mL/g], total pore area [m^2/g], average pore diameter, bulk density, skeletal density, and porosity. The porosity is calculated as follows:

$$\varphi(\%) = (1 - \frac{\rho_b}{\rho_s}) \times 100 \quad (24)$$

where φ , $\rho_b[\frac{g}{cm^3}]$, $\rho_s[\frac{g}{cm^3}]$ are porosity, bulk density, and skeletal density, respectively.

Table 12-Total intrusion volume, total pore area, average pore diameter, bulk density, skeletal density and porosity of biomass and biochars. n=1

Sample	Total intrusion Volume [mL/g]	Total Pore Area [m^2/g]	Average Pore Diameter [4V/A] [µm]	Bulk density at 0.54 psia [g/mL]	Skeletal Density [g/mL]	Porosity [%]
PS-Raw	2.47	0.47	20.83	0.31	1.35	76.94
EU-Raw	0.67	10.95	0.24	0.77	1.58	51.38
PS-C600	6.63	1.41	18.77	0.13	1.18	88.67
EU-C550	1.51	30.52	0.20	0.45	1.42	68.23
PS-AC	6.37	5.14	4.96	0.14	1.26	88.89
EU-AC	1.80	32.21	0.22	0.39	1.29	69.77

Table 13- Pore volume[mL/g] of different pore sizes according Soil Science Society of America (SSSA)

Pore Volume [mL/g]	Macropores (>75µm) [mL/g]	Mesopores (30-75µm) [mL/g]	Micropores (5-30µm) [mL/g]	Ultra-micropores (0.1-5µm) [mL/g]	Cryptopores (<0,1µm) [mL/g]
PS-Raw	9.18e-01	4.15e-01	1.04	9.50e-02	0.00
PS-C600	3.31	4.90e-01	2.49	3.37e-01	0.00
PS-AC	3.17	4.98e-01	2.35	3.43e-01	7.00e-03
EU-Raw	2.26e-01	5.80e-02	9.00e-02	2.51e-01	4.30e-02
EU-C550	6.12e-01	8.20e-02	2.61e-01	3.77e-01	1.76e-01
EU-AC	7.00e-01	8.60e-02	3.30e-01	4.90e-01	1.91e-01

Table 14- Pore volume[mL/g] of different pore sizes classified according to International Union of Pure and Applied Chemistry (IUPAC)

Pore Volume [mL/g]	Macropores (>50 nm) [mL/g]	Mesopores (2-50 nm) [mL/g]	Micropores (< 2 nm) [mL/g]
PS-Raw	2.47	0.00	NA
PS-C600	6.63	0.00	NA
PS-AC	6.37	6.00e-03	NA
EU-Raw	6.36e-01	3.30e-02	NA
EU-C550	1.39	1.15e-01	NA
EU-AC	1.68	1.19e-01	NA

For PS-C600 and PS-AC, there is a slight difference in total intrusion volume (4%) being PS-C600 larger, due to the fact that also for the larger pore sizes there is a slight difference in terms of distribution, reflected in a slightly lower slope in the cumulative intrusion curve. In terms of skeletal density and bulk density they are also quite similar being the differences of an increase of 6% and 4% (PS-AC in relation to PS-C600), respectively. Consequently, the difference between the porosities is 0.24%.

On the other hand, there is a difference in relation to the total pore area being PS-AC 3.6 times higher than PS-C600, due to the fact that for the activated biochar there is a pore range between 9 to 6 nm and in the intermediate range there is also a slight offset of the pores to the right. Comparing the results of the biochar at 600°C with the raw biomass, there is a 63% decrease of total intrusion volume which is mainly due to the fact that the number of high-end pores (400 to 200 µm) is relatively lower compared to their biochars. There is also a reduction of bulk and skeletal density comparing raw pine with its biochar (-57% and -13%, respectively), which comes from the release of volatile matter from the slow pyrolysis process.

In relation to eucalyptus biochars, an increase (for EU-AC) of 19%, 5%, 2% occurs for total intrusion volume, total pore area and porosity, respectively. Regarding the total intrusion volume,

although the pore size distribution is practically equal, the density of this same distribution is higher for the EU-AC hence in those parameters that also comes from the lower density that the EU-AC has in relation to the EU-C550 (-14%, -10% bulk and skeletal) resulting once again from the fact that the activated biochar has passed through a process that allows a greater release of matter. The eucalyptus raw has an intrusion volume 2.3 times lower than the EU-C550, due to the lower distribution amount of pores (it has higher amount in certain pore size than the respective biochars) and also to the differences observed in the distribution itself.

It should be noted that the total pore area presented in **Table *12*** is not related to the specific area presented in the section regarding the BET test, this area refers to the pore size range studied here. It can be proved that the total pore area per unit mass will be higher as bigger is the amount of smaller pore sizes (the materials which have higher density on the right side have larger area).

Table *13* and **Table *14*** represent the distribution of total pore volume by pore classification according to Soil Science Society of America (SSSA) and IUPAC, respectively. This distinction was made since the classification by SSSA gives a better insight into the volume distribution than the IUPAC classification and is also commonly used in research of this nature. These results are in line (or according) with **Figure *29*** and **Figure *30***, showing that EU has higher representativeness for smaller pore range while PS has higher representativeness for larger pore range. Looking at the last column (cryptopores) the effect of activation on PS is evident, since for PS-C600 this volume is 0 mL/g and for PS-AC it is 0.007 mL/g. It is verified the same effect for EU-AC, with an increase of 9% in relation to EU-C550.

In accordance with the results presented in this section, despite the different densities (absolute values presented in distribution charts) of the pore size distribution, there is a significant correlation between the raw biomass and their respective biochars, proving that many of the pores present in the biochars are residual biological capillary structures of the raw material. This result is consistent with other studies carried out by Zhang and You[55], and Wildan and Derbyshire [86]. It brings out that this relationship is more perceptible for Pine than for Eucalyptus, and for this reason a structural morphological analysis was performed using SEM tests. Furthermore, it is also possible to see the emergence of pyrogenic pores (resulting from the thermochemical process, pyrolysis) in relation to its raw biomass, either by BET area as well as in the cases of biochar activated by the cryptopores volumes present in **Table *13***. The emergence of such pores may be associated with the phenomenon of tar cracking within the matrix of the material itself since it is more likely to occur for high temperatures.

Scanning Electron Microscope

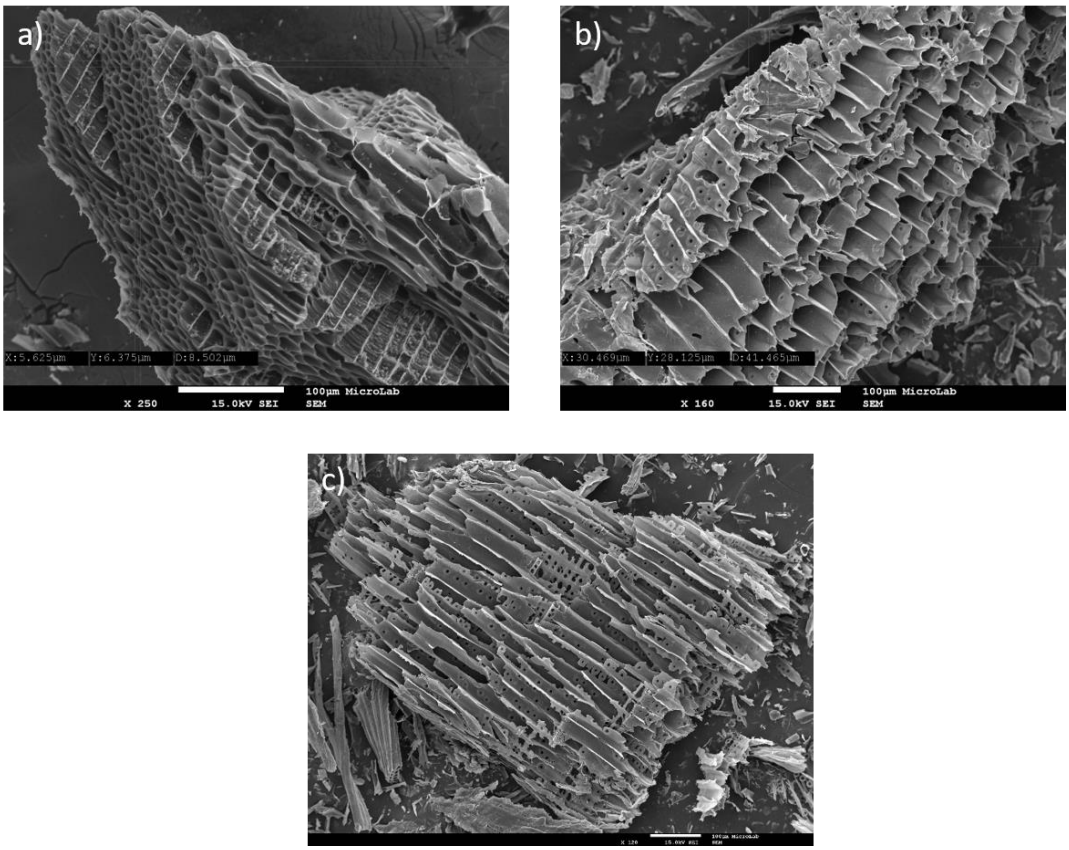

Figure 31- SEM images a) represents PS-RAW, b) PS-C600 and c) PS-AC, (resolution of 100 µm).

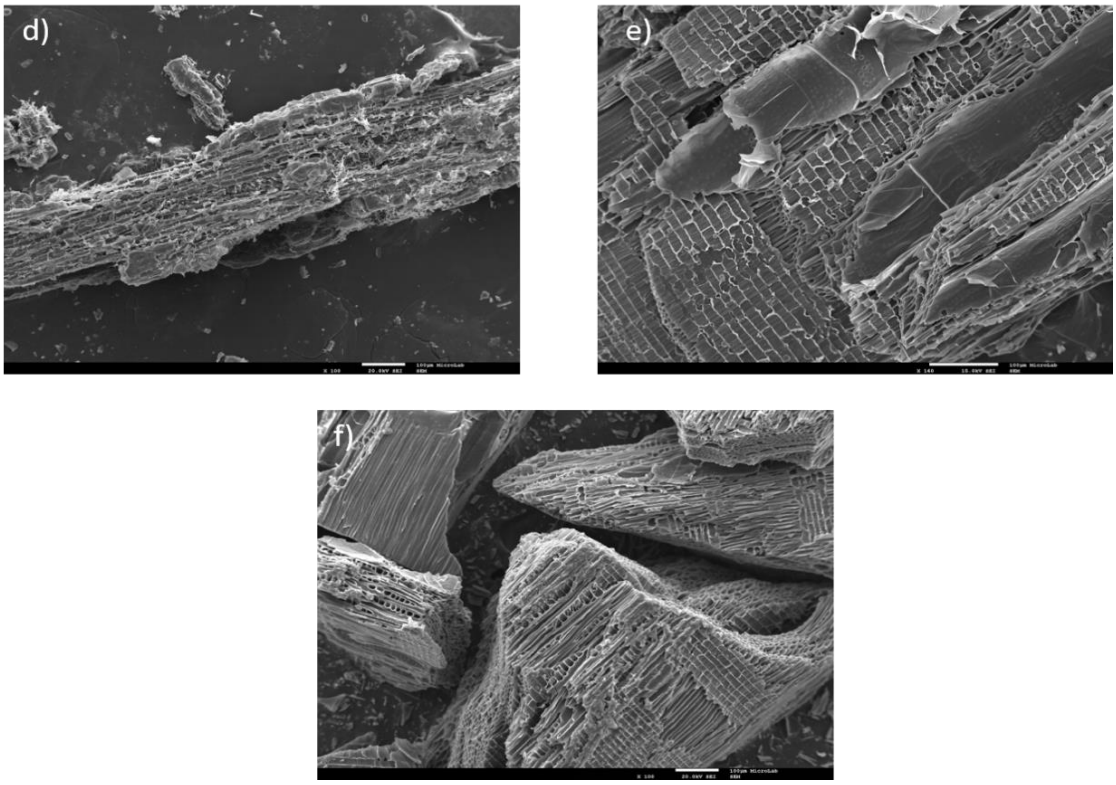

Figure 32-SEM images represents d) EU-Raw, e) EU-C550 and f) EU-AC (resolution of 100 µm).

Figure *31* and **Figure *32***, represent SEM images of the morphological structure of pine and its biochars and eucalyptus and its biochars, respectively. SEM images are used to check samples at the microscopic level, the images can be used to determine the structure and distribution of pores present on the surface of biomasses and biochars. The size of the pores that can be measured depends greatly on the resolution of the image. In this work, a resolution of 100 µm was used and only macropores can be observed. **Figure *31* a)** has represented the raw pine, where it is possible to see a very porous structure with pores with different dimensions in the range of tens of microns, presenting a similar elongated structure with variable section. **Figure *31* b)** and **c)** represent the biochar at 600 ºC and activated respectively, ratifying that the structure for this range of pores is quite similar with the raw biomass. It can also be seen in the figure for the biochars certain circular holes that correspond to the structure of the biomass, they are called plasmodesmata and are channels that cross the plant cells allowing the transport and communication between them.

On the other hand, it can be seen in **Figure *32* e)** and **f)** that the pores for the eucalyptus biochars are also elongated in a cylindrical shape and it is also visible that there is a considerable number of pores with a size smaller than that observed for the pine, which agrees with the mercury porosimetry results. Observing **Figure *32* d)** it is possible to see that the pore structure is also similar to its biochars however they are quite clogged and constricted (occurring this release during the thermochemical process), which contrasts with the results of **Figure *30***, i.e., hence there is also a considerable difference in the pore distribution of biomass and biochar.

4.3. Equilibrium Moisture Content

In this section the results regarding the moisture adsorption by both biomass and its respective biochars are presented and discussed. In the first phase, the results are presented on a volume and mass basis, then an estimate of the mass diffusivity of water based on the one-dimensional model described in section 3.4.1 is made and finally the single experimental point for the moisture sportion isotherm of each material is shown.

4.3.1. Volume Basis

In the following figures, are represented the water adsorption curves for the tests referred in section 3.4. It should be noted that the tests were performed for a constant relative humidity (conditions of T=20 ºC and HR=72%) and the mass variations were recorded for 4 hours to ensure that the balance between the amount of moisture adsorbed by the material and the relative humidity of the atmosphere was reached. Thus, it can be seen that, in a first phase we have the transition phase (where the greatest increase of moisture in the material occurs) and then we have the equilibrium phase (this phase was maintained for a longer time to ensure that there were no significant changes of moisture).

Figure *33* shows the materials related to pine. It possible to observed that PS-AC is the material that absorbs more moisture (0.0130 gcm^{-3}), however, pure pine adsorbs a large amount of moisture (0.0127gcm^{-3}). Where the latter is very close to activated carbon, being the difference only 3.2%. On the other hand, the BC-C600 adsorbs less moisture (0.0056 gcm^{-3}), representing approximately 2.4 times less than the corresponding activation.

Figure *34* shows that eucalyptus raw adsorbs more moisture than its respective biochars (0.0157 gcm^{-3}), being 1.2 and 1.6 times higher than EU-C550 and EU-AC, respectively. Regarding their biochars, contrary to what would be expected the moisture absorbed by EU-C550 is 1.3 times higher than EU-AC. Thus, the results on a volume basis give us a perspective of the absolute value of the adsorbed moisture, since the same volume was used for all the samples. This shows that the raw biomasses themselves adsorb more water than their biochars, thus demonstrating that the porous structure is not the only parameter influencing wate adsorption, as explained at the end of this section.

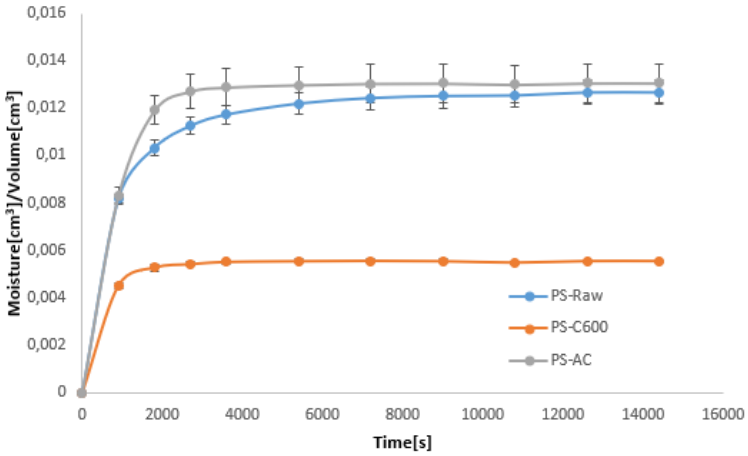

Figure 33-EMC curves for PS-Raw, PS-C600 and PS-AC, on a volume basis.

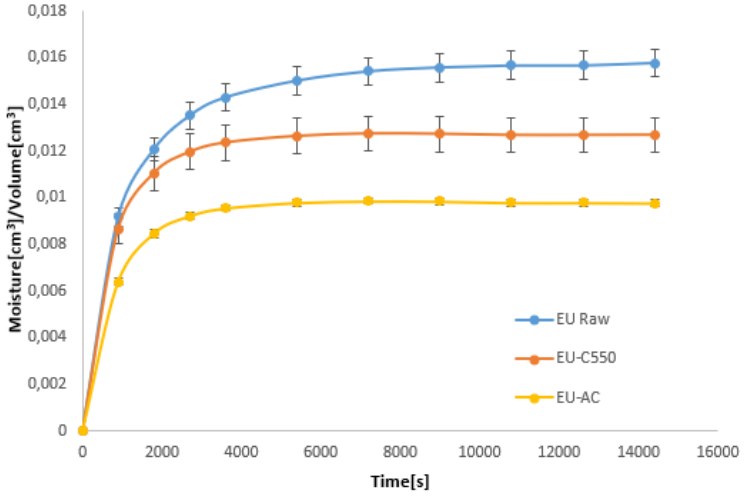

Figure 34-EMC curves for EU-Raw, EU-C550 and EU-AC, on a volume basis.

4.3.2. Mass Basis

It is also important to understand the amount of moisture adsorbed per unit mass of the material, since these are materials with different densities, due first to the type of biomass to which the material corresponds and then due to the changes they undergo in the slow pyrolysis process. Thus, in **Figure *35*** it is possible to see that on a mass basis PS-AC becomes the material with the highest value, due to its porous structure and the low yield of the process (**Table *8***), thus the amount of moisture adsorbed per unit mass becomes representing a value of 0.168 g/g, 2.8 and 1.7 times higher than PS-C600 and PS-Raw, respectively. In relation to the value of PS-C600, although the density is 2.3 times less than the density of PS-Raw, the value it adsorbed in absolute terms is not enough to be superior on a mass basis in relation to its biomass. Represented thus, PS-Raw a value of 0.0975 g/g and PS-C600 a value of 0.0611 g/g.

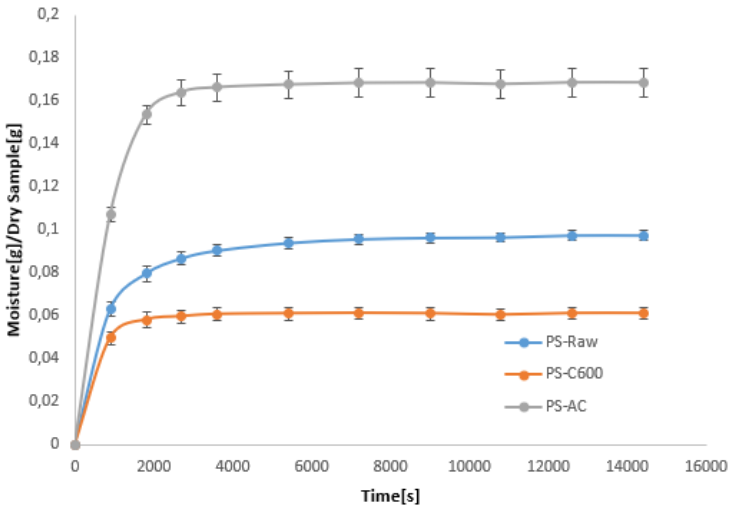

Figure 35- EMC curves for PS-Raw, PS-C600 and PS-AC, on a mass basis.

For the eucalyptus (**Figure *36***) it is possible to see that the raw biomass then has a lower amount of moisture per unit mass (0.0352 g/g) resulting from once again the decrease in density resulting from the conversion process.

Comparing the biochars, both EU-C550 (0.0482 g/g) and EU-AC (0.0374 g/g) it appears that the ratio between them remains nearly constant (1.28 times higher) because although there is a reduction in density of the activated biochar, it is not significant and therefore this ratio remains almost constant. In **Table *13*** are represented the bulk densities calculated for these tests, note that bulk densities can vary with those shown in **Table *12*** because: 1) the material is heterogeneous (are particles from 400 µm to 1 mm) and 2) there is the compaction factor that will have a very large influence on bulk density.

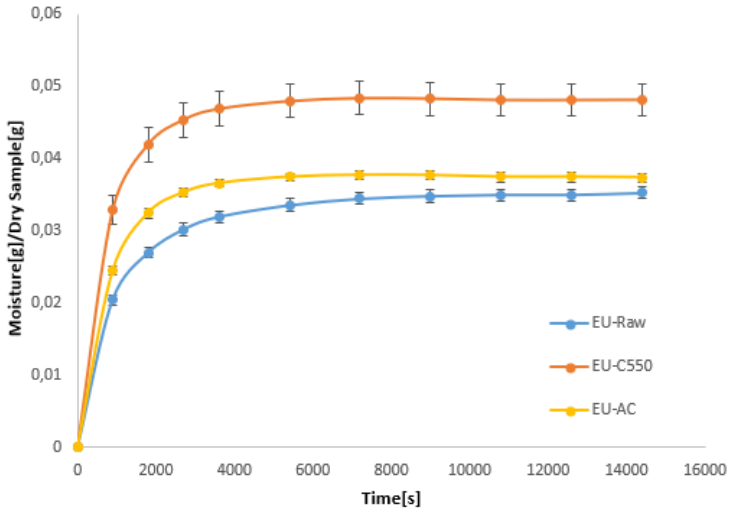

Figure 36-EMC curves for EU-Raw, EU-C550 and EU-AC, on a mass basis.

Table 15- Bulk density used in moisture adsorption tests

	PS Raw	PS-C600	PS-AC	EU Raw	EU-C550	EU-AC
Density [g/cm^3]	1,30e-01	9,09e-02	7,76e-02	4,48e-01	2,63e-01	2,62e-01

4.3.3. Effective water mass diffusivity

Considering the material as a film in macroscopic terms (not considering the phenomena that occur in the material due to its pore and functional groups on the surface) it's determined the effective diffusivity associated with each material. **Figure *37*** and **Figure *38*** represent respectively, the experimental points and the fitting curves according to the established in section 4.1, and therefore the results are presented in a dimensionless form. Since it was intended to determine the effective diffusivity in the transition phase, we considered only the points of the curves until 5400s, which is the moment from which the amount of water remains stable.

Table *14* shows the different effective diffusivities and their respective least squares errors (method used for fitting). The value of the effective diffusivity gives us the perception of how quickly the material absorbs moisture until it reaches equilibrium (in which there is no longer any moisture exchange), and the PS-C600 has the highest value of effective diffusivity, 709 µm^2/s. The PS-AC has a diffusivity value slightly above the PS-Raw (10% higher), since looking at **Figure *33***, it is perceptible the difference in reaching equilibrium around 2000s, being the biochar activated faster. Relative to eucalyptus is the raw biomass takes longer to reach equilibrium compared to its biochars, as it is perceptible in **Figure *34***. EU-C550 is slightly higher (7%) compared to EU-AC.

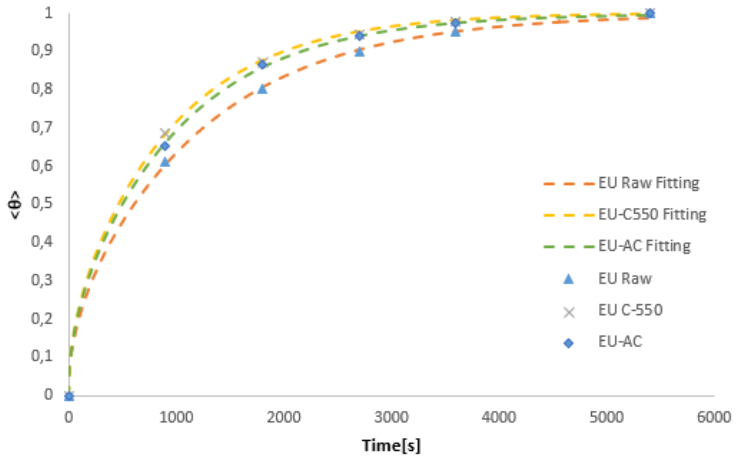

Figure 37-Experimental points and fitting curves for moisture diffusion curves for EU Raw, EU550, EU-AC

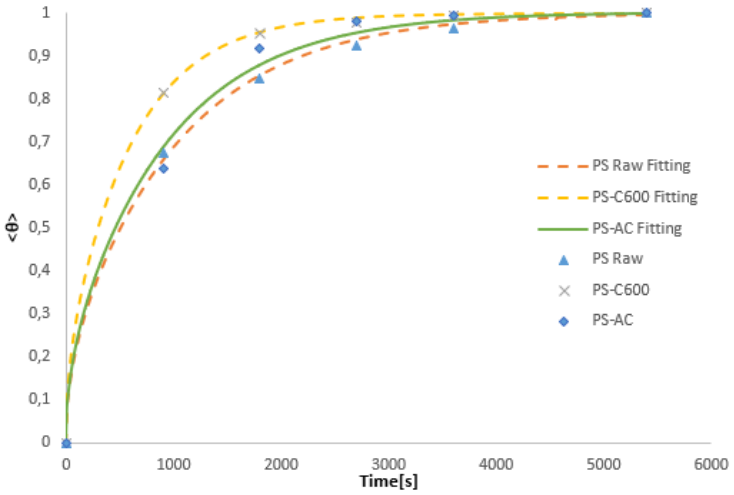

Figure 38- Experimental points and fitting curves for moisture diffusion curves for PS Raw PS-C600, PS-AC.

Table 16- Effective mass diffusivity of water for pine and eucalyptus materials.

	PS Raw	PS-C600	PS-AC	EU Raw	EU-C550	EU-AC
D_{eff} [µm²/s]	417.28	709.03	459.24	349.37	455.79	425.21
LSS	7.04e-04	1.94e-04	4.47e-03	2.08e-04	6.22e-05	1.29e-04

4.3.4. Moisture Sportion Isotherm

As referred in section 2.5.1, the set of equilibrium moisture content for the different relative humidities correspond to the moisture sportion isotherm, which is unique for each material due to different interactions (colligative, capillary, and surface functionality effects) between the water and the solid components. However, in this work, a point of this curve was produced for the humidity of 72% and T=20 ºC. In **Figure *39***, it is possible to see the point determined for the biomasses and their respective biochars of pine and eucalyptus.

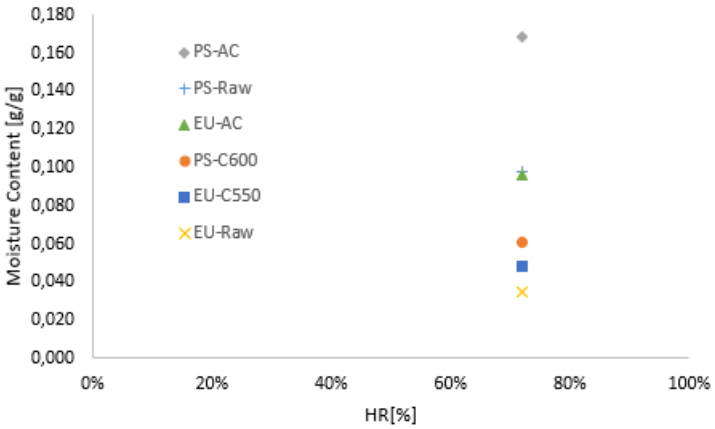

Figure 39-Moisture sportion isotherm experimental point for pine and eucalyptus biomasses and biochars.

Regarding the pine materials, the PS-AC is the one with the highest value (0.168 g/g).It would be expected since being an activated carbon it would have activated sites that provide a higher adsorption, as proved by a study with several activated carbons produced with different methods [87]. Furthermore, in **Table *13*** where the pore volume distribution by classification is shown, it can be seen that PS-AC has 0.006 mL/g of mesoporosity, which leads one to consider that the phenomenon of capillary condensation may have an effect since the points shown are for a moisture content that is within the range considered for this phenomenon to happen (section 2.4). On the other hand, PS-Raw (0.097 g/g) and PS-C600 (0.061 g/g) have no volume in the range of mesoporosity, so the adsorption is due to its surface functionality which as present in **Figure *26***. PS-Raw has more functional groups, hence shows higher value.

On the other hand, for eucalyptus both EU-Raw, EU-C550 and EU-AC have a pore volume in mesoporosity of 0.033 mL/g, 0.115 mL/g and 0.119 mL/g , respectively. With EU-AC having the highest value of 0.096 g/g. However it cannot be stated that it is directly correlated with mesoporosity and capillary condensation effect. Given that the pearson correlation between moisture content and mesoporosity for these values is 0.69 . In this case, the EU-Raw was the lowest value, being necessary the characterization of the surface functionality to conclude in relation to eucalyptus.

Nevertheless, the Pearson correlation between the moisture content of all biochars (excluding raw biomasses) with their specific area determined by BET is 0.86. Although it is a considerable value, it should be careful to conclude that there is a positive correlation between these two parameters since only a complementary study of the functionality will make it clearer.

4.4. Water Holding Capacity

Understanding the processes of water uptake is crucial to producing effective products that can be used practically in applications requiring water retention and uptake. Thus, water uptake in porous media depends on capillary forces, which can act to either allow or prevent water from entering the pores. The strength of these capillary forces depends on the chemical composition of the surface and the physical properties of the medium, and is generally described by Young-Laplace equation, given by:

$$P_c = \frac{2\gamma \cos\theta}{r} \tag{25}$$

Where $P_c[\frac{N}{m^2}], \gamma\left[\frac{N}{m}\right], \theta[°], r[m]$ are the differential capillary pressure across the liquid-gas interface, surface tension of water, contact angle of water (which depends on interfacial energies and thus biochar surface chemistry) and the pore radius, respectively. These forces can be positive or negative depending on the surface properties of the material, if the contact angle is less than 90° positive forces are generated leading the water to enter the pores, if it is greater than 90° negative forces are generated preventing the water from entering the pores. As can be seen from the

equation, the magnitude of the capital force is inversely proportional to the pore size, so hydrophobic surfaces in nanopores can generate quite high capillary forces. Thus, the amount of water absorbed by the material will have a high dependence on capillary forces and total porosity.

In addition, there are some important factors that can influence the WHC and water absorption rate (WAR) of biomass carbon: surface functional groups, porosity structure, and specific surface area.[55] **Figure *40*** shows the water holding capacity in a mass and volume basis.

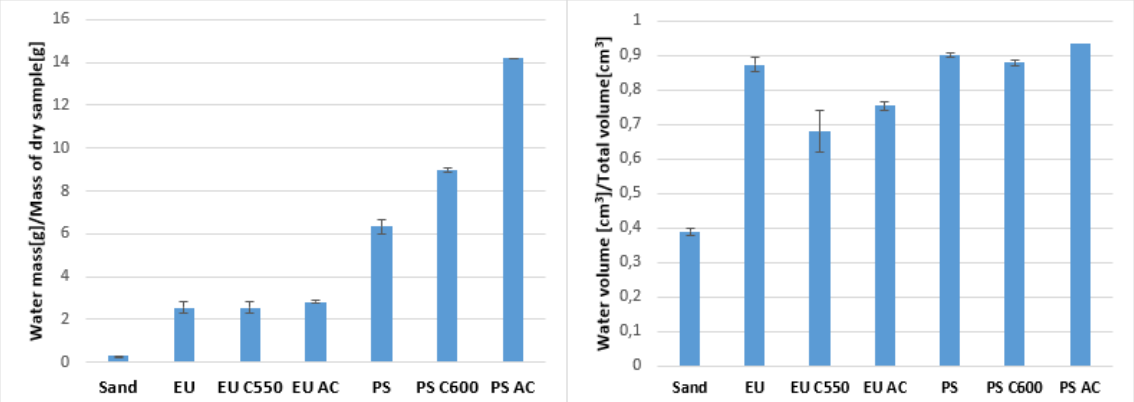

Figure 40- Water holding capacity of biomasses and biochars on a mass basis (left) and volume basis (right).

Analysing **Figure *40*** it is possible to see the water holding capacity for the pine biomasses and their respective biochars, as well as for the sand, described in section 3, used as control. In the figure on the right side, correspond to the WHC on a volume-by-volume basis, while on the left side to the WHC on a mass by volume basis. If there were no functional groups on the surfaces of the materials then their WHC would coincide with their total intrusion volume (this is to say their porosity, information in **Table *12***). In **Table *17*** we can see these two variables. Firstly, it is necessary to say that the particle size studied is from 1mm to 400 µm, and the maximum range of pores studied is up to 400 µm so in **Table *17*** it is not considered this larger range of pores that will also have an influence on WHC. However, looking at the eucalyptus results, it is possible to see that EU-AC has only slightly WHC than EU-C550, and it can be seen through the standard deviation that they may even coincide. This result is contrary to what is expected since besides the porosity of EU-AC being slightly larger. Furthermore, the effect of hydrophobicity should be lower for EU-AC (therefore it should have a higher WHC), since as shown by Gray et.al.[59], there is a decrease of surface functional groups that cause this hydrophobicity, with the increase of the pyrolysis temperature. Anyway, as it was not possible to perform an F-TIR evaluation to these two materials, so it is not possible to conclude about their surface functionality. On the other hand, looking at PS-C600 and PS-AC, it can be seen that the WHC of PS-AC is 6% higher than PS-C600, which is also true for its porosity.

Regarding the raw biomass, eucalyptus and pine, both show a high WHC (0.893 and 0.910 cm^3 /cm^3, respectively), demonstrating well the water absorption capacity of woody biomass. Thus, these results, in addition to substantiate, once again that most of the pores come from the

biological structure of biomass itself, it is necessary to take into account other phenomenas that occur in biomass, including the swelling. This is a phenomenon that occurs mainly on woody biomasses, due to the expansion of the fibres of the biomass itself, since its stiffness is lower than their respective biochars (in the slow pyrolysis occurs precisely a significant increase of fixed carbon, making the material more rigid). This phenomenon has been reported by several studies, including on [88]. Besides, other effects that are preponderant in the relation of biomass with water is its chemical composition, namely its extractives (non-structural components such as fats, resins, simple sugars, starches, etc.) which can lead to the increase of WHC. Due to work limitations, it was not possible to perform the chemical composition of biomass, so the interference of extractives is not possible to quantify.

Thus, considering only the biochars of the respective biomasses, the Pearson's correlation between the WHC and the total pore volume (presents in **Table *17***) is 0.95, meaning a positive correlation between the WHC and the total pore volume. On the other hand, comparing the results with the specific area determined by BET tests, the Pearson correlation obtained was 0.83 demonstrating that there is no clear strong correlation between the specific area at nanopore level and the WHC. These results are in agreement with that presented by Zhang and You[55] , which obtained the same correlation for two different biochars of poplar and pine.

It is also noted that the results when analysed on a mass basis (**Figure *40*-left**), the mass of water per unit of dry mass of sample is of the order of 2 g/g for EU-Raw, EU-C550 and EU-AC, while for PS-Raw, PS-C600 and PS-AC is of the order of 6.2 g/g, 9 g/g and 14 g/g. This is due to the differences in the densities of the materials. Eucalyptus being a denser material, then the amount of water retained at saturation for the same amount of mass consider will be lower.

Table 17- Total intrusion volume, Water Holding capacity, Specific Area from BET for Pine and Eucalyptus biomasses and biochars

	PS-Raw	**EU-Raw**	**PS-C600**	**EU-C550**	**PS-AC**	**EU-AC**
Total Intrusion Volume [cm^3/cm^3]	7.69e-01	5.14e-01	8.89e-01	6.82e-01	8.92e-01	6.97e-01
WHC [cm^3/cm^3]	9.10e-01	8.93e-01	8.84e-01	6.85e-01	9.36e-01	7.69e-01
A_{BET} [m^2g^{-1}]	0.34	NA	375	20	112	112

4.5. Water Retention Curves

In this section the results in relation to the water retention curves are presented and discussed. The curve used as a control is the sand curve, and for each graph this control is considered. Then the representation of biomass/biochar at 10% on a volume basis, followed by 50% and finally 100% of biomass/biochar is made. Note also that soil water potential is composed by pressure potential, gravitational potential, osmotic potential. However, in the present study only the pressure potential (mainly capillary pressure) is considered since pre-treated sand was used and in a soil without solutes there is no osmotic potential. The gravitational potential is also neglected due to the low elevation.

4.5.1. Sand and biomasses

In **Figure *41*** to **Figure *45*** are represented the experimental points obtained for the biomasses (PS-Raw, EU-Raw), and for the biochars (EU-C550, EU-AC and PS-C660). Furthermore **Table *18***, summarises all the values obtained for this test together with other parameters such as total pore volume, specific area BET and the error of the least squares method (LSS).

The curves for the PS-AC were not obtained, due to the low yield of the activation process which led to not having enough quantity to perform the water retention tests. It should also be noted that the fitting performed through the Van Genutchen model described in section 3.6.2, to obtain the most accurate empirical parameters (n and α) should be used more points along the entire curve, as performed in other studies[56], [89]. However, these are tests with a long duration time and the most critical points were determined, being possible to make a qualitative comparison between the empirical parameters. On the other hand, the fitting of the curves for the elements, i.e., for biomasses and biochars at 100% was not considered since values for the parameters that are not within the scope of the model would be obtained.

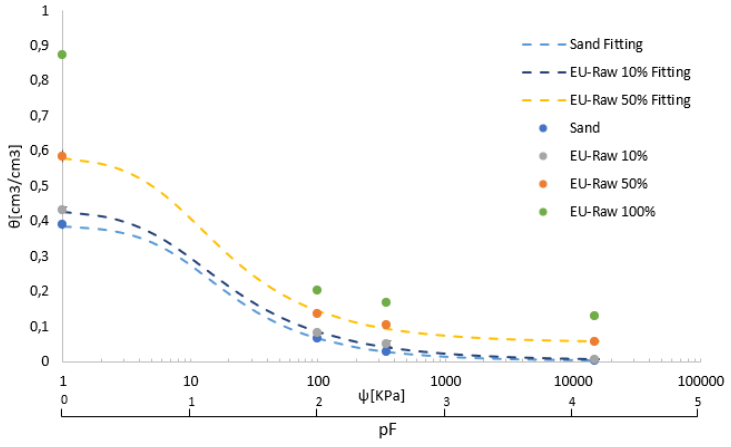

Figure 41-Water retention curves for sand, EU-Raw 10%, EU-Raw-50%, EU-Raw 100% and respective fitting curves.

In relation to pine biomass (**Figure *41***), PS-Raw, there is an increase of 12%, 17%, reduction of 13% and change of 0% for pF points 0, 2, 2.54 and 4.2 for 10% biomass in the mixture with sand. Increase of 46%,75%,228% and 1233% for pF points 0,2,2.54 and 4.2 for 50% mixing with sand. And increase of 132%, 157%,469% and 3433% for 100% PS-Raw for pF points 0, 2, 2.54 and 4.2.

Considering EU-Raw (**Figure *42***) there is an increase of 11%, 22%,75% and 67% for pF points 0, 2, 2.54 and 4.2 for 10% biomass in the mixture with sand. Increase of 51%,108%,261% and 1733% for the points of pF 0,2,2.54 and 4.2 for 50% of mixture with sand. And increase of 125%, 205%,483% and 4200% for 100% EU-Raw for pF points 0, 2, 2.54 and 4.2.

Thus, it can be observed that an increase occurs for all points comparing only with the isolated sand, taking away a value for PS-Raw for pF 2.54 that could represent an outlier. However, although it has been concluded that much of the larger scale pores come from the biological structure of the biomass, it is difficult to correlate this water retention with the porosity of the biomass alone for several reasons. One of them, as already mentioned in sub-section 4.4, is the fact that there is the phenomenon of swelling that is always difficult to quantify since it is due to the expansion of biomass fibres. On the other hand, the extractives can also have a significant effect. And lastly, since raw biomass is not a very rigid structure unlike biochar, pore deformation may occur when pressure is applied.

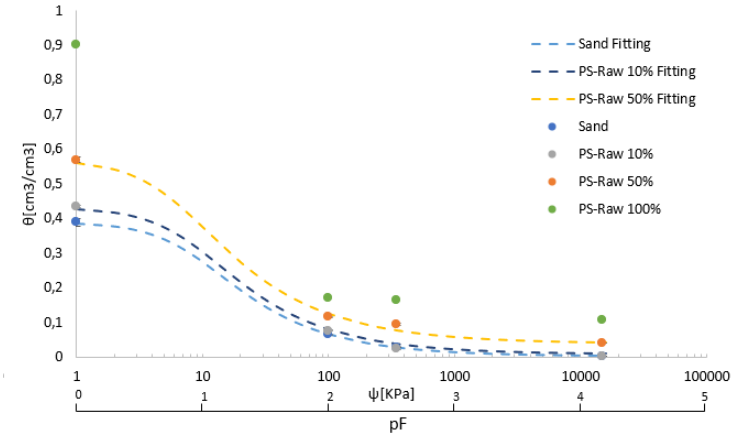

Figure 42- Water retention curves for sand, PS-Raw 10%, PS-Raw-50%, PS-Raw 100% and respective fitting curves.

4.5.2. Sand and biochars

With respect to EU-C550 (**Figure *43***), an increase of 11%, 16%, 48% and 167% for pF points 0, 2, 2.54 and 4.2 for 10% biochar in the mixture with sand is found. Increase of 22%,73%,203% and 667% for pF points 0,2,2.54 and 4.2 for 50% mixing with sand. And increase of 75%, 58%,72% and 21.33% for 100% of EU-C550 for pF points 0.2,2.54 and 4.2.

As for EU-AC (**Figure *44***), an increase of 10%, 18%, 58% and 67% for pF points 0, 2, 2.54 and 4.2 is found for 10% biochar in the mixture with sand. Increase of 36%,89%,236% and 1967% for pF points 0,2,2.54 and 4.2 for 50% mixing with sand. And increase of 94%, 93%,507% and 5000% for 100% EU-AC for pF points 0,2,2.54 and 4.2.

For PS-C600 (**Figure *45***), an increase of 17%, 14%, 34% and 0% for pF points 0, 2, 2.54 and 4.2 for 10% biochar in the mixture with sand is found. Increase of 56%,95%,173% and 1033% for pF points 0,2,2.5 and 4.2 for 50% mixing with sand. And increase of 126%, 189%,345% and 2667% for 100% of PS-C600 for pF points 0,2,2.54 and 4.2.

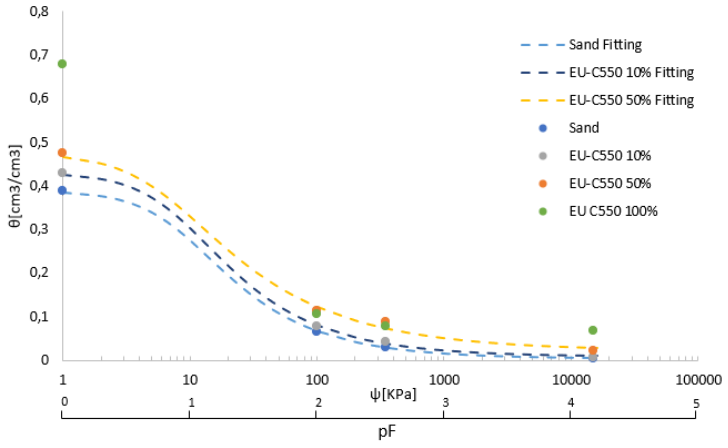

Figure 43- Water retention curves for sand, EU-C550 10%, EU-C550 50%, EU-C550 100% and respective fitting curves.

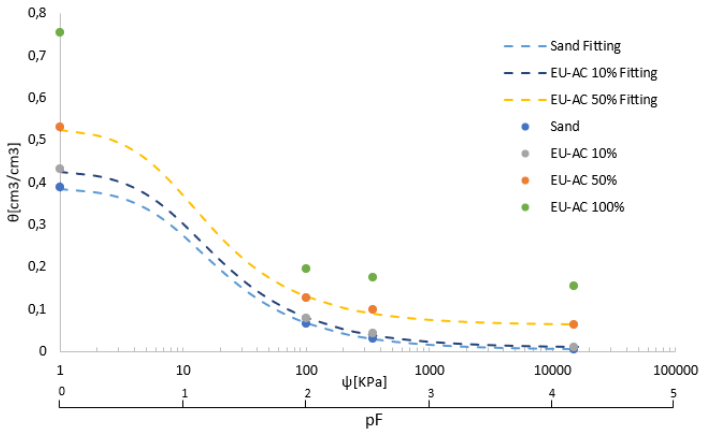

Figure 44- Water retention curves for sand, EU-AC 10%, EU-AC 50%, EU-AC 100% and respective fitting curves.

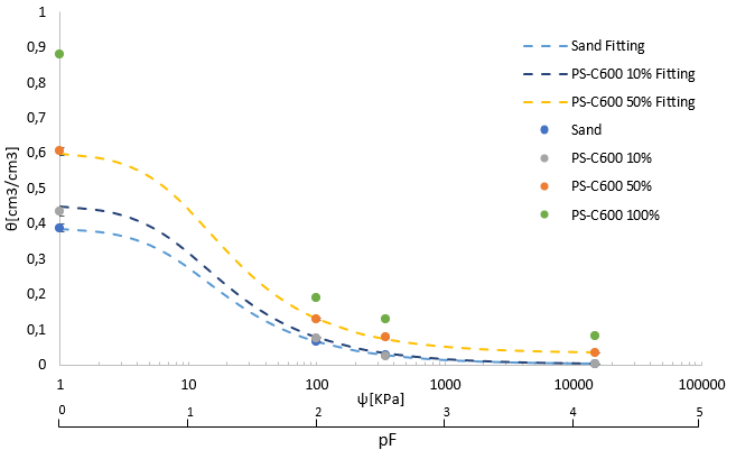

Figure 45- Water retention curves for sand, PS-C600 10%, PS-C600 50%, PS-C600 100% and respective fitting curves.

The effect of biochar and biomass when compared to the sand control is visible. Furthermore, it is also noted that biomass has a positive response in terms of water retention when mixed with sand, which is not generally considered as an object of study in the literature. There is also a non-linearity concerning the percentage of element used with the sand, this is due to the fact that there are several parameters that will affect the water retention, namely the interpores between the sand and biomass/biochar particles and the intrapores of the biochar itself.

However as reported by Yi et.al [89], considering the same particle size range for both sand and biochar, the effect of inter-pores is diminished, hence the same size for both elements (400µm to 1mm) was selected for this work. Thus, looking at the values, it can be seen that for biochars there is an increase to θ_{fc}, $\theta_{pF=2.54}$, θ_{wp} for all biochars due mainly to the intraporous. This is because if capillary potential is the main effect, then capillary forces are the main factor in water retention. These are described by the Young-Laplace equation (equation 25), which indicates that the smaller the pore, the greater the pressure to remove the water from that pore, which agrees with the fact that the water retention values for biochar mixtures at the wilting point are much

higher than for sand, since this is the point of greatest pressure and only the smallest pores retain water. However, looking at the formula there is also the effect of the contact angle which depends on hydrophobicity, hence the relationship is not entirely direct between smaller pores and more water retained. In relation to this point, it should be noted that Kynney et.al.[90] found that hydrophobicity can be reduced by exposure to water (so if it is 24 hours saturated then that hydrophobicity will also be reduced).

To prove this capillarity effect, Pearson correlation was made (table in appendix B) between the values obtained for water retention (θ_s, θ_{fc}, θ_{paw}, θ_{wp}), being that for mixtures of 10% a correlation value of 0.76 is obtained for between the volume of crypotores (according to SSSA - <0.1µm) and θ_{wp}. For 50% mixtures there is a correlation of 0.86 between the volume of ultramicropores (according to SSSA 0.1 µm to 5 µm). For 100% elements there is a correlation of 0.91 between ultramicropores volume and θ_{wp}. Thus, demonstrating that intrapores are the main factor responsible for increased water retention, specially at greater pressures (wilting point). These results are in line with Liu et.al.[56] for medium-sized materials, considered in their study from 0.25 mm to 0.853 mm, which is quite close to the range considered in this study.

That said, from a practical point of view we introduce a parameter described in section 2.3.1, the θ_{paw} (plant available water) which is calculated as follows:

$$\theta_{paw} = \theta_{fc} - \theta_{wp} \tag{26}$$

where $\theta_{fc}[\frac{cm^3}{cm^3}]$ is the field capacity and $\theta_{wp}[\frac{cm^3}{cm^3}]$ is the wilting point.

In **Table *18***, as is present the summary of the parameters for all mixtures and materials, it can be seen that the material that has higher θ_{paw} is the PS-C600 at 100% (71% higher) with a value of 0.1080 [cm^3/cm^3], however only two materials have a plant available water lower than the sand, which are EU-AC and EU-C550 as elements (without mixing), due to the fact that the amount of water retained at the wilting point is still high due to water retention in the intra-pores, leading to the fact that the available water between the field capacity and the wilting point is not high. This leads to the conclusion that the use of biochar has to be considered, because if it is used in a high percentage the retention value for the wilting point can be so high that it makes the value of plant available water lower than that of sand alone.

However, it is not feasible to apply 100% biochar in a practical way, so it is also necessary to quantify which would be the best with the mixtures in function of the percentages. Thus, a 50% mixture of PS-C600 improves 50% over sand, while a 10% mixture improves 16%. The EU-C550 improves 45% and 9% in a mixture at 50% and 10%, respectively. As for biomasses, PS-Raw improves 19% and 17% in a 50% and 10% mixture, respectively. While EU-Raw improves 31% and 20% in a mixture of 50% and 10%, respectively.

Table 18-Summary table with WRC parameters and material characteristics

Category	Volume %	Sample	θ_s[cm^3/cm^3]	θ_{fc}[cm^3/cm^3]	θ_{paw}[cm^3/cm^3]	θ_{wp}[cm^3/cm^3]	α [cm^{-1}]	n	Total Pore Volume [mL/g]	Specific Area BET[m^2/g]	SSL
Mixtures		**Sand**	3.89e-01	6.62e-02	6.32e-02	3.00e-03	1.16e-01	1.74			2.73e-06
Mixtures	**10%**	**EU Raw**	4.33e-01	8.07e-02	7.57e-02	5.00e-03	1.40e-01	1.63			1,51e-04
Mixtures	**10%**	**PS-Raw**	4.34e-01	7.72e-02	7.42e-02	3.00e-03	5.81e-02	1.99			8.58e-07
Mixtures	**10%**	**PS-C600**	4.55e-01	7.55e-02	7.35e-02	3.00e-03	1.20e-01	1.71			1.48e-04
Mixtures	**10%**	**EU-AC**	4.28e-01	7.81e-02	7.31e-02	5.00e-03	1.31e-01	1.66			9.71e-05
Mixtures	**10%**	**EU-C550**	4.30e-01	7.70e-02	6.90e-02	8.00e-03	1.21e-01	1.71			5.70e-05
Mixtures	**50%**	**PS-C600**	6.05e-01	1.29e-01	9.50e-02	3.40e-02	1.13e-01	1.73			1.80e-04
Mixtures	**50%**	**EU-C550**	4.74e-01	1.15e-01	9.16e-02	2.30e-02	1.57e-01	1.54			3.79e-04
Mixtures	**50%**	**EU Raw**	5.86e-01	1.38e-01	8.25e-02	5.50e-02	1.41e-01	1.67			2.26e-04
Mixtures	**50%**	**PS-Raw**	5.68e-01	1.16e-01	7.56e-02	4.00e-02	1.60e-01	1.66			4.84e-04
Mixtures	**50%**	**EU-AC**	5.30e-01	1.25e-01	6.32e-02	6.20e-02	1.35e-01	1.74			1.25e-04
Elements	**100%**	**PS-C600**	8.79e-01	1.91e-01	1.08e-01	8.30e-02	NA	NA	6.63	375	
Elements	**100%**	**EU Raw**	8.73e-01	2.02e-01	7.28e-02	1.29e-01	NA	NA	0.67	0	
Elements	**100%**	**PS-Raw**	9.02e-01	1.70e-01	6.43e-02	1.06e-01	NA	NA	2.47	0.34	
Elements	**100%**	**EU-AC**	7.54e-01	1.94e-01	4.09e-02	1.53e-01	NA	NA	1.80	112	
Elements	**100%**	**EU-C550**	6.79e-01	1.05e-01	3.78e-02	6.70e-02	NA	NA	1.51	20	

4.6. Enhancement of biochar from the industrial process

Since the industrial process conditions are not well known and the results showed that comparing eucalyptus biochar with pine biochar, it could indicate that the processing conditions of eucalyptus biochar were not ideal to obtain a structure with higher specific area, higher water retention capacity and higher moisture adsorption capacity. In this sense, it was carried out a slow pyrolysis of EU-Raw during 1 hour in a muffle furnace at 600°C (EU-C600) in inert atmosphere (without oxygen) and the same tests were performed to be compared with EU-C550 and EU-AC.

Table *19* shows the proximate analysis on a dry basis, including the new biochar produced EU-C600. While **Figure *46*-Figure *48*** show the water holding capacity (WHC), equilibrium moisture content (EMC) and water retention curves (WRC) for Eucalyptus biomass and biochars, including EU-C660, respectively.

Table 19- Proximate Analysis on a dry basis with EU-C600

	Dry Basis				
Sample Type	Moisture (%)	Volatile Matter (%)	Ash (%)	Fixed Carbon (%)	Calorific Value [MJ/kg]
EU-C550	-	20,03	0,83	79,14	31,10
EU-AC	-	18,32	0,45	81,23	31,58
EU-600	-	16,18	0,34	83,48	32,04

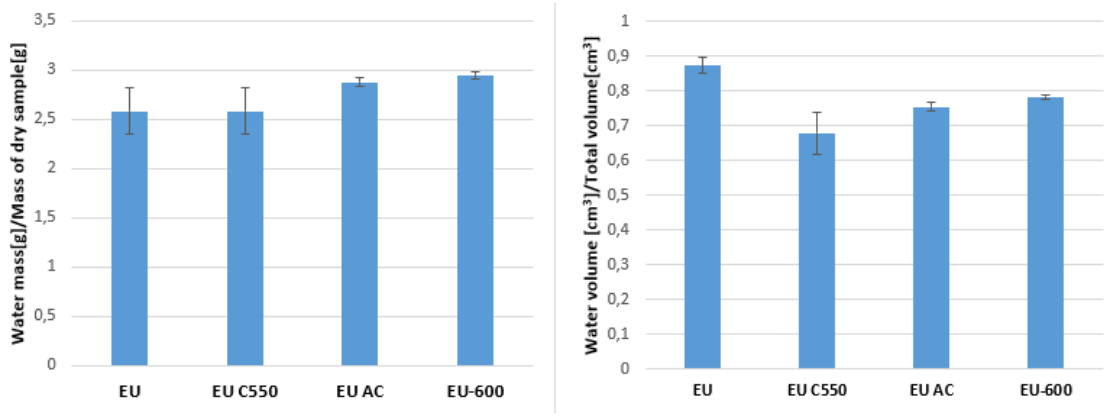

Figure 46- WHC for Eucalyptus biomass and biochars, including EU-C600.

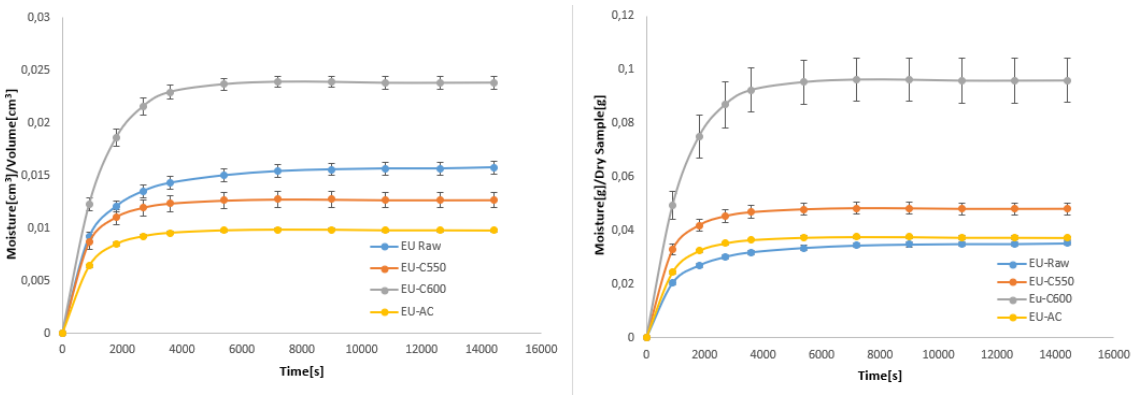

Figure 47- EMC curves for EU-Raw, EU-C550, EU-AC and EU-C600, on a volume basis.

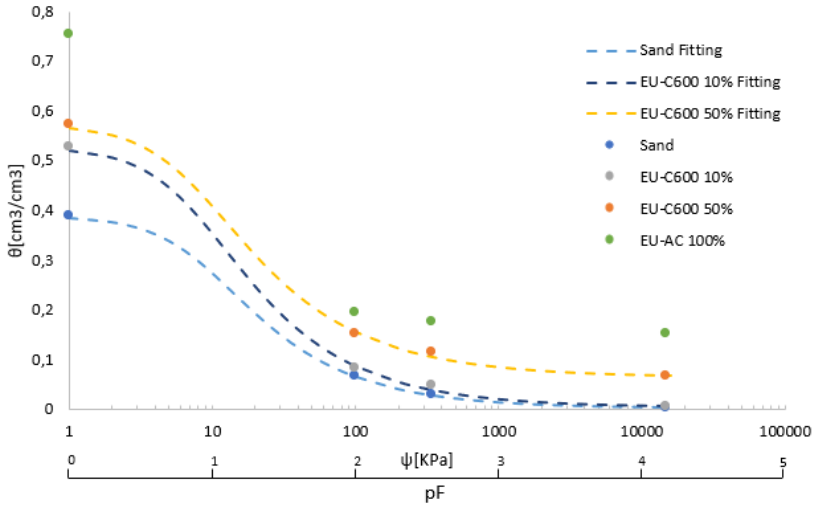

Figure 48- Water retention curves for sand, PS-C600 10%, PS-C600 50%, PS-C600 100% and respective fitting curves.

Analysing **Table *19***, there was a decrease of 3.85% in volatile matter of EU-C600 compared to EU-C550 and an increase of 4.34% in fixed carbon, thus proving that the thermochemical process used allowed a greater devolatilization. From **Figure *46***, in terms of WHC there was an increase of 14% and 15% in relation to EU-C550, on a mass and volume basis respectively. And observing **Figure *47***, it can be seen that the greatest effect occurs in the moisture content equilibrium with an increase of 100% and 88% in relation to EU-C550, mass and volume basis.

With respect to **Figure *48***, comparing first with sand, there is an increase in plant-available water of 23%, 36% and 31% for EU-C600 volume percentages of 10%, 50% and 100%, respectively (the other volume percentage is sand).Comparing the values obtained for EU-C600 against Eu-C550, there is an increase of 13%, decrease of 6% and increase of 120% for volume bases of 10%, 50% and 100%.Thus EU-C600, is only not beneficial for the 50% mixture in relation to EU-550. However, this is because the plant-available water depends on the water retained for pF 2

and pF 4.2. That is, for the case of the 50% mixture, the wilting point value (maximum pressure) is higher for EU-C600, meaning that it retains more water for higher pressures, which leads to the conclusion that it has a larger intraporous structure than EU-C550.

Given these results, it can be concluded that the industrial process can be improved and optimized to obtain biochars with characteristics suitable for use in soils, in particular to improve their porous structure.

4.7. Technical – economic analysis: a qualitative approach

Regarding the results from section 4.5. although both biomasses and the respective biochars present positive effects in relation to water retention in sandy soils, it is necessary to discuss in relation to their feasibility in technical and economic terms. Having said that from an economic point of view it would not be profitable to put 50% of material in volume terms in relation to the soil (this analysis was only done to understand the parametric variation in relation to the volume amount used). Therefore, only mixtures with 10% volume are considered in this section.

From a technical economic point of view the parameters that have to be assessed are:

1. The effect and improvement that biomass and biochar has in terms of water retention in soil.
   Thus, considering this parameter, consulting **Table *18*** (for mixtures at 10%), it can be observed that for the parameter of plant available water θ_{paw}, for PS-Raw there is an increase of 17% in relation to sand while for PS-C600 there is an increase of 16%. While for Eucalyptus the increase in relation to sand is 20%,16% and 9% for EU-Raw, EU-AC and EU-C550, respectively.
   That said, with regard to the first criterion it can even be concluded that biomass increases the amount of water available although the difference is not very substantial, however these values are on a volume basis which means that for industrial applications a small difference in percentage points can mean a large amount of water.

2. The cost effectiveness of the process from getting the biomass through the process to getting the final product.
   Evaluating this point, obtaining raw biomass is significantly cheaper than obtaining biochar or activated biochar, because the costs associated with raw biomass, would be the pre-treatment (drying, milling, etc.) while for biochar would have to involve costs related to the more expensive thermochemical process. In addition, if activation is considered, it makes the process even more expensive due to the material needed to carry it out (either physical or chemical activation).

3. The yield of the thermochemical conversion process used, i.e., the final amount obtained compared to the initial amount.
   The yield of the process considered the raw biomass is much higher than the biochar, in biomass the yield will be very close to 100% while for biochar or activated carbon the yield will be much lower due to the release of volatile matter (**Figure *23*** and **Table *8***).

4. The durability (life span) of the additional element in the soil, since different conditions of conversion processes lead to different structures and consequently different life spans.
   For this point, raw biomass has a much less stable structure than biochar and its lifetime in the soil can be very short, while biochar can last a long time in the soil due to its rigid solid structure.
5. Additional effects that may interfere with soils other than water retention.
   Finally, biochar in case of having a high BET surface area can add cation exchange effect in soils, while for biomass this value is very low. And in addition, biochar can be considered as a means to sequester carbon [91]. However, it is necessary to highlight the complexity of the phenomenon and the multidisciplinary research requirements.

In general, the major disadvantage of biomass is its life span in the soil, which can be very short, but the availability of woody biomass in countries with high forestation is also abundant and could be replaced more regularly. This being said, it will be necessary to do further research and evaluate the factors that make the whole process more profitable.

5.Conclusions

The results of this thesis include the investigation of two biomasses, pine and eucalyptus, produced by different processes, laboratory (batch process) and industrial (continuous process) in order to investigate their porous structure, their behaviour in relation to water and together with the sand-based soil. Six materials were thus studied, raw pine (PS-Raw), biochar at 600ºC (PS-C600), activated pine biochar (PS-C600), raw eucalyptus (EU-Raw), eucalyptus biochar at 550ºC (EU-C550) and activated biochar (EU-AC).

From the results of the pine biochar production, it is concluded that the largest decrease (12.78%) in yield is affected at lower temperatures (300-400ºC), lowering this decrease as the temperature increases, due to the fact that the major constituents (cellulose, hemicellulose, lignin) of woody biomass decompose in these temperature ranges as can be concluded by thermogravimetric tests (TGA).

Regarding the activation process, it is concluded that its yield is low (11.79%) due to the reaction with CO2. The results of the approximate analysis show that the eucalyptus biochars have a higher amount of volatiles (20.3%), which indicates that the industrial process may not be optimized in relation to the slow pyrolysis parameters. From the analysis carried out on the functionality of the pine surfaces, a reduction of this functionality was observed with the increase of temperature. Regarding the porous structures evaluated, the BET tests showed that the activation process produced the biochar with the highest surface area (PS-AC) of 937 m^2g^{-1}, concluding that the temperature increase and consequent activation in pyrolysis processes have a positive effect on the specific area, providing most sites for nutrient adsorption, cation exchange and soil microbial. However, evaluating from the industrial point of view with large application, the PS-C600 (392 m^2g^{-1}) is the best choice from the technical-economic point of view even having the specific area lower than the activated one, because the yield is very low (11.79%) and the production costs very high (it requires more control, more time and introduction of new gases). Regarding pores of a scale greater than 4nm, it is concluded that most of the pores are based on the biological structure of the raw biomass (r=0.73 for pine materials), and the eucalyptus biochars showed a lower range of pores than the pine biochars, also verified in the SEM images. From the results of the moisture adsorption curves, it can be concluded that activation produces more activity sites that lead to greater water adsorption (0.13 cm^3/cm^3 and 0.17 g/g), not being possible to obtain clear conclusions regarding the eucalyptus since information on the functionality of their surfaces would be necessary. In the water holding capacity, there is a strong correlation (r=0.95) with the total pore volume, being noteworthy the swelling and extractives effects that lead the raw biomass to have results close to the biochars.

Regarding the water retention curves, there was an increase for all the measured pressure levels in relation to the control used (sand only), concluding that the intra-pores of biomass/biochar have a great influence due to capillary phenomena, with macropores having a greater influence for lower pressures and smaller pore sizes having a greater influence for higher pressures (wilting

point). For biomass the referred effects may exist. It was also found that there is no linearity between the percentage of biomass/biochar used, due precisely to the interporous-intraporous relationship between sand and biochar. Therefore, from a practical point of view, in order to optimize the plant available water, the ideal mixture will be between 10% and 50% so that the high retention value at the wilting point does not harm the amount of available water. Considering the mixtures, the greatest increase in plant-available water was 50% (PS-C600) for mixture on a 50% volume basis, and 20% (EU-Raw) on a 10% volume basis.

Making an analysis from the technical-economical point of view for pine with the purpose of application in industrial scales, evaluating the results for pine the PS-C600 at 50% presents an increase of 50% and the raw biomass PS-Raw at 50% presents an improvement of 20%. From an economic point of view, the raw biomass will be the best option since the costs are reduced compared to biochar, since it does not need to go through the thermochemical process. However, the stability and durability of biomass is much lower than that of biochar, besides biochar can provide other advantages such as cation exchange and used as a mean for carbon sequestration.

Finally, it is concluded that eucalyptus biochar can be enhanced by increasing its WHC (14% and 15%, mass and volume basis), moisture content equilibrium (100% and 80% mass and volume basis) and plant water available (120%, comparison with EU-C550).

5.1. Recommendation for further research

For the continuation of this work the following points are proposed:

1. To study the functional groups of both biomasses and biochars, namely those obtained through the industrial process. Using different methods such as Fourier-Transform infrared spectroscopy (FTIR) and X-ray photoelectron spectroscopy (XPS). As well as doing the chemical characterization of biomasses to quantify the effect of extractives.
2. For eucalyptus in the industrial process, several operational parameters (temperature, heating rate, residence time) can be varied in order to find the optimal conditions to obtain a biochar with a larger BET surface area.
3. For the laboratory process, vary the parameters during the physical activation, use steam instead of CO2 and compare with the specific area value obtained. Activate chemically and then analyse the yield of both processes in relation to the specific area obtained.
4. With a controlled atmosphere chamber, obtain for the various biomasses/biochars the equilibrium content moistures points for different relative humidities and thus obtain the different moisture sportion isotherm.
5. In the laboratory process, for the horizontal tube furnace, build a heat exchange system to use the gases released during the slow pyrolysis to maintain the temperature of the process itself.
6. For future research, activated carbons and biochars should be used for adsportion of specific compounds such as e.g., pharmaceuticals, heavy metals etc. to check its suitability for an industrial application.

7. Regarding the water retention curves, carry out the tests for more pressure points in order to obtain a more accurate fitting due to the greater number of points.
8. In this work, the experiment was done from a laboratory point of view and one of the future works will be to experiment with biomass/biochar at an industrial level in longer periods of more than 1 year and to prove the effect both in terms of water retention and in terms of nutrient and cation exchange effects. As well as exploring the effect on soils other than sandy (desert soils).
9. Carry out a quantitative Technical Economic Analysis in order to obtain the profitability of the process from the beginning to the end.
10. Consider different biomasses to be added to this work, not only woody biomasses but also herbaceous biomasses and animal/human waste biomass

6. References

[1] U.S. Energy Information Admnistration, “Internaltional Energy Outlook 2019,” *U.S. Energy Inf. Adm.*, vol. September, no. 09, pp. 25–150, 2019.

[2] J. Delbeke, A. Runge-Metzger, Y. Slingenberg, and J. Werksman, “The paris agreement,” *Towar. a Clim. Eur. Curbing Trend*, pp. 24–45, 2019, doi: 10.4324/9789276082569-2.

[3] S. R. Bull, “Renewable energy today and tomorrow,” *Proc. IEEE*, vol. 89, no. 8, pp. 1216–1226, 2001, doi: 10.1109/5.940290.

[4] B. Global, “Statistical Review of World Energy - Global,” *Br. Pet.*, 2020.

[5] D. Gielen, F. Boshell, D. Saygin, M. D. Bazilian, N. Wagner, and R. Gorini, “The role of renewable energy in the global energy transformation,” *Energy Strateg. Rev.*, vol. 24, no. June 2018, pp. 38–50, 2019, doi: 10.1016/j.esr.2019.01.006.

[6] International Renewable Energy Agency, *IRENA (2019), Global Energy Transformation: A Roadmap to 2050*. 2019.

[7] “Fuels from Biomass,” in *Biohydrogen: For Future Engine Fuel Demands*, London: Springer London, 2009, pp. 43–59.

[8] R. A. Houghton, F. Hall, and S. J. Goetz, “Importance of biomass in the global carbon cycle,” *J. Geophys. Res. Biogeosciences*, vol. 114, no. 3, 2009, doi: 10.1029/2009JG000935.

[9] United Nations Environment Programme, “Converting Waste Agricultural Biomass into a Resource - Compendium of Technologies,” 2009.

[10] M. A. Perea-Moreno, E. Samerón-Manzano, and A. J. Perea-Moreno, “Biomass as renewable energy: Worldwide research trends,” *Sustain.*, vol. 11, no. 3, pp. 1–21, 2019, doi: 10.3390/su11030863.

[11] The World Bank, “Water in Agriculture - World Bank,” 2020. [Online]. Available: https://www.worldbank.org/en/topic/water-in-agriculture#1.

[12] S. V. Vassilev, D. Baxter, L. K. Andersen, C. G. Vassileva, and T. J. Morgan, “An overview of the organic and inorganic phase composition of biomass,” *Fuel*, vol. 94, pp. 1–33, 2012, doi: 10.1016/j.fuel.2011.09.030.

[13] P. Basu, “Chapter 3 - Biomass Characteristics,” in *Biomass Gasification, Pyrolysis and Torrefaction (Second Edition)*, Second Edi., P. Basu, Ed. Boston: Academic Press, 2013, pp. 47–86.

[14] F. Shafizadeh, “Introduction to pyrolysis of biomass,” *J. Anal. Appl. Pyrolysis*, vol. 3, no. 4, pp. 283–305, 1982, doi: https://doi.org/10.1016/0165-2370(82)80017-X.

[15] A. Anca-couce, “Reaction mechanisms and multi-scale modelling of lignocellulosic biomass pyrolysis,” *Prog. Energy Combust. Sci.*, vol. 53, no. 2016, pp. 41–79, 2020, doi: 10.1016/j.pecs.2015.10.002.

[16] D. M. Alonso, S. G. Wettstein, and J. A. Dumesic, “Bimetallic catalysts for upgrading of biomass to fuels and chemicals,” *Chem. Soc. Rev.*, vol. 41, no. 24, pp. 8075–8098, 2012, doi: 10.1039/c2cs35188a.

[17] P. Basu, “Chapter 1 - Introduction,” in *Biomass Gasification, Pyrolysis and Torrefaction*

(Second Edition), Second Edi., P. Basu, Ed. Boston: Academic Press, 2013, pp. 1–27.

[18] R. C. Saxena, D. K. Adhikari, and H. B. Goyal, “Biomass-based energy fuel through biochemical routes: A review,” *Renew. Sustain. Energy Rev.*, vol. 13, no. 1, pp. 167–178, 2009, doi: 10.1016/j.rser.2007.07.011.

[19] P. Basu, “Chapter 5 - Pyrolysis,” in *Biomass Gasification, Pyrolysis and Torrefaction (Second Edition)*, Second Edi., P. Basu, Ed. Boston: Academic Press, 2013, pp. 147–176.

[20] P. Basu, “Chapter 7 - Gasification Theory,” in *Biomass Gasification, Pyrolysis and Torrefaction (Second Edition)*, Second Edi., P. Basu, Ed. Boston: Academic Press, 2013, pp. 199–248.

[21] S. Zhou, B. Pecha, M. van Kuppevelt, A. G. McDonald, and M. Garcia-Perez, “Slow and fast pyrolysis of Douglas-fir lignin: Importance of liquid-intermediate formation on the distribution of products,” *Biomass and Bioenergy*, vol. 66, pp. 398–409, 2014, doi: https://doi.org/10.1016/j.biombioe.2014.03.064.

[22] A. V. Bridgwater, “Review of fast pyrolysis of biomass and product upgrading,” *Biomass and Bioenergy*, vol. 38, pp. 68–94, 2012, doi: 10.1016/j.biombioe.2011.01.048.

[23] M. Van de Velden, J. Baeyens, A. Brems, B. Janssens, and R. Dewil, “Fundamentals, kinetics and endothermicity of the biomass pyrolysis reaction,” *Renew. Energy*, vol. 35, no. 1, pp. 232–242, 2010, doi: https://doi.org/10.1016/j.renene.2009.04.019.

[24] F. Ronsse, R. W. Nachenius, and W. Prins, *Carbonization of Biomass*. Elsevier B.V., 2015.

[25] A. Demirbas, “The influence of temperature on the yields of compounds existing in bio-oils obtained from biomass samples via pyrolysis,” *Fuel Process. Technol.*, vol. 88, no. 6, pp. 591–597, 2007, doi: https://doi.org/10.1016/j.fuproc.2007.01.010.

[26] A. Demirbas, “Effects of temperature and particle size on bio-char yield from pyrolysis of agricultural residues,” *J. Anal. Appl. Pyrolysis*, vol. 72, no. 2, pp. 243–248, 2004, doi: https://doi.org/10.1016/j.jaap.2004.07.003.

[27] M. Guerrero, M. P. Ruiz, M. U. Alzueta, R. Bilbao, and A. Millera, “Pyrolysis of eucalyptus at different heating rates: studies of char characterization and oxidative reactivity,” *J. Anal. Appl. Pyrolysis*, vol. 74, no. 1, pp. 307–314, 2005, doi: https://doi.org/10.1016/j.jaap.2004.12.008.

[28] G. KUMAR, A. K. PANDA, and R. K. SINGH, “Optimization of process for the production of bio-oil from eucalyptus wood,” *J. Fuel Chem. Technol.*, vol. 38, no. 2, pp. 162–167, 2010, doi: https://doi.org/10.1016/S1872-5813(10)60028-X.

[29] K. Weber and P. Quicker, “Properties of biochar,” vol. 217, no. September 2017, pp. 240–261, 2018, doi: 10.1016/j.fuel.2017.12.054.

[30] M. Kumar, R. C. Gupta, and T. Sharma, “Effects of carbonisation conditions on the yield and chemical composition of Acacia and Eucalyptus wood chars,” *Biomass and Bioenergy*, vol. 3, no. 6, pp. 411–417, 1992, doi: https://doi.org/10.1016/0961-9534(92)90037-Q.

[31] M. Heidari, A. Dutta, B. Acharya, and S. Mahmud, “A review of the current knowledge and challenges of hydrothermal carbonization for biomass conversion,” *J. Energy Inst.*, vol. 92, no. 6, pp. 1779–1799, 2019, doi: 10.1016/j.joei.2018.12.003.

[32] A. V Bridgwater, “Renewable fuels and chemicals by thermal processing of biomass,”

Chem. Eng. J., vol. 91, no. 2, pp. 87–102, 2003, doi: https://doi.org/10.1016/S1385-8947(02)00142-0.

[33] J. Lehmann and S. Joseph, "Biochar for environmental management: Science and technology," *Biochar Environ. Manag. Sci. Technol.*, pp. 1–416, 2012, doi: 10.4324/9781849770552.

[34] E. S. Krull, C. W. Swanston, J. O. Skjemstad, and J. A. McGowan, "Importance of charcoal in determining the age and chemistry of organic carbon in surface soils," *J. Geophys. Res. Biogeosciences*, vol. 111, no. 4, pp. 1–9, 2006, doi: 10.1029/2006JG000194.

[35] J. Lee, B. Hawkins, D. Day, and D. Reicosky, "Sustainability: The capacity of smokeless biomass pyrolysis for energy production, global carbon capture and sequestration," *Energy Environ. Sci.*, vol. 3, 2010, doi: 10.1039/C004561F.

[36] B. L. C. Pereira, A. de Angélica de C.O. Carneiro, A. M. M. L. Carvalho, J. L. Colodette, A. C. Oliveira, and M. P. F. Fontes, "Influence of Chemical Composition of Eucalyptus Wood on Gravimetric Yield and Charcoal Properties," *BioResources*, vol. 8, no. 2, pp. 4574–4592, 2013.

[37] D. W. VAN KREVELEN, "Graphical-statistical method for the study of structure and reaction processes of coal," *Fuel*, vol. 29, pp. 269–284, 1950.

[38] D. Rutherford, R. Wershaw, and L. Cox, "Changes in Composition and Porosity Occurring During the Thermal Degradation of Wood and Wood Components: U.S. Geological Survey Scientific Investigations Report 2004-5292," p. 79, 2005.

[39] R. Conti, A. G. Rombolà, A. Modelli, C. Torri, and D. Fabbri, "Evaluation of the thermal and environmental stability of switchgrass biochars by Py-GC-MS," *J. Anal. Appl. Pyrolysis*, vol. 110, no. 1, pp. 239–247, 2014, doi: 10.1016/j.jaap.2014.09.010.

[40] S. V. Vassilev, D. Baxter, L. K. Andersen, and C. G. Vassileva, "An overview of the chemical composition of biomass," *Fuel*, vol. 89, no. 5, pp. 913–933, 2010, doi: 10.1016/j.fuel.2009.10.022.

[41] Y. Wang, Y. Hu, X. Zhao, S. Wang, and G. Xing, "Comparisons of biochar properties from wood material and crop residues at different temperatures and residence times," *Energy and Fuels*, vol. 27, no. 10, pp. 5890–5899, 2013, doi: 10.1021/ef400972z.

[42] S. V. Vassilev, D. Baxter, L. K. Andersen, and C. G. Vassileva, "An overview of the composition and application of biomass ash. Part 1. Phase-mineral and chemical composition and classification," *Fuel*, vol. 105, pp. 40–76, 2013, doi: 10.1016/j.fuel.2012.09.041.

[43] M. Plötze and P. Niemz, "Porosity and pore size distribution of different wood types as determined by mercury intrusion porosimetry," *Eur. J. Wood Wood Prod.*, vol. 69, no. 4, pp. 649–657, 2011, doi: 10.1007/s00107-010-0504-0.

[44] L. Pulido-Novicio, T. Hata, Y. Kurimoto, S. Doi, S. Ishihara, and Y. Imamura, "Adsorption capacities and related characteristics of wood charcoals carbonized using a one-step or two-step process," *J. Wood Sci.*, vol. 47, no. 1, pp. 48–57, 2001, doi: 10.1007/BF00776645.

[45] J. Lehmann, "Bio-energy in the black," *Front. Ecol. Environ.*, vol. 5, no. 7, pp. 381–387, 2007, doi: 10.1890/1540-9295(2007)5[381:BITB]2.0.CO;2.

[46] C. E. Brewer *et al.*, "New approaches to measuring biochar density and porosity," *Biomass*

and Bioenergy, vol. 66, pp. 176–185, 2014, doi: 10.1016/j.biombioe.2014.03.059.

[47] L. Leng *et al.*, “An overview on engineering the surface area and porosity of biochar,” *Sci. Total Environ.*, vol. 763, p. 144204, 2021, doi: 10.1016/j.scitotenv.2020.144204.

[48] F. R. Oliveira, A. K. Patel, D. P. Jaisi, S. Adhikari, H. Lu, and S. K. Khanal, “Environmental application of biochar: Current status and perspectives,” *Bioresour. Technol.*, vol. 246, no. July, pp. 110–122, 2017, doi: 10.1016/j.biortech.2017.08.122.

[49] M. Carrier, T. Hugo, J. Gorgens, and H. Knoetze, “Comparison of slow and vacuum pyrolysis of sugar cane bagasse,” *J. Anal. Appl. Pyrolysis*, vol. 90, no. 1, pp. 18–26, 2011, doi: https://doi.org/10.1016/j.jaap.2010.10.001.

[50] A. K. Sakhiya, A. Anand, and P. Kaushal, *Production, activation, and applications of biochar in recent times*, vol. 2, no. 3. Springer Singapore, 2020.

[51] J. Zhang, Q. Chen, and C. You, “Biochar Effect on Water Evaporation and Hydraulic Conductivity in Sandy Soil,” *Pedosphere*, vol. 26, no. 2, pp. 265–272, 2016, doi: 10.1016/S1002-0160(15)60041-8.

[52] H. Jiang, “Desertification in China: Problems with Policies and Perceptions,” 2010, pp. 13–40.

[53] D. A. Laird, P. Fleming, D. D. Davis, R. Horton, B. Wang, and D. L. Karlen, “Impact of biochar amendments on the quality of a typical Midwestern agricultural soil,” *Geoderma*, vol. 158, no. 3, pp. 443–449, 2010, doi: https://doi.org/10.1016/j.geoderma.2010.05.013.

[54] Y. Wang, R. Yin, and R. Liu, “Characterization of biochar from fast pyrolysis and its effect on chemical properties of the tea garden soil,” *J. Anal. Appl. Pyrolysis*, vol. 110, pp. 375–381, 2014, doi: https://doi.org/10.1016/j.jaap.2014.10.006.

[55] J. Zhang and C. You, “Water holding capacity and absorption properties of wood chars,” *Energy and Fuels*, vol. 27, no. 5, pp. 2643–2648, 2013, doi: 10.1021/ef4000769.

[56] Z. Liu, B. Dugan, C. A. Masiello, and H. M. Gonnermann, “Biochar particle size, shape, and porosity act together to influence soil water properties,” *PLoS One*, vol. 12, no. 6, pp. 1–19, 2017, doi: 10.1371/journal.pone.0179079.

[57] C. Vittucci, “MICROWAVE ANALYSIS OF SOIL MOISTURE AND ITS IMPLICATION IN HYDROLOGY AND FOREST MONITORING,” 2015.

[58] S. Abel, A. Peters, S. Trinks, H. Schonsky, M. Facklam, and G. Wessolek, “Impact of biochar and hydrochar addition on water retention and water repellency of sandy soil,” *Geoderma*, vol. 202–203, pp. 183–191, 2013, doi: 10.1016/j.geoderma.2013.03.003.

[59] M. Gray, M. G. Johnson, M. I. Dragila, and M. Kleber, “Water uptake in biochars: The roles of porosity and hydrophobicity,” *Biomass and Bioenergy*, vol. 61, pp. 196–205, 2014, doi: 10.1016/j.biombioe.2013.12.010.

[60] F. Razzaghi, P. B. Obour, and E. Arthur, “Does biochar improve soil water retention? A systematic review and meta-analysis,” *Geoderma*, vol. 361, no. October 2019, p. 114055, 2020, doi: 10.1016/j.geoderma.2019.114055.

[61] C. Kosmas, N. G. Danalatos, J. Poesen, and B. Van Wesemael, “The effect of water vapour adsorption on soil moisture content under Mediterranean climatic conditions,” *Agric. Water Manag.*, vol. 36, no. 2, pp. 157–168, 1998, doi: 10.1016/S0378-3774(97)00050-4.

[62] United States Pharmacopeial Convention, “<786> Particle Size Distribution Estimation by Analytical Sieving,” *United States Pharmacop. Natl. Formul. 41*, vol. 30, no. 6, pp. 6970–6975, 2017.

[63] C. Grima-Olmedo, Ramírez-Gómez, D. Gómez-Limón, and C. Clemente-Jul, “Activated carbon from flash pyrolysis of eucalyptus residue,” *Heliyon*, vol. 2, no. 9, 2016, doi: 10.1016/j.heliyon.2016.e00155.

[64] T. Zhang, W. P. Walawender, L. T. Fan, M. Fan, D. Daugaard, and R. C. Brown, “Preparation of activated carbon from forest and agricultural residues through CO2 activation,” *Chem. Eng. J.*, vol. 105, no. 1–2, pp. 53–59, 2004, doi: 10.1016/j.cej.2004.06.011.

[65] A. F. Ferreira, J. P. Ribau, and M. Costa, “A decision support method for biochars characterization from carbonization of grape pomace,” *Biomass and Bioenergy*, vol. 145, no. December 2020, 2021, doi: 10.1016/j.biombioe.2020.105946.

[66] “No Title.” [Online]. Available: https://carbonationmachine.net/environmental-protection-characteristics-technical-advantages-municipal-solid-waste-carbonization-technology/.

[67] J. Parikh, S. A. Channiwala, and G. K. Ghosal, “A correlation for calculating HHV from proximate analysis of solid fuels,” *Fuel*, vol. 84, no. 5, pp. 487–494, 2005, doi: 10.1016/j.fuel.2004.10.010.

[68] M. Thommes *et al.*, “Physisorption of gases, with special reference to the evaluation of surface area and pore size distribution (IUPAC Technical Report),” *Pure Appl. Chem.*, vol. 87, 2015, doi: 10.1515/pac-2014-1117.

[69] M. Hajnos, “Porosimetry,” in *Encyclopedia of Agrophysics*, J. Gliński, J. Horabik, and J. Lipiec, Eds. Dordrecht: Springer Netherlands, 2011, pp. 647–650.

[70] D. Brabazon, “Chapter 18 - Nanocharacterization Techniques for Dental Implant Development,” in *Emerging Nanotechnologies in Dentistry*, K. Subramani and W. Ahmed, Eds. Boston: William Andrew Publishing, 2012, pp. 307–331.

[71] A. B. D. Nandiyanto, R. Oktiani, and R. Ragadhita, “How to read and interpret ftir spectroscope of organic material,” *Indones. J. Sci. Technol.*, vol. 4, no. 1, pp. 97–118, 2019, doi: 10.17509/ijost.v4i1.15806.

[72] W. E. L. Spiess and W. Wolf, “Critical evaluation of methods to determine moisture sorption isotherms,” in *Water activity: theory and applications to food*, Routledge, 2017, pp. 215–233.

[73] C. De Oliveira Romera, J. O. De Moraes, V. C. Zoldan, A. A. Pasa, and J. B. Laurindo, “Use of transient and steady-state methods and AFM technique for investigating the water transfer through starch-based films,” *J. Food Eng.*, vol. 109, no. 1, pp. 62–68, 2012, doi: 10.1016/j.jfoodeng.2011.09.033.

[74] M. M. R. Williams, “The mathematics of diffusion: By J. Crank. Clarendon Press, Oxford, £ 13.50, 1975, 414 pp.” Pergamon, 1977.

[75] S. Bikbulatova, A. Tahmasebi, Z. Zhang, S. K. Rish, and J. Yu, “Understanding water retention behavior and mechanism in bio-char,” *Fuel Process. Technol.*, vol. 169, no. September 2017, pp. 101–111, 2018, doi: 10.1016/j.fuproc.2017.09.025.

[76] M. T. van Genuchten, “A Closed-form Equation for Predicting the Hydraulic Conductivity of Unsaturated Soils,” *Soil Sci. Soc. Am. J.*, vol. 44, no. 5, pp. 892–898, 1980, doi:

https://doi.org/10.2136/sssaj1980.03615995004400050002x.

[77] W. Canal, A. Márcia, A. Oliveira, M. Magalhães, W. Cândido, and L. Fialho, “Comportamento térmico, emissão de gases condensáveis e não condensáveis no processo de carbonização da madeira,” *Pesqui. Florest. Bras.*, vol. 36, p. 261, 2016, doi: 10.4336/2016.pfb.36.87.1083.

[78] H. Yang, “Characteristics of hemicellulose , cellulose and lignin pyrolysis,” vol. 86, pp. 1781–1788, 2007, doi: 10.1016/j.fuel.2006.12.013.

[79] H. Marsh and F. Rodríguez-Reinoso, “CHAPTER 4 - Characterization of Activated Carbon,” in *Activated Carbon*, H. Marsh and F. Rodríguez-Reinoso, Eds. Oxford: Elsevier Science Ltd, 2006, pp. 143–242.

[80] S. Brunauer, P. H. Emmett, and E. Teller, “Adsorption of Gases in Multimolecular Layers,” *J. Am. Chem. Soc.*, vol. 60, no. 2, pp. 309–319, Feb. 1938, doi: 10.1021/ja01269a023.

[81] M. Keiluweit, P. S. Nico, M. Johnson, and M. Kleber, “Dynamic molecular structure of plant biomass-derived black carbon (biochar),” *Environ. Sci. Technol.*, vol. 44, no. 4, pp. 1247–1253, 2010, doi: 10.1021/es9031419.

[82] G. Chu *et al.*, “Phosphoric acid pretreatment enhances the specific surface areas of biochars by generation of micropores,” *Environ. Pollut.*, vol. 240, pp. 1–9, 2018, doi: 10.1016/j.envpol.2018.04.003.

[83] M. J. Fernandes *et al.*, “Evaluation of the adsorption potential of biochars prepared from forest and agri-food wastes for the removal of fluoxetine,” *Bioresour. Technol.*, vol. 292, p. 121973, 2019, doi: 10.1016/j.biortech.2019.121973.

[84] S. Mopoung and N. Dejang, “Activated carbon preparation from eucalyptus wood chips using continuous carbonization–steam activation process in a batch intermittent rotary kiln,” *Sci. Rep.*, vol. 11, no. 1, pp. 1–9, 2021, doi: 10.1038/s41598-021-93249-x.

[85] Y. Chun, G. Sheng, G. T. Chiou, and B. Xing, “Compositions and sorptive properties of crop residue-derived chars,” *Environ. Sci. Technol.*, vol. 38, no. 17, pp. 4649–4655, 2004, doi: 10.1021/es035034w.

[86] J. Wildman and F. Derbyshire, “Origins and functions of macroporosity in activated carbons from coal and wood precursors,” *Fuel*, vol. 70, no. 5, pp. 655–661, 1991, doi: https://doi.org/10.1016/0016-2361(91)90181-9.

[87] J. Alcañiz-Monge, A. Linares-Solano, and B. Rand, “Water adsorption on activated carbons: Study of water adsorption in micro- and mesopores,” *J. Phys. Chem. B*, vol. 105, no. 33, pp. 7998–8006, 2001, doi: 10.1021/jp010674b.

[88] U. Aslam, N. Ramzan, Z. Aslam, and T. Iqbal, “Enhancement of fuel characteristics of rice husk via torrefaction process,” no. October, 2019, doi: 10.1177/0734242X19838620.

[89] S. Yi, N. Y. Chang, and P. T. Imhoff, “Advances in Water Resources Predicting water retention of biochar-amended soil from independent measurements of biochar and soil properties,” vol. 142, no. February 2019, 2020, doi: 10.1016/j.advwatres.2020.103638.

[90] T. J. Kinney *et al.*, “Hydrologic properties of biochars produced at different temperatures,” *Biomass and Bioenergy*, vol. 41, pp. 34–43, 2012, doi: 10.1016/j.biombioe.2012.01.033.

[91] J. H. Windeatt, A. B. Ross, P. T. Williams, P. M. Forster, M. A. Nahil, and S. Singh, “Characteristics of biochars from crop residues: Potential for carbon sequestration and soil

amendment," *J. Environ. Manage.*, vol. 146, pp. 189–197, 2014, doi: 10.1016/j.jenvman.2014.08.003.

[92] R. Yin, R. Liu, Y. Mei, W. Fei, and X. Sun, "Characterization of bio-oil and bio-char obtained from sweet sorghum bagasse fast pyrolysis with fractional condensers," *Fuel*, vol. 112, pp. 96–104, 2013, doi: 10.1016/j.fuel.2013.04.090.

7.Appendix

List of figures

List of tables

7.1. Appendix A

Materials and Methods

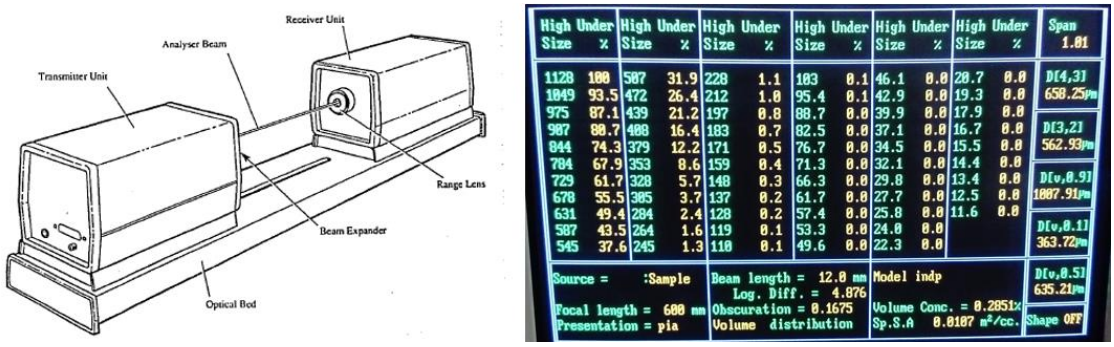

Appendix Figure 1- Scheme of Malvern Series 2600 (left) and sand particle size distribution (right).

Appendix Figure 2- Proximate analysis tests, volatile matter (left) and ash (right).

Appendix Figure 3- Perkinelmer spectrum two FT-IR spectrometers.

Appendix Figure 4- Crucibles with pine biochar resulting from the horizontal electrical furnace

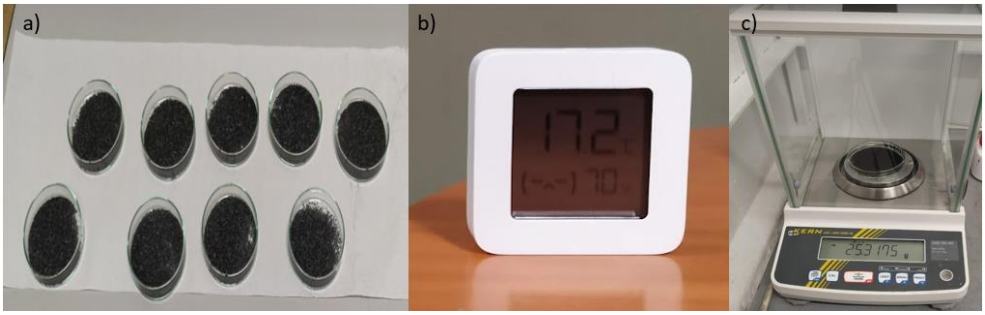

Appendix Figure 5- Equilibrium moisture content test, a) samples; b) hygrometer; c) precision balance Kern ABJ-NM ABS 80-4N.

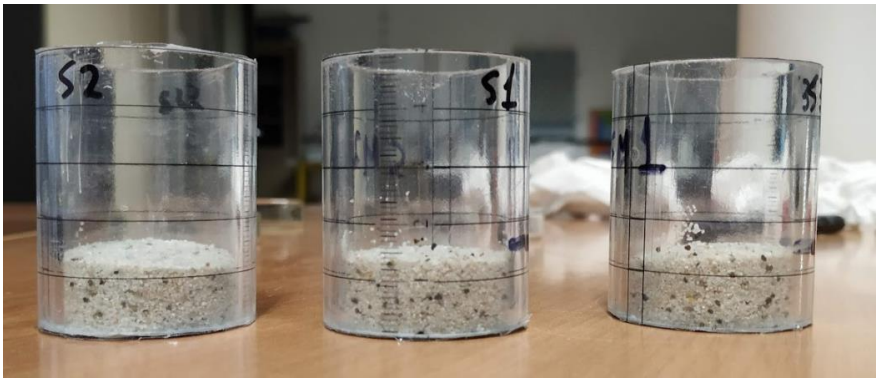

Appendix Figure 6- acrylic tubes used for water holding capacity tests

7.2. Appendix B

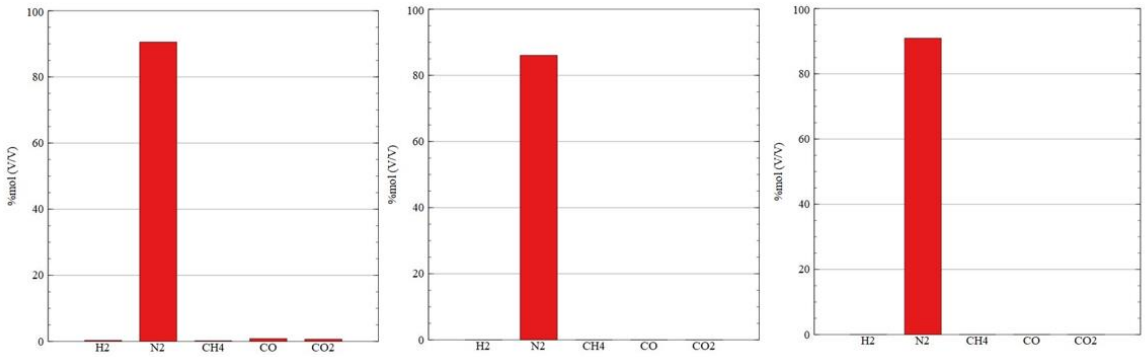

Appendix Figure 7- Gases released during the slow pyrolysis process for 20, 45, 75 min from left to right.

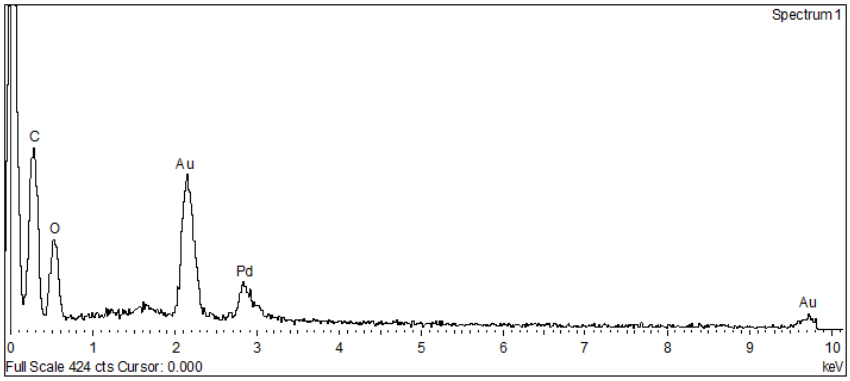

Appendix Figure 8- Elemental analysis for PS-Raw.

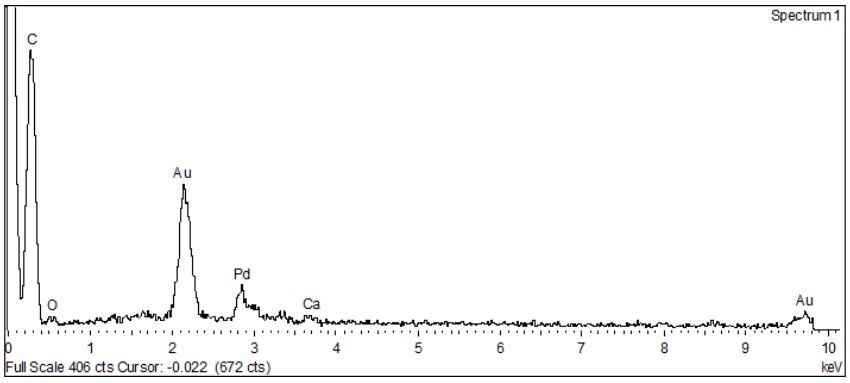

Appendix Figure 9- Elemental analysis for PS-C600.

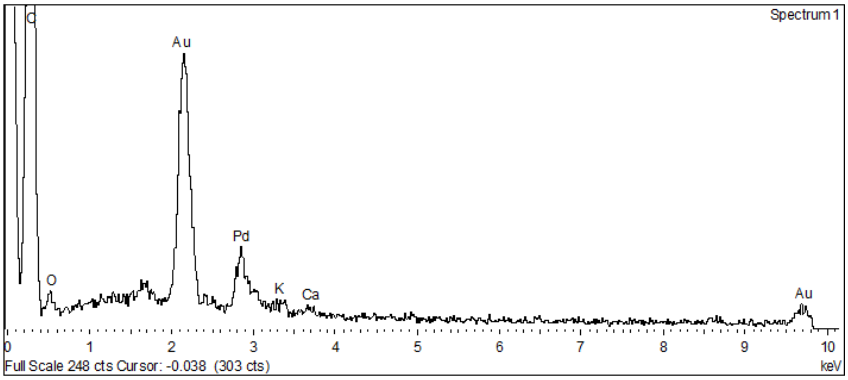

Appendix Figure 10- Elemental analysis for PS-AC.

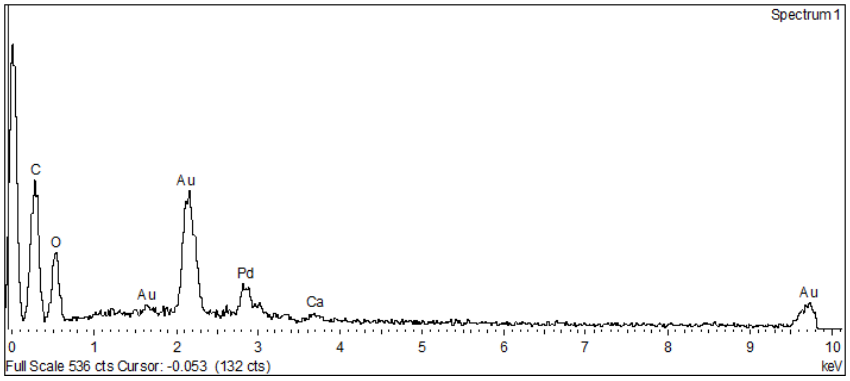

Appendix Figure 11- Elemental analysis for EU-Raw.

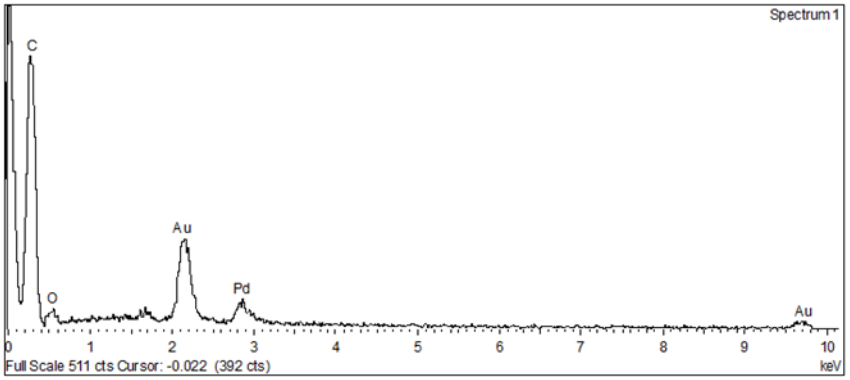

Appendix Figure 12-Elemental analysis for EU-C550.

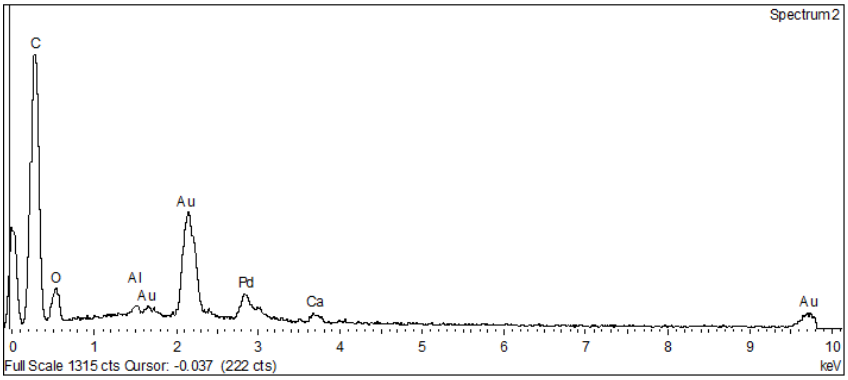

Appendix Figure 13- Elemental analysis for EU-AC.

Appendix Table 1- Pearson correlation between the variables of water retention curves and pore volume per pore size, for mixtures with 10% element volume.

10%	θs[cm3/cm3]	θfc[cm3/cm3]	θpaw[cm3/cm3]	θwp[cm3/cm3]
θ_s[cm^3/cm^3]	1.00			
θ_{fc}[cm3/cm3]	-0.94	1.00		
θ_{paw}[cm3/cm3]	0.30	0.05	1.00	
θ_{wp}[cm3/cm3]	-0.75	0.48	-0.86	1.00
Total Pore Volume [mL/g]	0.99	-0.88	0.42	-0.83
Macropores Volume [mL/g]	0.99	-0.89	0.40	-0.82
Mesopores Volume [mL/g]	1.00	-0.90	0.39	-0.81
Micropores Volume [mL/g]	0.99	-0.90	0.40	-0.82
Ultramicropores Volume [mL/g]	-0.76	0.94	0.39	0.14
Cryptopores Volume [mL/g]	-1.00	0.93	-0.31	0.76
Specific Area BET[m2/g]	0.94	-0.77	0.60	-0.93

Appendix Table 2- Pearson correlation between the variables of water retention curves and pore volume per pore size, for mixtures with 50% element volume.

50%	θs[cm3/cm3]	θfc[cm3/cm3]	θpaw[cm3/cm3]	θwp[cm3/cm3]
θ_s[cm^3/cm^3]	1.00			
θ_{fc}[cm3/cm3]	0.94	1.00		
θ_{paw}[cm3/cm3]	0.18	-0.16	1.00	
θ_{wp}[cm3/cm3]	0.19	0.52	-0.93	1.00
Total Pore Volume [mL/g]	0.92	0.74	0.54	-0.20
Macropores Volume [mL/g]	0.92	0.72	0.56	-0.22
Mesopores Volume [mL/g]	0.91	0.71	0.58	-0.24
Micropores Volume [mL/g]	0.92	0.72	0.56	-0.22
Ultramicropores Volume [mL/g]	-0.33	0.01	-0.99	0.86
Cryptopores Volume [mL/g]	-0.87	-0.65	-0.64	0.31

Specific Area BET[m2/g]	0.98	0.86	0.36	0.01

Appendix Table 3 Pearson correlation between the variables of water retention curves and pore volume per pore size, for elements.

100%	**θs[cm3/cm3]**	**θfc[cm3/cm3]**	**θpaw[cm3/cm3]**	**θwp[cm3/cm3]**
θs[cm3/cm3]	1.00			
θfc[cm3/cm3]	0.77	1.00		
θpaw[cm3/cm3]	0.94	0.51	1.00	
θwp[cm3/cm3]	0.03	0.67	-0.30	1.00
Total Pore Volume [mL/g]	0.95	0.52	1.00	-0.29
Macropores Volume [mL/g]	0.94	0.50	1.00	-0.31
Mesopores Volume [mL/g]	0.93	0.48	1.00	-0.33
Micropores Volume [mL/g]	0.94	0.50	1.00	-0.32
Ultramicropores Volume [mL/g]	-0.39	0.29	-0.67	0.91
Cryptopores Volume [mL/g]	-0.90	-0.41	-0.99	0.41
Specific Area BET[m2/g]	0.99	0.68	0.98	-0.10

Appendix Table 4- FTIR band interpretation according to the wavenumber(cm^{-1}) [92]

Wave number (cm^{-1})	**Functional groups**
3355	O-H stretching vibration
2935	C-H stretching vibration
2075	C≡C stretching vibration
1735–1705	Aromatic carbonyl/carboxyl C═O stretching
1605	C═C stretching vibration
1515	Aromatic C═C ring stretching
1445	Aliphatic CH_2 deformation
1370–1385	Aliphatic CH_3 deformation
1225–1270	Aromatic C-H stretching
1110	Ketone or ester bonding
1050	Aliphatic ether C-O and alcohol C-O stretching
840–885	Aromatic C-H out of plane deformation
760	Adjacent aromatic C-H deformation
615	Phenol O-H out of plane deformation

7.3. Appendix C

Mercury Porosimetry Reports

LA - REQUIMTE

AutoPore IV 9500 V1.09 Serial: 622 Port: 2/1 Page 1

Sample: 001-719 Pine Sawdust
Operator: 21P006r
Submitter: Rodrigo Santos / IST
File: C:\9500\DATA\001-719.SMP

LP Analysis Time: 03-05-2021 9:00:41
HP Analysis Time: 03-05-2021 13:02:59
Report Time: 07-05-2021 1:17:15

Sample Weight: 0.0734 g
Correction Type: None
Show Neg. Int: No

Summary Report

Penetrometer parameters

Penetrometer:	0660 - (14) 3 Bulb, 0.412 Stem, Powder		
Pen. Constant:	11.117 µL/pF	Pen. Weight:	62.7966 g
Stem Volume:	0.4120 mL	Max. Head Pressure:	4.6800 psia
Pen. Volume:	3.2068 mL	Assembly Weight:	103.0852 g

Hg Parameters

Adv. Contact Angle:	140.000 degrees	Rec. Contact Angle:	125.000 degrees
Hg Surface Tension:	480.000 dynes/cm	Hg Density:	13.5335 g/mL

User Parameters

Param 1:	0.000	Param 2:	0.000	Param 3:	0.000

Low Pressure:

Evacuation Pressure:	50 µmHg
Evacuation Time:	5 mins
Mercury Filling Pressure:	0.54 psia
Equilibration Time:	20 secs
Maximum Intrusion Volume:	100.000 mL/g

High Pressure:

Equilibration Time:	20 secs
Maximum Intrusion Volume:	100.000 mL/g

No Blank Correction

(From Pressure 0.50 to 33000.00 psia)

Intrusion Data Summary

Total Intrusion Volume =	2.4662 mL/g
Total Pore Area =	0.473 m²/g
Median Pore Diameter (Volume) =	34.8184 µm
Median Pore Diameter (Area) =	11.0531 µm
Average Pore Diameter (4V/A) =	20.8339 µm
Bulk Density at 0.54 psia =	0.3120 g/mL
Apparent (skeletal) Density =	1.3529 g/mL
Porosity =	76.9401 %
Stem Volume Used =	44 %

Appendix Figure 14- Mercury porosimetry report for PS-Raw

LA - REQUIMTE

AutoPore IV 9500 V1.09 Serial: 622 Port: 2/1 Page 1

Sample: 001-721 BIOCHAR Pine Sawdust
Operator: 21P006
Submitter: Rodrigo Santos / IST
File: C:\9500\DATA\001-721.SMP

LP Analysis Time: 06-05-2021 23:29:59
HP Analysis Time: 07-05-2021 1:03:01
Report Time: 07-05-2021 1:03:01

Sample Weight: 0.0391 g
Correction Type: None
Show Neg. Int: No

Summary Report

Penetrometer parameters

Penetrometer:	0660 - (14) 3 Bulb, 0.412 Stem, Powder		
Pen. Constant:	11.117 µL/pF	Pen. Weight:	62.7321 g
Stem Volume:	0.4120 mL	Max. Head Pressure:	4.6800 psia
Pen. Volume:	3.2068 mL	Assembly Weight:	102.2130 g

Hg Parameters

Adv. Contact Angle:	140.000 degrees	Rec. Contact Angle:	125.000 degrees
Hg Surface Tension:	480.000 dynes/cm	Hg Density:	13.5335 g/mL

User Parameters

Param 1:	0.000	Param 2:	0.000	Param 3:	0.000

Low Pressure:

Evacuation Pressure:	50 µmHg
Evacuation Time:	5 mins
Mercury Filling Pressure:	0.55 psia
Equilibration Time:	20 secs
Maximum Intrusion Volume:	100.000 mL/g

High Pressure:

Equilibration Time:	20 secs
Maximum Intrusion Volume:	100.000 mL/g

No Blank Correction

(From Pressure 0.50 to 33000.00 psia)

Intrusion Data Summary

Total Intrusion Volume =	6.6313 mL/g
Total Pore Area =	1.413 m²/g
Median Pore Diameter (Volume) =	76.2206 µm
Median Pore Diameter (Area) =	8.0420 µm
Average Pore Diameter (4V/A) =	18.7691 µm
Bulk Density at 0.55 psia =	0.1337 g/mL
Apparent (skeletal) Density =	1.1801 g/mL
Porosity =	88.6691 %
Stem Volume Used =	63 %

Appendix Figure 15- Mercury porosimetry report for PS-C600

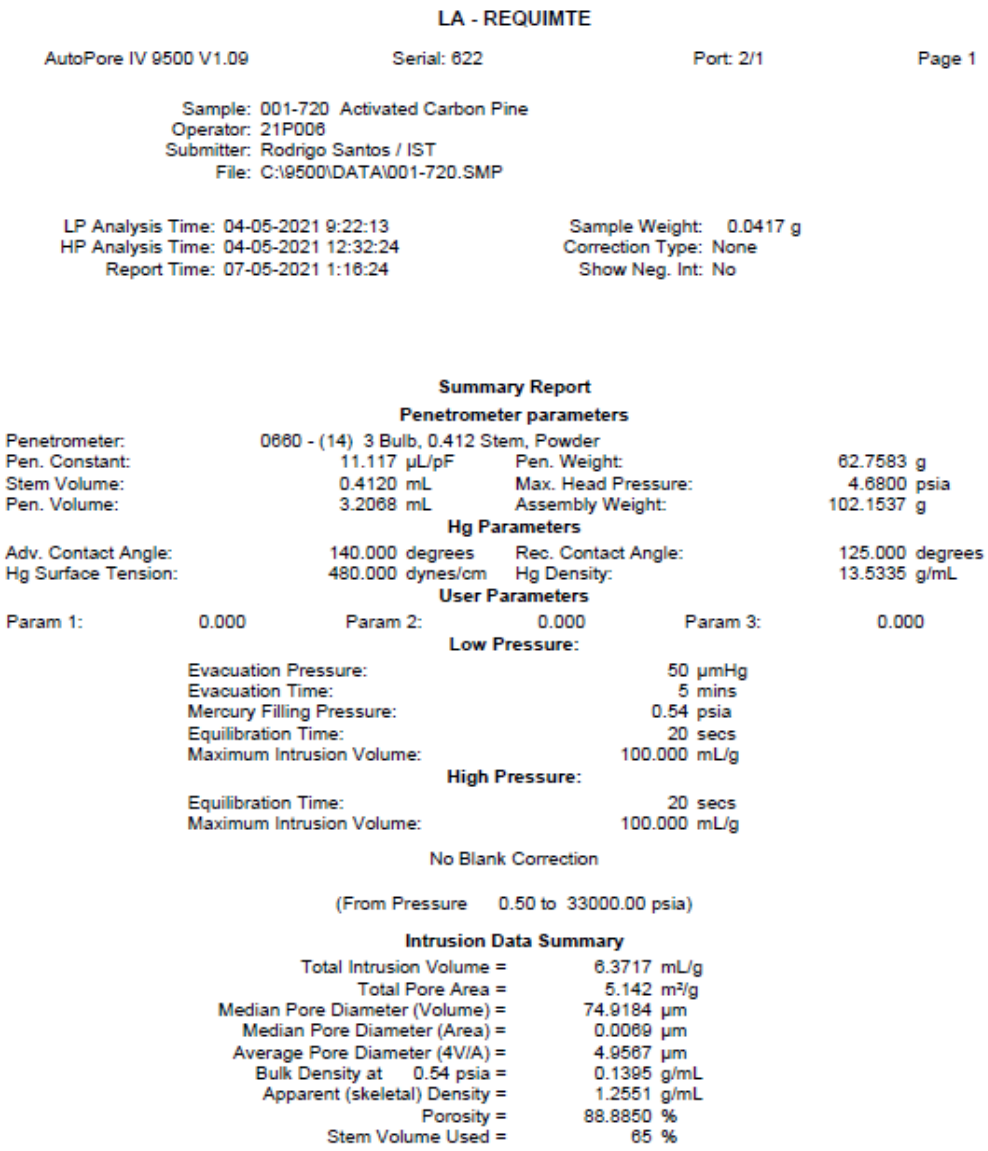

LA - REQUIMTE

AutoPore IV 9500 V1.09 Serial: 622 Port: 2/1 Page 1

Sample: 001-720 Activated Carbon Pine
Operator: 21P006
Submitter: Rodrigo Santos / IST
File: C:\9500\DATA\001-720.SMP

LP Analysis Time: 04-05-2021 9:22:13
HP Analysis Time: 04-05-2021 12:32:24
Report Time: 07-05-2021 1:16:24

Sample Weight: 0.0417 g
Correction Type: None
Show Neg. Int: No

Summary Report

Penetrometer parameters

Penetrometer:	0660 - (14) 3 Bulb, 0.412 Stem, Powder		
Pen. Constant:	11.117 µL/pF	Pen. Weight:	62.7583 g
Stem Volume:	0.4120 mL	Max. Head Pressure:	4.6800 psia
Pen. Volume:	3.2068 mL	Assembly Weight:	102.1537 g

Hg Parameters

Adv. Contact Angle:	140.000 degrees	Rec. Contact Angle:	125.000 degrees
Hg Surface Tension:	480.000 dynes/cm	Hg Density:	13.5335 g/mL

User Parameters

Param 1:	0.000	Param 2:	0.000	Param 3:	0.000

Low Pressure:

Evacuation Pressure:	50 µmHg
Evacuation Time:	5 mins
Mercury Filling Pressure:	0.54 psia
Equilibration Time:	20 secs
Maximum Intrusion Volume:	100.000 mL/g

High Pressure:

Equilibration Time:	20 secs
Maximum Intrusion Volume:	100.000 mL/g

No Blank Correction

(From Pressure 0.50 to 33000.00 psia)

Intrusion Data Summary

Total Intrusion Volume =	6.3717 mL/g
Total Pore Area =	5.142 m²/g
Median Pore Diameter (Volume) =	74.9184 µm
Median Pore Diameter (Area) =	0.0069 µm
Average Pore Diameter (4V/A) =	4.9567 µm
Bulk Density at 0.54 psia =	0.1395 g/mL
Apparent (skeletal) Density =	1.2551 g/mL
Porosity =	88.8850 %
Stem Volume Used =	65 %

Appendix Figure 16 -Mercury porosimetry report for PS-AC

LA - REQUIMTE

AutoPore IV 9500 V1.09 Serial: 622 Port: 2/1 Page 1

Sample: 001-725 Eucalipto Saw
Operator: 21P008
Submitter: Rodrigo Santos / IST
File: C:\9500\DATA\001-725.SMP

LP Analysis Time: 08-05-2021 23:54:36
HP Analysis Time: 09-05-2021 1:18:01
Report Time: 09-05-2021 1:18:01

Sample Weight: 0.1567 g
Correction Type: None
Show Neg. Int: No

Summary Report

Penetrometer parameters

Penetrometer:	0660 - (14) 3 Bulb, 0.412 Stem, Powder		
Pen. Constant:	11.117 µL/pF	Pen. Weight:	62.7910 g
Stem Volume:	0.4120 mL	Max. Head Pressure:	4.6800 psia
Pen. Volume:	3.2068 mL	Assembly Weight:	103.5873 g

Hg Parameters

Adv. Contact Angle:	140.000 degrees	Rec. Contact Angle:	125.000 degrees
Hg Surface Tension:	480.000 dynes/cm	Hg Density:	13.5335 g/mL

User Parameters

Param 1:	0.000	Param 2:	0.000	Param 3:	0.000

Low Pressure:

Evacuation Pressure:	50 µmHg
Evacuation Time:	5 mins
Mercury Filling Pressure:	0.54 psia
Equilibration Time:	20 secs
Maximum Intrusion Volume:	100.000 mL/g

High Pressure:

Equilibration Time:	20 secs
Maximum Intrusion Volume:	100.000 mL/g

No Blank Correction

(From Pressure 0.50 to 33000.00 psia)

Intrusion Data Summary

Total Intrusion Volume =	0.6686 mL/g
Total Pore Area =	10.951 m²/g
Median Pore Diameter (Volume) =	11.2703 µm
Median Pore Diameter (Area) =	0.0138 µm
Average Pore Diameter (4V/A) =	0.2442 µm
Bulk Density at 0.54 psia =	0.7685 g/mL
Apparent (skeletal) Density =	1.5807 g/mL
Porosity =	51.3828 %
Stem Volume Used =	26 %

Appendix Figure 17- Mercury porosimetry report for EU-Raw

LA - REQUIMTE

AutoPore IV 9500 V1.09 Serial: 622 Port: 2/1 Page 1

Sample: 001-717 BIOCHAR EUCALIPTO
Operator: 21P006r
Submitter: Rodrigo Santos / IST
File: C:\9500\DATA\001-717.SMP

LP Analysis Time: 02-05-2021 13:39:08
HP Analysis Time: 02-05-2021 15:03:16
Report Time: 07-05-2021 1:17:15

Sample Weight: 0.1086 g
Correction Type: None
Show Neg. Int: No

Summary Report

Penetrometer parameters

Penetrometer:	0660 - (14) 3 Bulb, 0.412 Stem, Powder				
Pen. Constant:	11.117	µL/pF	Pen. Weight:	62.7350	g
Stem Volume:	0.4120	mL	Max. Head Pressure:	4.6800	psia
Pen. Volume:	3.2068	mL	Assembly Weight:	102.9930	g

Hg Parameters

Adv. Contact Angle:	140.000	degrees	Rec. Contact Angle:	125.000	degrees
Hg Surface Tension:	480.000	dynes/cm	Hg Density:	13.5335	g/mL

User Parameters

Param 1:	0.000	Param 2:	0.000	Param 3:	0.000

Low Pressure:

Evacuation Pressure:	50	µmHg
Evacuation Time:	5	mins
Mercury Filling Pressure:	0.54	psia
Equilibration Time:	20	secs
Maximum Intrusion Volume:	100.000	mL/g

High Pressure:

Equilibration Time:	20	secs
Maximum Intrusion Volume:	100.000	mL/g

No Blank Correction

(From Pressure 0.50 to 33000.00 psia)

Intrusion Data Summary

Total Intrusion Volume =	1.5086	mL/g
Total Pore Area =	30.517	m²/g
Median Pore Diameter (Volume) =	14.7940	µm
Median Pore Diameter (Area) =	0.0205	µm
Average Pore Diameter (4V/A) =	0.1977	µm
Bulk Density at 0.54 psia =	0.4523	g/mL
Apparent (skeletal) Density =	1.4234	g/mL
Porosity =	68.2272	%
Stem Volume Used =	40	%

Appendix Figure 18- Mercury porosimetry report for EU-C550

LA - REQUIMTE

AutoPore IV 9500 V1.09 Serial: 622 Port: 2/1 Page 1

Sample: 001-726 Eucalipto Ativado
Operator: 21P008
Submitter: Rodrigo Santos / IST
File: C:\9500\DATA\001-726.SMP

LP Analysis Time: 09-05-2021 23:03:28
HP Analysis Time: 10-05-2021 2:34:13
Report Time: 10-05-2021 2:34:13

Sample Weight: 0.1080 g
Correction Type: None
Show Neg. Int: No

Summary Report

Penetrometer parameters

Penetrometer:	0660 - (14) 3 Bulb, 0.412 Stem, Powder		
Pen. Constant:	11.117 µL/pF	Pen. Weight:	62.8161 g
Stem Volume:	0.4120 mL	Max. Head Pressure:	4.6800 psia
Pen. Volume:	3.2068 mL	Assembly Weight:	102.5592 g

Hg Parameters

Adv. Contact Angle:	140.000 degrees	Rec. Contact Angle:	125.000 degrees
Hg Surface Tension:	480.000 dynes/cm	Hg Density:	13.5335 g/mL

User Parameters

Param 1:	0.000	Param 2:	0.000	Param 3:	0.000

Low Pressure:

Evacuation Pressure:	50 µmHg
Evacuation Time:	5 mins
Mercury Filling Pressure:	0.55 psia
Equilibration Time:	20 secs
Maximum Intrusion Volume:	100.000 mL/g

High Pressure:

Equilibration Time:	20 secs
Maximum Intrusion Volume:	100.000 mL/g

No Blank Correction

(From Pressure 0.50 to 33000.00 psia)

Intrusion Data Summary

Total Intrusion Volume =	1.7969	mL/g
Total Pore Area =	32.213	m²/g
Median Pore Diameter (Volume) =	11.0217	µm
Median Pore Diameter (Area) =	0.0226	µm
Average Pore Diameter (4V/A) =	0.2231	µm
Bulk Density at 0.55 psia =	0.3883	g/mL
Apparent (skeletal) Density =	1.2846	g/mL
Porosity =	69.7731	%
Stem Volume Used =	47	%

Appendix Figure 19- Mercury porosimetry report for EU-AC